Experimentele studie van atmosferische niet-thermische plasma's
voor oppervlaktemodificatie

Experimental Study of Non-Thermal Plasmas
at Atmospheric Pressure for Surface Modification

Eef Temmerman

Promotor: prof. dr. ir. C. Leys
Proefschrift ingediend tot het behalen van de graad van
Doctor in de Ingenieurswetenschappen: Toegepaste Natuurkunde

Vakgroep Toegepaste Fysica
Voorzitter: prof. dr. W. Wieme
Faculteit Ingenieurswetenschappen
Academiejaar 2005 - 2006

UNIVERSITEIT
GENT

ISBN 90-8578-101-9
NUR 926, 971
Wettelijk depot: D/2006/10.500/59

PROMOTOR

prof. dr. ir. Christophe Leys

Universiteit Gent, Vakgroep Toegepaste Fysica IR17

VOORZITTER VAN DE EXAMENCOMMISSIE

prof. dr. ir. Luc Taerwe

Universiteit Gent, Academisch Secretaris

OVERIGE LEDEN VAN DE EXAMENCOMMISSIE

prof. dr. Yuri Akishev

State Research Centre of Russian Federation Triniti, Troitsk, Moscow Region

prof. dr. ir. Lieva Van Langenhove

Universiteit Gent, Vakgroep Textielkunde IR11

prof. dr. ir. Guido Van Oost

Universiteit Gent, Vakgroep Toegepaste Fysica IR17

prof. dr. Marc Van Parys

Hogeschool Gent, Textielinstituut

prof. dr. Willem Wieme

Universiteit Gent, Vakgroep Toegepaste Fysica IR17

Universiteit Gent
Faculteit Ingenieurswetenschappen
Vakgroep Toegepaste Fysica IR17
Rozier 44, B-9000 Gent

DANKWOORD

De eerste pagina van mijn doctoraatswerk is met stip voorbehouden aan alle mensen die ik wil bedanken voor hun directe of indirecte bijdrage aan dit resultaat van 6 jaar onderzoek.

Prof. dr. W. Wieme ben ik dankbaar voor de kans die mij geboden is om een onderdeel te vormen van de Vakgroep Toegepaste Fysica en onderzoek te verrichten in een aangename omgeving.

Prof. dr. ir. C. Leys, die het promotorschap op zich nam, wil ik bedanken voor de motiverende ondersteuning en samenwerking tijdens de experimentele arbeid en de nuttige discussies achteraf.

I would like to thank prof. dr. Y. Akishev for the pleasant cooperation and the many interesting discussions.

De leden van de lees-en examencommissie wil ik bedanken voor de waardevolle commentaren en suggesties.

Mijn woorden van dank gaan ook uit naar dr. Jo Verschuren die op elk moment bereid was te helpen bij vragen of problemen. Zijn interesse en gedrevenheid zijn voor mij een stimulerend voorbeeld geweest.

De vakgroep Vaste-stofwetenschappen en in het bijzonder prof. dr. D. Depla wil ik bedanken voor het ter beschikking stellen van hun apparatuur voor de uitvoering van de XPS metingen.

Ik maak van deze gelegenheid ook graag gebruik om de mensen van het atelier in de spotlights te zetten. Wetenschappelijke ideeën ombouwen tot een concreet haalbare en werkende labo-opstelling is dikwijls geen sinecure en vergt veel ervaring, precisie en vooral veel geduld om telkens weer klaar te staan om hier een aanpassing of daar een verbetering aan te brengen. Ik denk dat elk succesvol experiment, elk gepubliceerd artikel en elk afgewerkt doctoraat ook voor een deel hun verdienste is en ik hoop dan ook dat dit voor hen evenveel voldoening mag geven. Bedankt!

Uiteraard wil ik al mijn collega's van de vakgroep bedanken voor de vruchtbare samenwerking en de aangename werksfeer. Het doet bovendien goed om ook naast de werkvloer een "team" te kunnen vormen.

Tot slot zou ik nog één iemand willen bedanken, maar ik weet dat woorden van dank tekort zullen schieten voor de enorme steun en toeverlaat die hij voor mij was en altijd zal blijven. Ik draag dit boek dan ook graag op aan mijn rots-in-de-branding en liefhebbende echtgenoot, Thomas.

Eef Temmerman

CONTENT

LIST OF SYMBOLS AND ABBREVIATIONS

AC	Alternating Current
BCD	Barrier Corona Discharge
C_{cell}	Total capacitance [F]
C_{die}	Capacitance of the dielectric(s) [F]
C_{gas}	Capacitance of the gas [F]
C_m	Measuring capacitor [F]
CVD	Chemical Vapour Deposition
c	Speed of light [m s^{-1}]
D	Energy dose [J m^{-2}]
d	Interelectrode distance [m]
d_i	effective information depth [m]
DBD	Dielectric Barrier Discharge
DC	Direct Current
E	Electric field strength [V m^{-1}]
E_0	Amplitude of electromagnetic field [V m^{-1}]
E_b	Binding energy [eV]
E_k	Kinetic energy [eV]
e	Electron charge [C]
ECR	Electron Cyclotron Resonance
f	Frequency [Hz]
FWHM	Full Width at Half Maximum [eV]
G	Distance between cathodes and sample [m]
H	Height relative to the anode plate [m]

h	Planck's constant [J s]
I	Discharge current [A]
I_A	Intensity of the XPS peak corresponding to A [%]
I/U	Reduced current [A V^{-1}]
L	Power loading [W m^{-2}]
m_e	Electron mass [kg]
MW	Microwave
n	Gas density [m^{-3}]
n_c	Cut-off density [m^{-3}]
n_e	Electron density [m^{-3}]
P	Discharge power [W]
P_{abs}	Absorbed power [W]
P_{plasma}	Mean power dissipated by the plasma in a DBD discharge [W]
$\mathscr{P}$	Power density [W m^{-3}]
p	Pressure [mbar]
PE-CVD	Plasma Enhanced Chemical Vapour Deposition
PET	Poly(ethylene)therephthalate
PP	Polypropylene
Q_{cell}	Total charge [C]
Q_{die}	Charge on the dielectric [C]
R	Resistance [Ω]
RF	Radio Frequency
S_A	Sensitivity factor of the XPS detector for A []
T	Period [s]
t	Ageing time [s]

U	Discharge voltage [V]
U_0	Corona inception voltage [V]
UHV	Ultra High Vacuum
u_b	Effective gas breakdown voltage [V]
u_{cell}	Total applied sinusoidal voltage [V]
u_{gas}	Voltage across the gas [V]
u_{peak}	Peak value of the applied sinusoidal voltage [V]
V	Volume [m^3]
V_b	Breakdown voltage [V]
v_s	Substrate velocity [m s^{-1}]
W_A	Liquid absorptive capacity [%]
W_{plasma}	Energy deposited into the plasma during 1 cycle of a DBD discharge [J]
X_A	Concentration of element A [%]
XPS	X-ray Photoelectron Spectroscopy

δ_s	Skin depth [m]
ε_0	Permittivity of the vacuum [F m^{-1}]
$\theta_{untreated}$	Contact angle for the untreated material [°]
θ_D	Contact angle for material treated with energy dose D [°]
λ	Wavelength [m]
λ_a	Attenuation length [m]
ν_c	Electron-neutral collision frequency [Hz]
τ	Treatment time [s]

ϕ	Work function [eV]
ω	Angular frequency [rad s^{-1}]
ω_c	Electron cyclotron frequency [rad s^{-1}]
ω_{pe}	Electron plasma frequency [rad s^{-1}]

SUMMARY

Polymers are extensively used in industry due to their excellent bulk properties, but the surface properties of polymers are often a stumbling block in the production process. The low surface energy and chemical inertia causes them to be non-perceptive to bonding with other substrates. These materials therefore usually require surface modification. Plasma technology offers an environmentally friendly alternative to the conventional wet chemical methods to improve the surface properties.

Most industrially used plasmas are cold plasmas. A plasma is a gaseous mixture of neutral and charged particles. The word “cold” refers to a thermal unequilibrium between the electrons and the neutral gas. Initially, the application of a strong electrical field causes ionisation. The created charged particles are accelerated in the applied field. Especially the light electrons receive energy and reach high temperatures. The neutral particles and the ions stay relatively “cold” (the gas temperature is lower than 200°C). Due to collisions between the high energetic electrons and the neutral molecules, radicals are created. These radicals determine the chemical reactivity of the plasma.

Surface treatment with a plasma is usually focused on increasing the surface energy to make the surface more perceptive to water, printing inks, coatings, … In general, the plasma-surface interactions can be divided into the following mechanisms:

- Etching of the surface: The ions in the plasma bombard the surface and thereby remove molecules from the treated surface.
- Cleaning of the surface: Dust particles and other contamination are removed from the surface.
- Activation or functionalisation of the surface: Chemical reactions between activated gaseous particles in the plasma and surface

molecules lead to the formation of functional polar groups at the surface (e.g. hydroxyl- or carboxyl-groups).

- Plasma-enhanced deposition of functional coatings by adding gaseous or fluid precursors to the plasma gas.

This dry, environmentally friendly modification method influences the outermost molecular surface layers without changing the bulk properties. The resulting treatment effect depends on easily adjustable discharge parameters, like gas composition, power, treatment time, … The plasma treatment is therefore a versatile and multifunctional process. Moreover, on account of using non-thermal plasma, the treatment can be applied to heat-sensitive materials.

Different types of plasma sources can be used for the surface treatment. Initially, low pressure plasmas were used, where the discharge is generated by high-frequency electromagnetic waves (radio frequency or microwave discharge). Plasma technology at low pressure ensures a stable and easily controllable discharge. The long mean free path of the gas particles guarantees a high density of chemically active species. However, this technology has to deal with some disadvantages such as the expensive vacuum equipment and the batchwise processing. Consequently, recent development of new plasma technology for practical applications is stressed on atmospheric plasma sources, which offer besides economical benefits also the possibility of in-line processing. In the field of material processing we can distinguish active and remote treatment, depending on the location of the treated material with respect to the plasma chamber. In the active plasma treatment, the sample to be treated usually passes between the electrodes, while in remote treatment the sample is located outside the plasma chamber and is treated in the gas stream that runs through the plasma chamber and is loaded with radicals and other active species. An active plasma treatment has the advantage of a higher concentration of active species near the sample surface, while the remote plasma treatment has a low risk on damaging or backside treatment and allows treatment of materials of any thickness and geometry. The choice for

a specific plasma source will depend on the application and the demands of the producer.

In this thesis the atmospheric dielectric barrier discharge (DBD) in air is examined as an active plasma source. The atmospheric DC glow discharge and the pulsed streamer discharge in air are examined in a remote setup.

The quantification of the plasma effect is carried out by measurement of the change in hydrophilicity after the plasma treatment by means of contact angle and absorption measurements. The surface energy is derived from the contact angle of small (3 µl) water droplets on the surface and is applied on surfaces with a closed structure (such as polymer foils). If the material has a more open structure, the liquid absorptive capacity is measured, which gives the amount of water that a fabric has absorbed during one minute of immersion in water, relative to its own weight. Alternatively, the wicking rate can be measured. In this case the material is suspended in (coloured) water while the rate of vertical capillary rise is recorded at fixed times. X-ray Photoelectron Spectroscopy (XPS) is applied to perform a quantitative analysis of the atomic surface composition.

By means of Lissajous figures and current time variations the classical DBD is compared with a combination of a corona and a barrier discharge, namely a pin-to-plate discharge and a wedge-to-plate discharge with a dielectric layer at the plate electrode. An active treatment of a poly(ethylene terephthalate) foil (PET-foil) in a wedge-to-plate configuration in He + 2 % O_2 at atmospheric pressure and a frequency of 50 kHz during 2 minutes is used to examine the spatial extension of the treatment effect. With the naked eye, oval opaque imprints of the plasma filaments are visible (size up to 7 mm), indicating an overtreatment. The long treatment time is chosen to magnify the plasma effect, so we have a clear view on the area with maximum effect of the plasma treatment. UV transmission spectroscopy shows that the effect is gradual and extends beyond the imprints observed with the naked eye. A Brightfield microscopic image of the surface reveals microscopic spherical pits. This effect causes

the foil to become non-transparent near the imprints. After a more gentle treatment at 50 Hz during 10 seconds the PET-foil surface shows no visible transformation. The effect is noticed by the spreading of water droplets deposited on the treated area of the surface. A systematic measurement of the contact angle is done on PET-foil treated at medium pressure (50 mbar) with the classical DBD. The contact angle for untreated PET-foil is 72°. The value decreases fast as a function of the treatment time, but levels off at a value of 33° for treatment times longer than 0.5 s. The active nature of the DBD treatment leads to a relatively efficient treatment, but the inhomogeneity of the effect, the risk on damages and the limitation on thickness and geometry of the treated material has stimulated the research towards a new treatment technique.

The remote treatment is based on DC pin-to-plate discharges placed in parallel in order to obtain a linear plasma source, easily scaled up to industrial roll widths. A fast transverse airflow ensures the plasma stability and transports the active species towards the surface to be treated. Moreover, the turbulent mixing of inhomogeneities in the density of the active species results in a uniform treatment.

The contact angle on PET-foil decreases with treatment time during the first second of treatment and stabilizes afterwards at 33°. This behaviour of the plasma effect is observed for most materials and could be explained by the incorporation of polar molecular groups at the surface. XPS measurements on the treated PET-foil reveal a good correlation between the wettability and the concentration of the oxygen containing functional groups versus treatment time.

Contact angle measurements on different positions of the sample pointed out that the treatment effect is uniform in the region of the surface that is directly exposed to the flowing afterglow. Outside the directly exposed zone, the effect decreases gradually depending on the local velocity of the gas flow. Finally, an ageing effect is observed on PET-foil. This means that a relapse in the wettability is observed as a function of the time after treatment, due to a relaxation in the structure and orientation of plasma-created polar groups at the

surface. After a storage time of about 5 hours, this decrease levels off. However, after 50 hours of ageing the contact angle is still considerably lower than the value for an untreated surface and results in a wettability that is sufficient for many practical purposes.

The results on other materials show that plasma treatment with the DC glow discharge in the remote setup can be involved in various applications where improvement of hydrophilicity, adhesion or dyebility is desirable.

To have an idea of the local influence of different parameters on the plasma effect, an active treatment in the linear DC glow discharge was carried out on cotton yarn. The results show that the wicking rate of the treated cotton yarn increases with the treatment time and the discharge power. The wicking rate tends to be higher when the yarn is positioned in the vicinity of the electrodes. The variation of the plasma effect in the direction of the airflow reflects the asymmetry in the plasma profile due to the fast gas flow.

To improve the treatment efficiency, a new setup is designed where the remote regime is combined with an intense contact between the plasma and the surface in order to reach a high concentration of active species near the treated surface. The linear pin-to-plate plasma source is therefore redesigned to perform in a regime where the plasma consists of high density current filaments (streamers) that are forced to slide along the surface by the fast airflow. This type of surface treatment ensures higher treatment efficiency without losing the flexibility in thickness and geometry of the materials to be treated. The results on Polypropylene foil (PP-foil) treated in the streamer discharge demonstrate a good permanency of the effect.

SAMENVATTING

Polymeren worden veelvuldig gebruikt in de industrie omwille van hun excellente bulkeigenschappen. De oppervlakte-eigenschappen van polymeren betekenen echter dikwijls een groot struikelblok tijdens het productieproces. De lage oppervlakte-energie en chemische inertie zorgen voor een slechte hechting, bedrukbaarheid en bevochtiging. Daarom vergen deze materialen voor verwerking meestal één of andere vorm van oppervlaktebehandeling. Plasmatechnologie vormt hierbij een milieuvriendelijk alternatief voor de klassieke, natchemische methoden die een verbetering van de oppervlakte-eigenschappen nastreven.

De meeste industrieel aangewende plasma's zijn koude plasma's. Een plasma is een gasvormig mengsel van neutrale en geladen deeltjes. Het adjectief "koud" slaat op een thermisch onevenwicht tussen de elektronen en het neutrale gas. Het aanleggen van een sterk elektrisch veld zorgt in eerste instantie voor ionisatie. De gecreëerde geladen deeltjes worden vervolgens versneld in het aangelegde veld. Vooral de lichte elektronen winnen hierdoor energie en bereiken hoge temperaturen. De neutrale deeltjes en de ionen blijven evenwel "koud" (de gastemperatuur stijgt niet hoger dan 200°C). Bij botsingen tussen de energetische elektronen en neutrale moleculen ontstaan radicalen. Deze radicalen bepalen de chemische reactiviteit van het plasma.

Een plasmabehandeling van het oppervlak is meestal gericht op een verhoging van de oppervlakte-energie om het oppervlak ontvankelijk te maken voor water, verf, coatings, … De interactie tussen het plasma en het oppervlak kan algemeen onderverdeeld worden in verschillende processen:

- Etsen van het oppervlak: De ionen in het plasma bombarderen het oppervlak waardoor moleculen van het behandelde oppervlak verwijderd worden.

- Reiniging van het oppervlak: Stofdeeltjes en andere contaminatie aan het oppervlak worden verwijderd.
- Activatie of functionalisatie van het oppervlak: De reactieve deeltjes in het plasma reageren met het oppervlak, waardoor functionele polaire groepen ingebouwd worden (bv. hydroxyl- of carboxylgroepen).
- Plasmageassisteerde depositie van functionele coatings door toevoeging van gasvormige of vloeibare precursoren in het gasmengsel.

Deze droge, milieuvriendelijke modificatiemethode beïnvloedt enkel de buitenste oppervlaktelaag en laat de bulkeigenschappen onveranderd. Het resulterende effect van de behandeling hangt af van ontladingsparameters die gemakkelijk aangepast kunnen worden, zoals gassamenstelling, vermogen, behandelingstijd,… Een plasmabehandeling is daardoor een veelzijdig en multifunctioneel proces. Bovendien kan een oppervlakte-behandeling met behulp van een plasma ook toegepast worden op hittegevoelige materialen.

Verschillende soorten plasmabronnen werden reeds aangewend voor oppervlaktebehandeling. Aanvankelijk werden vooral lagedruk plasma's ingezet, waarbij de ontlading opgewekt wordt door hoogfrequente elektromagnetische golven (radiofrequente ontlading en microgolfontlading). Plasmatechnologie bij lage druk zorgt voor stabiele en gemakkelijk controleerbare ontladingen. De lange vrije weglengte zorgt bovendien voor een hoge dichtheid aan chemisch reactieve deeltjes. Deze technologie kent echter enkele nadelen zoals de dure vacuüminstallatie en de batchgewijze procesvoering. Op dit ogenblik ligt het accent bij de ontwikkeling van nieuwe plasmatechnologie dan ook bij de atmosferische plasmabronnen, die naast een economisch voordeel ook de mogelijkheid tot in-line processing bieden. Bij de atmosferische plasmatechnologie die aangewend wordt in de materiaaltechnologie kunnen we onderscheid maken tussen actieve en remote behandeling, afhankelijk van de plaats waar het te behandelen materiaal zich bevindt ten opzichte van de ontladingskamer. Bij een actieve plasmabehandeling wordt het monster meestal tussen de elektroden geplaatst, terwijl bij een remote

behandeling het monster zich buiten de plasmakamer bevindt en behandeld wordt in de met actieve deeltjes beladen gasstroom die door het plasma stroomt. Een actieve behandeling heeft het voordeel van een hoge efficiëntie wegens een hogere concentratie aan reactieve deeltjes, terwijl een remote behandeling een laag risico op beschadiging heeft en materialen met een willekeurige geometrie kan behandelen. De keuze van een plasmabron en zijn specifiek ontwerp zal afhangen van de toepassing en de eisen van de producent.

In deze scriptie wordt een atmosferische diëlektrische barrière ontlading (Engels: dielectric barrier discharge) in lucht besproken als actieve plasmabron. De DC glimontlading (Engels: DC glow discharge) en de gepulste streamerbron (Engels: pulsed streamer discharge) in lucht worden in een remote opstelling onderzocht.

De kwantificatie van het plasma-effect wordt onderzocht door de verandering in hydrofiliciteit na de plasmabehandeling te meten aan de hand van contacthoek- of absorptiemetingen. De contacthoek van kleine druppels (3 µl) gedistilleerd water die op het oppervlak worden aangebracht is een maat voor de oppervlakte-energie en wordt toegepast op oppervlakken met een gesloten structuur (zoals polymeerfolies). Wanneer het materiaal een meer open structuur heeft is men aangewezen op absorptiemetingen (Engels: liquid absorptive capacity), waarbij de hoeveelheid water wordt gemeten die door het monster geabsorbeerd wordt gedurende een vast tijdsinterval. Als alternatief kan ook de capillaire opstijgsnelheid gemeten worden (Engels: wicking rate). Het materiaal wordt deels in (gekleurd) water ondergedompeld terwijl de hoogte van de opstijgende watergrens op vaste tijdstippen wordt genoteerd. X-stralen fotoelektronenspectroscopie (Engels: X-ray Photoelectron Spectroscopy, XPS) wordt toegepast om een kwantitatieve analyse van de atomaire oppervlaktecompositie uit te voeren.

De klassieke diëlektrische barrière ontlading wordt vergeleken met een combinatie van een corona en een barrière ontlading aan de hand van Lissajous figuren en tijdsvariaties van de stroom. Het gaat hierbij om een pin-plaat (Engels: pin-to-plate discharge) en een mes-

plaat ontlading (Engels: wedge-to-plate discharge) met diëlektrische laag op de vlakke elektrode. Een actieve behandeling van een polyethyleentereftalaatfolie (PET-folie) in een mes-plaat ontlading in He + 2 % O_2 bij atmosfeerdruk en een frequentie van 50 kHz gedurende 2 minuten werd gebruikt om de ruimtelijke uitspreiding van het behandelingseffect te onderzoeken. Met het blote oog zijn ovale niet-transparante afdrukken van de plasma filamenten op het behandelde oppervlak zichtbaar die wijzen op een overbehandeling (afmetingen tot 7 mm). Dit stelt ons echter in staat om een duidelijker beeld te krijgen van de oppervlakte die het meest beïnvloed wordt door het plasma. UV transmissiespectroscopie toont aan dat het effect gradueel is en zich nog verder uitstrekt dan wat we met het blote oog waarnemen. Een Brightfield microscopisch beeld van het oppervlak onthult bovendien microscopische ronde “putjes” (Engels: pits) die de oorzaak zijn van het verdwijnen van de transparantie ter hoogte van de ovale afdrukken. Een mildere behandeling bij 50 Hz gedurende 10 seconden zorgt niet meer voor zichtbare beschadiging. Het effect werd hier zichtbaar door de uitspreiding van waterdruppels die op de behandelde zone van het oppervlak geplaatst werden. Een systematische meting van de contacthoek als functie van de behandelingstijd werd uitgevoerd op PET-folie die behandeld werd bij een medium druk (50 mbar) in de klassieke DBD. Onbehandeld bedraagt de contacthoek 72°. De waarde daalt vrij snel als functie van de behandelingstijd, maar satureert vanaf een behandelingstijd van 0.5 s op een waarde van 33°. Het actieve karakter van de behandeling met de DBD leidt tot een relatief efficiënte behandeling, maar de inhomogeniteit van het effect, het risico op beschadiging en de begrenzing in dikte en geometrie van de te behandelen materialen heeft het onderzoek naar een nieuwe behandelingstechniek gestimuleerd.

Een remote configuratie wordt ontworpen en uitgevoerd door DC pin-plaat ontladingen in het glimregime parallel aan elkaar te plaatsen om op die manier een lineaire plasmabron te verkrijgen die gemakkelijk opgeschaald kan worden naar industriële rolbreedtes. Een snelle transversale luchtstroming zorgt voor de stabiliteit in het plasma en

voor het transport van de actieve deeltjes naar het te behandelen oppervlak toe. De turbulente menging van de actieve deeltjes resulteert bovendien in een uniforme behandeling.

De contacthoek op PET-folie vertoont een daling gedurende de eerste seconde van de behandeling en stabiliseert daarna op 33°. Dit gedrag van het plasma effect wordt waargenomen bij de meeste materialen en kan verklaard worden door de vorming van polaire molecuulgroepen aan het oppervlak. XPS-metingen op de behandelde PET-folie duiden op een goede correlatie tussen de verhoging van de hydrofiliciteit en de inbouw van zuurstofhoudende polaire molecuulgroepen als functie van de behandelingstijd.

Contacthoekmetingen op verschillende posities op de PET-folie wijzen op een uniforme behandeling van de oppervlaktezone die rechtstreeks blootgesteld wordt aan de nagloed van het plasma (Engels: afterglow). Daarbuiten neemt het effect gradueel af, afhankelijk van de lokale snelheid van de luchtstroming. Tot slot wordt een degradatie van het effect waargenomen als functie van de tijd na behandeling (Engels: ageing effect), ten gevolge van een relaxatie in de structuur en oriëntatie van de ingebouwde polaire molecuulgroepen. Na een bewaartijd van ongeveer 5 uren stagneert deze daling. Na 50 uren bewaartijd blijft het oppervlak echter nog steeds een deel van zijn hydrofiliciteit behouden, wat voor vele praktische toepassingen nog voldoende zal zijn.

De resultaten op andere materialen wijzen erop dat een plasmabehandeling met de DC glimontlading ingeschakeld kan worden voor verschillende toepassingen waar een verhoging van de hydrofiliciteit of adhesie gewenst is.

De lokale invloed van verschillende parameters op het plasma effect wordt onderzocht door de actieve behandeling van katoengaren in de lineaire DC glimontlading. De resultaten tonen een verhoging van de opstijgsnelheid als functie van behandelingstijd en vermogen. Het plasma effect blijkt bovendien groter wanneer de katoendraad in de nabijheid van de elektrodes wordt geplaatst. Variatie van de plaats in

de richting van de luchtstroming wijst op de asymmetrie in het plasmaprofiel ten gevolge van de snelle luchtstroming.

Om de behandelingsefficiëntie te verhogen werd tenslotte gezocht naar een opstelling waar het remote karakter wordt gecombineerd met een intens contact tussen plasma en oppervlak zodat een hoge concentratie aan actieve deeltjes wordt verkregen ter hoogte van het oppervlak. De lineaire pin-plaat plasmabron werd aangepast om in een streamer regime te werken. Het plasmavolume bestaat hierbij uit dunne stroomfilamenten die parallel aan het oppervlak lopen en die door de snelle luchtstroming gedwongen worden om de weg tussen pin en plaat af te leggen langs het oppervlak van het te behandelen materiaal. Hierdoor wordt een hogere behandelingsefficiëntie nagestreefd zonder in te boeten aan flexibiliteit qua materiaaldikte en geometrie. De resultaten op Polypropyleenfolie (PP-folie) behandeld met behulp van de streamerontlading tonen een goede permanentie van het effect aan.

INTRODUCTION

Most plastic materials have chemically inert surfaces with low surface tension. This causes them to be non-perceptive to bonding with substrates, printing inks, coatings and adhesives. Traditional surface treatments of fabrics and foils to improve bonding characteristics often include liquid chemical processes (e.g. acid treatment). In comparison with these methods, dry plasma treatment forms an economical and environmentally friendly alternative. Many recently developed plasma sources operate at low pressure (see, for instance, [1, 2]) and demonstrate good treatment results. Plasma assisted surface techniques can already be found in for example the fabrication of microelectronic components, automotive and aerospace industries. The disadvantages of these plasma systems are that vacuum equipment is expensive and continuous processing is difficult because a batch process is always necessary.

As for atmospheric pressure plasma treatment, so-called corona treaters [3], based on alternative current (AC) dielectric barrier discharge powered with a typical frequency of about 20-30 kHz, are widely used today for cold plasma processing of various materials. Some of the large-size treaters are able to process sheets up to 10 m in width with linear velocities up to 8-10 m/s. Some other results on surface treatment using AC barrier discharge are published in [4, 5].

For dielectric materials, the applicability of AC treaters is limited to thin substrates, because the AC discharge current strongly decreases with increasing thickness of the treated materials, resulting in a dramatic reduction (down to zero) of the treatment intensity. Moreover, some industrial applications require higher treatment effect without altering the production speed. Therefore, new kinds of atmospheric pressure plasma treaters need to be developed, which are not sensitive to the thickness of the treated material and can process textile and other sheet materials at high linear velocities.

This work takes up the scientific challenge of developing innovative concepts for plasma surface treatment, combined with fundamental research on both the discharge mechanism and the characterization of the treated materials. An atmospheric pressure remote plasma treatment is produced that operates in ambient air. Besides, the plasma system based on the use of steady-state direct current (DC) discharge is developed to avoid thermal effects that would cause degradation of heat-sensitive materials when placed in direct contact with the plasma. The design of the plasma reactor also ensures scalability to industrial roll widths. An additional advantage of the proposed remote plasma source in comparison with AC discharge treaters is the absence of limitations on the thickness of the treated substrates as the substrate is not placed between the electrodes. In the case of AC discharge the electrodes are separated by a gap not higher than 5 mm. The atmospheric treatment technique is further refined by operating the setup in a pulsed streamer regime. This redesign increases the efficiency by an improvement of the contact between plasma and surface.

By means of a multidisciplinary approach the research has contributed to a scientific expertise in the field of plasma physics and surface characterization techniques. This work demonstrates that the newly designed plasma treatment concepts constitute an alternative technique for surface activation of polymers and textiles. In this respect, it forms a good starting point for a feasibility study about the introduction of the innovative plasma sources into an industrial environment.

OUTLINE

Chapter 1 starts with a commentary on the motivation to use plasma in material processing. Some basics of gas discharge physics are discussed and the interactions between the plasma and the surface are listed. Furthermore, it gives an overview of the plasma techniques applied for surface modification.

After plasma treatment, the modification of the treated surface is investigated by physico-chemical surface analysis. In chapter 2, the principles of the different analysing methods, used in this work, are discussed. The quantification of the treatment efficiency is tested by measuring changes in wettability by means of the contact angle, the liquid absorptive capacity or the wicking rate. The treatment effect on molecular level is examined in more detail by X-ray Photoelectron Spectroscopy (XPS).

In the following chapters, the results of the research are discussed. The results are subdivided in three chapters according to the type of plasma source used in the experiments.

In chapter 3, the electrical and surface treatment characteristics of a classical dielectric barrier discharge are compared with an alternative approach where the parallel-plate electrode configuration is replaced by a pin-to-plate and a wedge-to-plate configuration (AC barrier corona discharge). The first experiments on surface treatment are carried out using barrier discharge in order to become familiar with plasma activation of polymers and the characterization of the plasma effect and to be faced with the disadvantages of this technique.

The design of a new type of plasma source for surface modification is based on eliminating the disadvantages of the AC barrier corona, mainly the inhomogeneity at atmospheric pressure and the thereby caused risk of damaging the material to be treated. Chapter 4 presents an atmospheric DC glow discharge in a “remote” plasma treatment setup. Different polymer foils and fabrics are treated in the

afterglow of the plasma source and are analysed afterwards. Moreover, as a way to investigate the properties of the plasma source, the influence of different parameters on the plasma effect is examined by active treatment of a cotton yarn.

Finally, chapter 5 presents a setup designed for treatment of narrow material stripes, where the plasma source operates in the streamer regime. The plasma consists of high density current filaments (streamers) that are forced to slide along the surface to be treated by means of a strong gas flow. In this way, a high concentration of active species is ensured near the surface and high treatment efficiency can be reached.

Finally, chapter 6 gives the general conclusions of this work.

PUBLICATIONS

The results presented in this work can be found in the following scientific publications in international journals:

- E. Temmerman and C. Leys, “Surface modification with a remote atmospheric pressure plasma”, *Czechoslovak Journal of Physics* **54** (2004) C984-C989

- E. Temmerman, Y. Akishev, N. Trushkin, C. Leys and J. Verschuren, “Surface modification with a remote atmospheric pressure plasma: DC glow discharge and surface streamer regime”, *Journal of Physics D: Applied Physics* **38** (2005) 505-509

- E. Temmerman, C. Leys and Y. Akishev, “Surface modification of cotton yarn with a DC glow discharge in ambient air”, *Surface and Coatings Technology* **200** 1-4 (2005) 686-689

- B. Boschmans, M. Vanneste, L. Ruys, E. Temmerman, C. Leys and L. Van Vaeck, ”Static secondary ion mass Spectrometry (S-SIMS) analysis of atmospheric plasma treated polypropylene films”, *Applied Surface Science* **252** 19 (2006) 6660-6663

- C. Leys, D. Neirynck, R. Morent and E. Temmerman “DC-excited cold atmospheric pressure plasmas”, *Czechoslovak Journal of Physics* **56** (2006) B896-B902

1 PLASMA SURFACE TREATMENT

1.1 MOTIVATION

The use of synthetic materials in industry - mostly polymers - is widely spread and is still expanding in different areas of industrial production (e.g. textile industry). This is attributed to the superior bulk properties of polymers compared to other materials, such as their high strength-to-weight ratio, good resistance to corrosion and often low production costs. Despite these excellent bulk characteristics, hydrocarbon polymers have unfavourable surface properties for many applications. The low surface tension and chemical inertness causes them to be non-perceptive to bonding with substrates, printing inks, coatings and adhesives. This causes the need for modification of the surface properties, without changing the bulk properties.

Traditional surface treatments of polymeric fabrics and foils to improve bonding characteristics often include liquid chemical processes (e.g. acid treatment) [6]. However, ecological requirements force the industry to search for environmentally friendly alternatives. Plasma technology is one of the most promising and cheap solutions. Activation of the surface with a plasma treatment is based on the chemical interaction between the reactive species in the plasma and the outermost molecular layer of the treated surface.

In plasma technology, “cold” plasmas are generated by an electrical gas discharge. The word “cold” refers to the thermal non-equilibrium between the light electrons and the heavy neutral gas molecules. The application of a strong electric field ensures ionization in the gas volume. The created charged particles are accelerated in the applied electric field. The light electrons gain most energy and achieve high temperatures (1-10 eV), while the heavy ions efficiently exchange their energy by collisions with the background gas and thus remain “cold” (the gas temperature is below 200°C). On collision between energetic

electrons and neutral molecules, radicals are created. These radicals play an important role in the chemical reactivity of the plasma.

Surface treatment with plasma results in a dry, non-polluting modification method, which leaves the bulk properties unaffected. As the treatment effect depends on the working gas and other easily adjustable discharge conditions, plasma treatment is versatile and multifunctional. Moreover, plasma surface treatment is applicable to heat-sensitive materials due to the low gas temperature.

1.2 BASICS OF GAS DISCHARGE PHYSICS

Originally, the term “gas discharge” referred to the process of discharging a capacitor into a circuit incorporating a gap between electrodes [7]. However, the notion of a closed circuit is not necessary for a direct motion of charges and therefore the modern gas discharge physics takes up a wider range of discharge types. The effects observed in gases subjected to oscillating electric fields or electromagnetic waves are in principle the same as the DC phenomena. In these types of discharge, the energy of the field is dissipated through absorption of radiation, instead of through the release of Joule heating by electrical current. In order to introduce the main basic concepts of gas discharge physics, the discussion can be confined to a typical discharge in a constant electric field: the low pressure DC glow discharge.

The plasma in a low pressure DC glow discharge is sustained between two conductive parallel plate electrodes placed in a closed reactor chamber (Figure 1.1). A high impedance power supply is connected to the electrodes to provide the electric energy. Typical dimensions of the discharge tube are 10-100 cm in length and a radius of 1 cm. The pressure p is typically between 10^{-2} and 10^{2} mbar. The current has values in the order of 10^{-4}-10^{-1} A and the voltage is in the order of 10^{2}-10^{3} V.

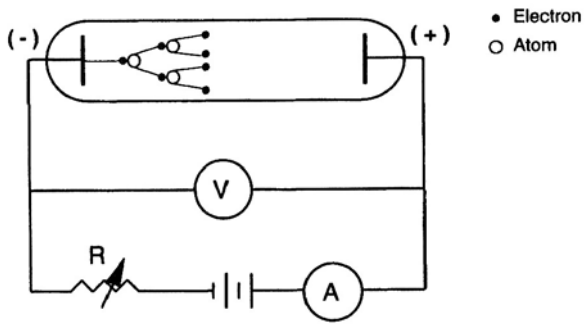

Figure 1.1 *Schematic setup of the low pressure DC glow discharge [8].*

The breakdown voltage in the DC glow discharge depends on the discharge gas, the gas pressure and the interelectrode distance according to the Paschen's law:

$$V_s = \frac{C_1(pd)}{C_2 + \ln(pd)} \tag{1.1}$$

where p is the pressure, d is the interelectrode distance and C_1 en C_2 are constants determined by the nature of the gas.

Figure 1.2 shows the Paschen's curves for different gases. For extreme values of the pd product, the breakdown voltage is high because the probability of ionization and/or ion collection will be small. Discharges are most easily initiated for values of pd in the range of 10^{-1}-10 torr cm since the breakdown voltage is at a minimum.

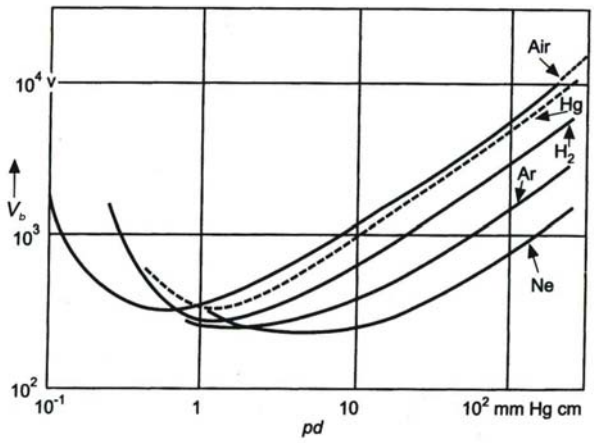

Figure 1.2 *Paschen's curve for various gases [8]*

Once the applied voltage exceeds the breakdown voltage, different types of discharges can be obtained depending on the discharge current. By adjusting the ballast resistor *R*, one can draw up the voltage-current characteristic (Figure 1.3). At low currents, the voltage increases very fast due to an electron multiplication process (*Townsend mechanism*). The gas discharge becomes self-sustained as soon as the breakdown voltage V_s is reached. An equilibrium is established between the rate of ion generation and the rate of electron-ion recombination and the electric field is independent of charge densities. This regime is called the *Townsend discharge*. On gradually increasing the current, the discharge voltage decreases, marking the transition to the *normal glow*. This regime has the remarkable property that the current density at the cathode is independent of the total current. This means that the area at the cathode surface through which the current flows changes. At the point where the plasma covers the entire cathode surface the further increase in current is attributed to an increase in voltage. This results in an increase in the cathode current density and corresponds to the *abnormal glow*. A further increase in the discharge current heats up the electrodes and eventually results in thermionic emission of

electrons and a fast decrease in voltage. This is known as an *arc discharge*.

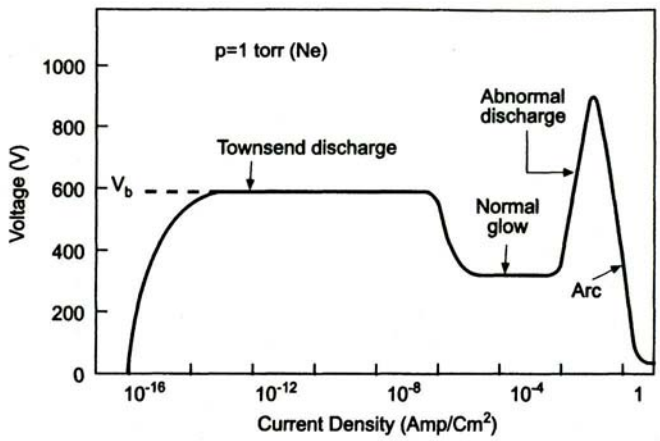

Figure 1.3 *Voltage-current characteristic of a low pressure DC glow discharge [8].*

In the low pressure DC glow discharge, we can distinguish several bright and dark regions along the discharge tube (Figure 1.4). These regions were first observed by Michael Faraday in 1830 and are so characteristic for the glow discharge that they received individual names. Near the cathode, we can see the *cathode glow* followed by the *Crooke's dark space*. The emission of light at the *cathode glow* comes from excited atoms sputtered off the cathode surface or from positive ions moving towards the cathode. The *Crooke's* or *cathode dark space* is a positive space charge, through which secondary electrons produced at the cathode gain energy. Over this region, a sharp voltage drop occurs, which is called the *cathode fall*. The thickness of this region is inversely proportional to the gas density. The brightest light intensity comes from the *negative glow*. The high-velocity electrons accelerated by the cathode fall produce intense ionization and excitation in the negative glow. These electrons are

slowed down in the *Faraday dark space*. The electron density decreases by recombination and diffusion. Most of the volume in the discharge tube is occupied by the *positive column*. This is a homogeneous and quasi-neutral region with a relatively small electric field. The positive column is separated from the anode by the *anode sheath*. The anode pulls electrons out of the positive column, while the positive ions are rejected. A negative space charge is formed near the anode, which creates the *anode dark space*. The *anode glow* is a bright region near the anode.

The presence of the different layers depends on the interelectrode distance. If this distance is lowered, the Faraday dark space and the positive column will shrink and finally disappear. For an interelectrode distance smaller than twice the thickness of the cathode dark space, it is impossible to generate a glow discharge.

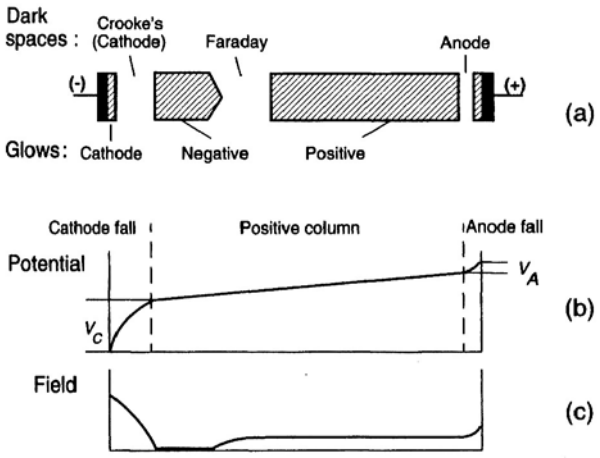

Figure 1.4 *Spatial distributions of (a) glow discharge regions (b) potential and (c) electric field along the discharge tube of a low pressure DC glow discharge with plane electrodes [8].*

1.3 PLASMA-SURFACE INTERACTIONS

As mentioned before, exposure of polymers to a plasma can cause chemical and physical changes to the uppermost surface layer, without affecting bulk properties. The desired result consists mostly of an increase in surface energy of the treated material, leading to an improved adhesion, printability or wettability. In general the plasma-surface interactions can be divided into different mechanisms. Which one is initiated depends on the plasma parameters and on the nature of both the plasma gas and the surface to be treated.

- *Etching* of the surface

  On exposure to plasma, molecules of the treated surface can be removed by an etching reaction. Chemical reactions produce volatile compounds containing atoms of the bulk material. For example, a polymer can be etched in an F_2-plasma, producing volatile CF_x.

- *Surface activation and functionalization*

  The most important process for surface modification during a plasma treatment is the implantation reaction. Chemical reactions between activated gaseous particles in the plasma and surface molecules lead to the formation of functional groups at the surface, e.g. hydroxyl (-OH), carbonyl (-C=O), carboxyl (-COOH) or amino groups ($-NH_x$). Plasma implantation or activation is performed in gases that do not polymerize. The bombardment of the surface with the reactive plasma particles breaks covalent bonds on the surface and leads to the formation of surface radicals on the treated material. These surface radicals react with the active species of the plasma to form various active chemical functional groups on the surface of the substrate [9]. Incorporated polar groups for example are responsible for an increase in

hydrophilicity of the surface. The presence of radicals or functional groups at the treated surface can also promote the covalent attachment of specific species, e.g. functionalization of polymer surfaces with aminogroups can allow the immobilization of biomolecules [10, 11].

- *Cleaning* of the surface

  Plasma can clean the surface by removing dust particles and other contaminants at the surface. This process is for example of high importance for the cleaning of wafers in the semiconductor industry. Residual organic and metallic contaminants can be removed completely from the silicon wafer in plasmas of inert gases and/or hydrogen. Plasma cleaning offers a good alternative to conventional wet cleaning, which is not always compatible with integrated chip processing [8].

- *Plasma-enhanced deposition of functional coatings*

  By adding organic gaseous or fluid precursors to the plasma gas, active fragments are created that react to form a film on the surface by polymerization. The properties of the coating are different from the properties of the substrate and strongly dependent on the plasma conditions (power input, flow rate of the organic gases introduced in the plasma, pressure, …) [8, 9]. This plasma enhanced chemical vapour deposition (PE-CVD) can change the mechanical (tribology), chemical (corrosion protection) and optical (reflective and decorative) properties of the material. PE-CVD can operate at much lower temperatures than the classical chemical vapour deposition (CVD), which simplifies the deposition of heat-sensitive coatings.

1.4 PLASMA TREATMENT PARAMETERS

In general, the plasma treatment is characterized by the following parameters.

In the first place, the plasma treatment depends on the power P [W] that is put into the discharge. The discharge current and the voltage determine the discharge power of the plasma source.

The power density $\mathcal{P}$ [W m^{-3}] is defined as the discharge power P divided by the discharge volume.

The power loading L [W m^{-2}] is defined as the discharge power P per exposed area of the sample surface.

The treatment time τ [s] is the time of exposure to the plasma. In most cases the substrate is moving, so the treatment time can also be given by:

$$\tau = \frac{d}{v_s} \tag{1.2}$$

where d is the active length of the discharge in the direction of the substrate movement and v_s is the substrate velocity.

The energy dose D [J m^{-2}] onto the treated surface is an important parameter to achieve desired surface properties. D is defined as the power loading L multiplied by the treatment time τ.

$$D = L\tau \tag{1.3}$$

1.5 PLASMA TECHNIQUES

The application field of plasma technology is growing very fast. Moreover, increasing demands from industry encourage the continuous development of more efficient and more flexible plasma techniques. One of these fast-growing areas is the use of plasma in

materials processing. This paragraph gives an overview of the different plasma techniques that can be used for surface modification. The choice of the plasma source and its particular design depend on the specific requirements of the application involved (cost, process rates, process uniformity, flexibility, etc.). However, it can be noticed that recent plasma research mainly emphasizes the development of atmospheric pressure technology.

1.5.1 LOW PRESSURE PLASMAS

Many developed plasma sources for surface treatment operate at low pressures (0.01-10 mbar), because at low pressure the discharge is more stable and it is easier to control the plasma reactions. Moreover, a long mean free path of the gas particles guarantees only few collisions and thus only small reduction in the number of chemically active species.

The low pressure plasmas used in the field of surface engineering are produced by means of generators with a radio frequency (RF) or microwave (MW) power supply [8, 12, 13].

1.5.1.1 Radio Frequency discharge

A plasma can be excited and sustained by high-frequency electromagnetic waves. When the frequency of the electromagnetic field increases, the ions and subsequently the electrons can no longer reach the electrode surface during the acceleration phase of the exciting external field. The interaction between the power supply and the plasma is now dominated by displacement rather than by real currents. The relation between the frequency of the applied electromagnetic field and the characteristic frequency of the electrons, the so-called *electron plasma frequency*, determines to what extent the electromagnetic wave interacts with the plasma. The electron plasma frequency ω_{pe} is given by:

$$\omega_{pe} = \sqrt{\frac{n_e e^2}{m_e \varepsilon_0}} \tag{1.4}$$

n_e = the electron density

e = electron charge

m_e = electron mass

ε_0 = permittivity of the vacuum

When an electromagnetic wave with a frequency above ω_{pe} is incident on the plasma, the electrons are too slow to follow the oscillations in the electric field of the wave. The electromagnetic wave does not interact with the individual electrons in the plasma, but interacts only weakly with the plasma through a collective interaction regime [14], as will be discussed in the next paragraph. When the incident wave has a frequency below ω_{pe}, as is the case for radio frequencies, the inertia of the electrons is relatively high enough to respond individually to the electric field of the wave. The electron density corresponding to the electron plasma frequency is also called the cut-off density, because the wave will be reflected if the electron density in the plasma is higher than this cut-off density. From equation (1.4) we can see that the cut-off density is given by:

$$n_c = \frac{\omega^2 \varepsilon_0 m_e}{e^2} \tag{1.5}$$

Due to the skin effect, the electromagnetic wave can only penetrate into the plasma over a small thickness, which is called the skin depth δ_s:

$$\delta_s = \sqrt{2}c\sqrt{\frac{\varepsilon_0 m_e \nu_c}{e^2 n_e \omega}} \tag{1.6}$$

c = speed of light

ν_c = electron-neutral collision frequency

ω = angular frequency of the electromagnetic field

In this region of the plasma, the electrons can absorb energy from the wave. The absorbed power per volume is given by

$$\frac{P_{abs}}{V} = \frac{n_e e^2 \nu_c E_0^2}{2m_e \left(\nu_c^2 + \omega^2\right)} \tag{1.7}$$

where E_0 is the amplitude of the electromagnetic field.

Radio frequency (RF) discharges operate in the frequency range of 1-100 MHz, most commonly at 13.56 MHz. The energy of the power supply is coupled to the plasma by displacement currents rather than real currents. In this way, the electrodes become less important for sustaining the plasma and *electrodeless discharges* become possible. This means that the electrodes can be placed outside the reactor chamber. As there is no direct contact between the electrodes and the discharge, impurities originating from the electrodes are no longer present in the treatment chamber and the lifetime of the electrodes is increased.

The power coupling in RF discharges can be accomplished by oscillating electric fields (capacitive coupling) or by oscillating magnetic fields (inductive coupling). Figure 1.5 shows the schematic setup of a capacitive and inductive coupling system in a plasma reactor for surface treatment.

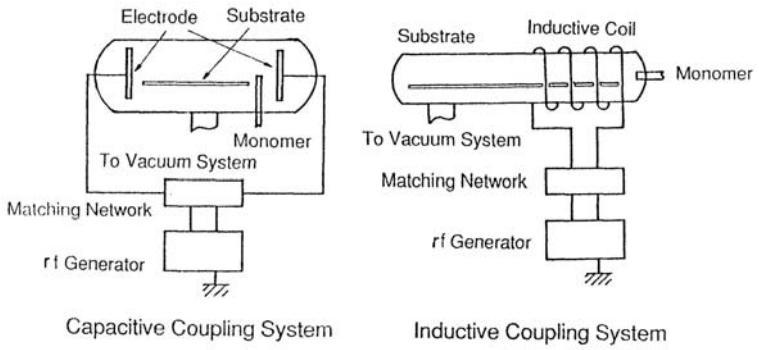

Figure 1.5 *Schematic diagram of the two different types of RF discharge reactors: capacitively and inductively coupled RF discharges [9].*

1.5.1.2 Microwave discharge

Electromagnetic radiation at microwave (MW) frequency interacts with a plasma in the collective regime. The interaction occurs between the radiation and the plasma as a dielectricum, rather than between the radiation and the individual electrons, as for RF plasmas. MW frequencies are at or above the electron plasma frequency. The energy in a typical MW plasma is supplied by a 2.45 GHz power supply. The microwaves are transmitted via coaxial cables at powers below 200 W and via hollow rectangular waveguides with high electrical conductivity at higher powers. The cross section of these transmission lines is determined by the wavelength of the microwave (λ = 12.24 cm). The microwaves propagate into the plasma reactor where they can be absorbed, leading to heating of the electrons and excitation of a discharge. In MW induced plasmas the electron kinetic temperature is typically 5 to 15 eV, where it is only 1-2 eV for the DC and RF discharges. Due to the higher electron kinetic temperatures, MW discharges have a higher fraction of ionization than DC or RF plasmas, which is an important advantage in many applications.

In general, a MW plasma reactor consists of a MW power supply, a circulator, the applicator and the plasma load (Figure 1.6). The circulator protects the power supply from reflected power due to an impedance mismatch. The applicator optimizes the energy transfer from the power supply to the plasma and minimizes the power reflection.

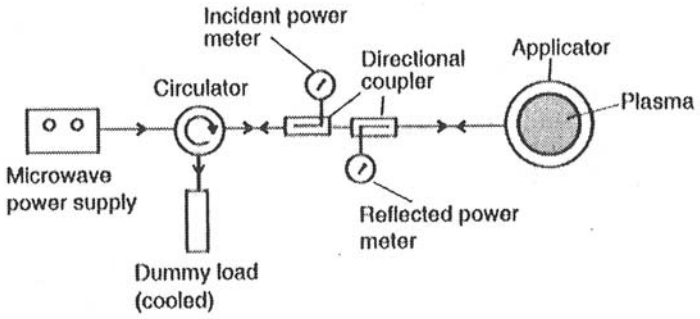

Figure 1.6 *General setup of a MW reactor [8].*

Different types of MW discharges are available, which ensures that MW plasmas can be operated over a wide range of conditions, with pressures ranging from 0.1 Pa up to atmospheric pressure.

One of the simplest and most used MW plasma generation configurations is the *waveguide coupled reactor*. The MW power is directly coupled to the plasma by inserting a dielectric (quartz) tube reactor through a rectangular waveguide, as shown in Figure 1.7. The plasma is initiated and maintained due to the axial high electric field at MW frequency located at the place where the waveguide surrounds the dielectric tube, which contains the working gas at low pressure.

In a *resonant* or *multimode cavity reactor* the MW power is fed through a window separating the waveguide from the cylindrical vacuum cavity, where the plasma is generated (Figure 1.8). In a *resonant cavity reactor* the cavity radius and length are comparable to the free space wavelength of the radiation (λ_0 = 12.24 cm for $\nu_{radiation}$ = 2.45 GHz) and electromagnetic modal structures are formed. If the

radius and length of the cavity are sufficiently larger than λ_0, the reactor is called a *multimode cavity reactor*. Here, the MW power is spread more uniformly throughout the cavity volume and confinement is improved by a lower surface-to-volume ratio.

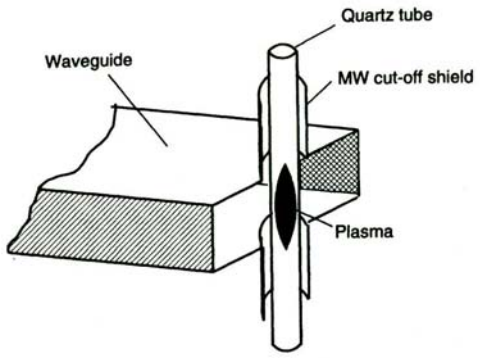

Figure 1.7 *Basic principle of a waveguide coupled reactor [8].*

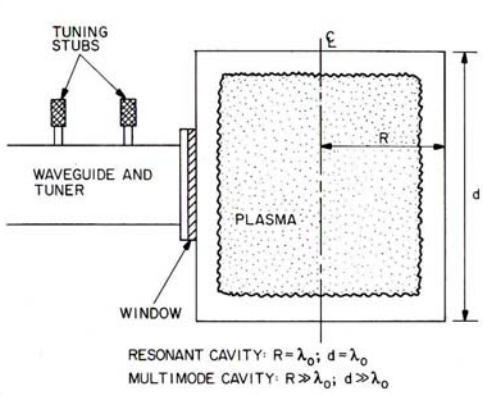

Figure 1.8 *A schematic of a resonant or multimode cavity microwave plasma reactor [14].*

Operation at high density without increasing the cavity dimensions is possible by applying an additional strong DC magnetic field, in which the electron cyclotron frequency ω_c equals the applied electromagnetic wave frequency ω. In this way the magnetic field ensures high plasma confinement as well as high power absorption.

This is especially favourable for low-pressure sources where the low collision frequency involves low power absorption (equation (1.7) approaches zero for $\nu << \omega$). Due to the *cyclotron resonance*, the electron gyration around the magnetic field lines is in phase with the applied right-hand circularly polarized wave. The electrons will "feel" a steady electric field over many gyro-orbits and absorb the energy by a collisionless heating mechanism. This allows using much lower field strengths as the electrons can absorb the energy over a longer time. Figure 1.9 shows an example of an *electron cyclotron resonance reactor* (ECR). The DC magnetic field is generated by one or more magnetic field coils and varies in axial direction. A linearly polarized microwave is axially applied through a quartz window into the plasma. This linearly polarized wave can be decomposed into two counter rotating circularly polarized waves. At the resonance zone, the electrons will be in phase with the right-hand circularly polarized wave and can absorb energy from the wave. The created plasma flows along the magnetic field lines from the resonance zone into the process chamber, where the energetic ions and free radicals impinge on the sample surface. Optionally, a magnet coil near the sample holder can be used to improve the uniformity of ion current density at the sample and to ensure that the ions hit the surface perpendicular. For the typically used microwave frequency of 2.45 GHz, the resonant magnetic field strength is 87.5 mT. Several other ECR configurations have been developed as these sources became a popular etching and deposition tool in microelectronics.

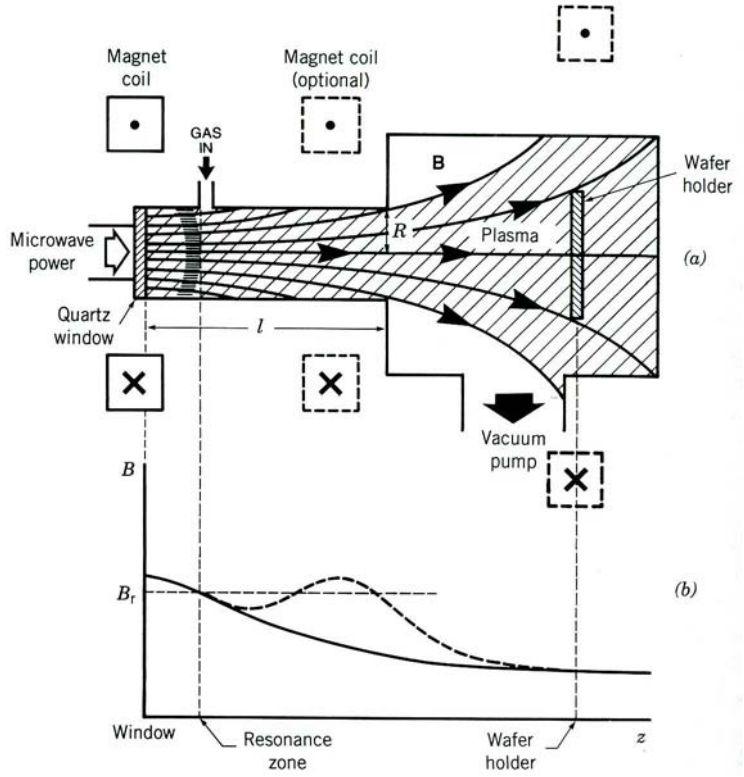

Figure 1.9 *A typical ECR configuration for material processing applications, together with the axial magnetic field variation [15].*

The low pressure techniques discussed above have been shown to be useful and suitable to modify surfaces for more than 50 years, for example large-area etching of polymers [16], surface cleaning in an oxygen RF plasma [17], treatment of fabric webs [18], etching and thin film deposition in an ECR configuration [19]. However, the disadvantages of these plasma systems are that vacuum equipment is very expensive and continuous processing is difficult because a batch process is always necessary. For industrial applications where a vacuum environment is not required, as in the case of surface activation, atmospheric pressure plasmas are much more desirable.

1.5.2 ATMOSPHERIC PRESSURE PLASMAS

To overcome the disadvantages of low pressure technology, efforts are made to develop atmospheric plasma sources. Because there is no need for vacuum devices, the investment costs are much lower and the atmospheric plasma technology can easily be scaled up to industrial dimensions and integrated in in-line processing.

The difficulty of working at atmospheric pressure is that instabilities in the discharge arise rapidly, so that accumulation of species with low ionization potentials and eventually transition to an arc discharge is likely to take place. This transition is undesirable because of the loss of homogeneity as the discharge constricts towards a narrow current channel. Moreover, the high current density causes an increase in gas temperature, which dispels the non-thermal character of the discharge. Therefore, the primary challenge when developing an atmospheric plasma technique is finding a mechanism to prevent this transition. A generally applied attempt to achieve a stable plasma is to introduce a negative feedback between the discharge current and voltage by means of a ballast resistor. But a mere ballast resistor seemed not to be sufficient to prevent the transition to a thermal arc. Different other solutions for additional stabilisation have come up, mostly based on limiting the discharge maintenance time [20]. A pulsed regime can prevent that instabilities have enough time to develop. In this way, for example pulsed corona and microwave discharge can be operated at atmospheric pressure. Dielectric barrier discharges prevent the transition to arc discharge by auto-pulsation of the discharge in an AC arrangement with a dielectric barrier on one or both parallel plate electrodes. Another method to prevent accumulation of charges is to apply a fast gas flow in transverse direction so that instabilities are “blown” away, for example in the DC glow discharge arrangement.

The surface treatment with atmospheric plasma technology can be divided into *active* and *remote plasma treatment*, according to the location of the treated sample with respect to the gas discharge chamber. In the *active plasma treatment*, the sample to be treated will

pass between the electrodes. There is a direct contact between the sample surface and the active plasma. In *remote plasma treatment*, the sample is located outside the plasma chamber, but passes in the gas stream that runs through the plasma chamber and is loaded with radicals and other active species. We can say that the sample is treated in the *afterglow* of the plasma. Figure 1.10 illustrates the difference between active and remote plasma treatment. An active plasma treatment has the advantage of a higher concentration of active species near the sample surface, while for remote plasma treatment, the concentration of active species in the afterglow decreases as a function of the distance to the plasma chamber due to collisions. On the other hand, the active plasma treatment faces a risk of backside treatment and pin-holing, while the remote treatment prevents damages from the discharge as the discharge current does not flow through the sample. Moreover, remote treatment allows the possibility to treat the surface of materials of any thickness and geometry (3D objects). The active treatment is limited to thin substrates, due to the dimensions of the interelectrode space.

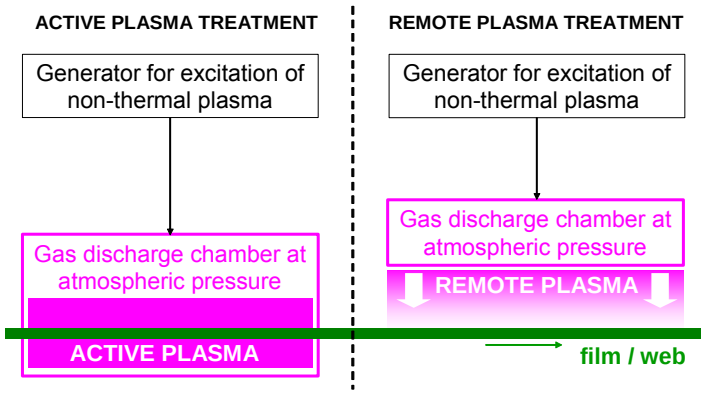

Figure 1.10 *Non-thermal atmospheric plasma treatment can be divided into active and remote plasma treatment.*

In the following paragraphs, the most important atmospheric plasma sources for surface treatment are described.

1.5.2.1 Active plasma treatment

Dielectric barrier discharge reactors

A well-known active plasma source at atmospheric pressure is the *dielectric barrier discharge* (DBD). In Figure 1.11, the general configuration is shown. An alternating current (AC) voltage is applied between two parallel plates, where at least one of the electrodes is covered with a dielectric layer (e.g. ceramic or glass plate). The interelectrode distance is typically only a few millimetres. The discharge is sustained by a voltage of 1-100 kV with frequencies of 50 Hz - 1 MHz. The discharge usually operates in the *filamentary* mode. Here, the discharge leads to the formation of a large number of parallel current filaments with a diameter in the order of 100 µm, randomly distributed in space and time [21]. These *microdischarges* are essentially streamer discharges whose lifetime is governed by the capacitance of the dielectric barrier (typically in the order of 10 ns). This capacitance is locally charged by the filament. The charge build-up at the dielectric surface creates an opposite electric field into the gap and eventually terminates the discharge. Because of the alternating applied voltage this phenomenon is repeated every half cycle. By raising the applied voltage, the number of filaments increases.

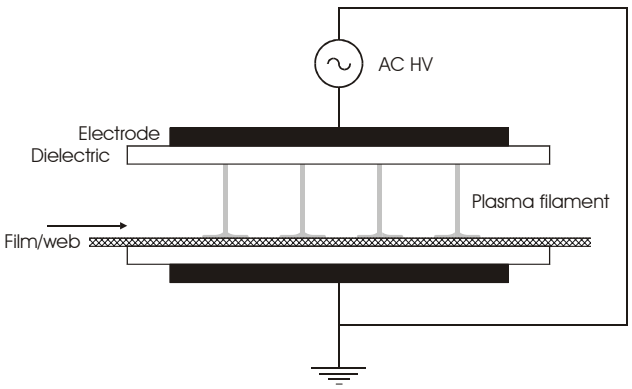

Figure 1.11 *Schematic diagram of the DBD configuration for surface treatment.*

Siemens used this type of discharge already in 1857 for the generation of ozone from air or oxygen [22]. Later, the dielectric barrier discharge is also used for surface modification. The already industrially wide-spread '*corona treatment*' of surfaces is based on a DBD [3, 23-25]. In a *corona discharge*, the electric field at one or both the electrodes is much higher than in the rest of the interelectrode space. This happens typically when the curvature of the electrode is much smaller than the interelectrode distance, for example when one of the electrodes has a sharp edge. The film to be treated often acts as the dielectric barrier. Some of the large-sized treaters are able to process sheets up to 10 m in width with linear velocities up to 8-10 m s^{-1}. The linear power density ranges up to 4-5 kW m^{-1}, and the maximum energy dose delivered by the AC discharge onto the surface at maximum linear velocity is about 25 kJ m^{-2}. Unfortunately the filamentary character of the discharge results in a non-homogeneous surface treatment and the risk of damaging the surface. Due to the perpendicular orientation of the filaments the treatment efficiency is not optimal. As mentioned before, the interelectrode distance (in the order of millimeters) also limits the substrate thickness. New developments in DBD technology are focused on avoiding these disadvantages.

With specific conditions of electrode structure, carrier gas and operating frequency, researchers made it possible to generate a stable *homogeneous glow discharge* in a dielectric barrier configuration at atmospheric pressure [26-28]. Figure 1.12 shows clear differences in time variation of the current between filamentary and glow regime. The filamentary regime reveals many current pulses of nanosecond duration per half cycle corresponding to the microdischarges, while the glow regime is characterized by only one current pulse per half cycle. Results on surface treatment using AC barrier discharge in the glow mode are published in [4, 5].

a)

b)

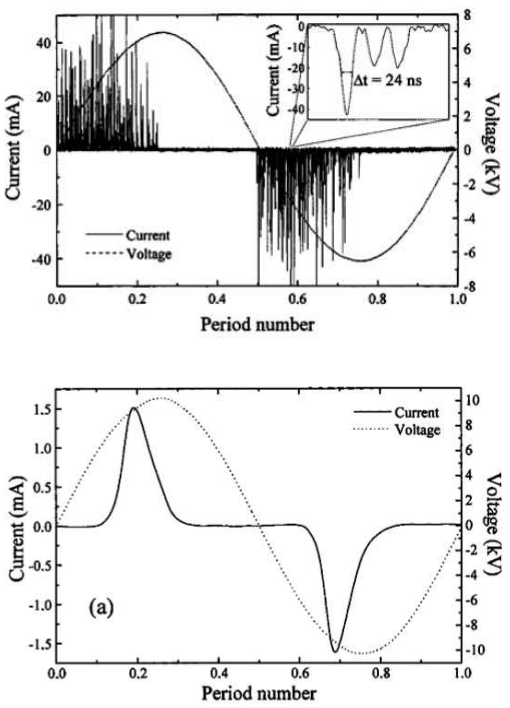

Figure 1.12 *Time variation of the discharge current in an atmospheric dielectric barrier discharge in nitrogen in a) filamentary regime b) glow regime [29].*

Another development in DBD technology is focused on changing the electrode configuration in order to avoid the limitation on the substrate thickness due to the restricted interelectrode distance. Besides the above mentioned parallel plate configuration (also called the *volume discharge*), the *surface discharge* is an alternative arrangement for generating DBDs [30]. The surface discharge arrangement consists of a dielectric plate with one or a number of electrodes on one side and a plane counter-electrode on its reverse side, as shown in Figure 1.13a. The function of the microdischarges in the volume discharge is here taken over by discharge steps propagating along the dielectric

surface. Increasing the applied voltage causes an increase in discharge area on the dielectric surface.

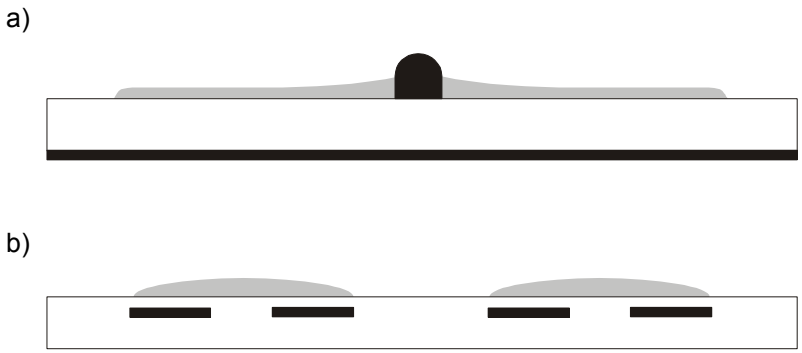

Figure 1.13 *Schematic of a) the surface discharge b) coplanar arrangement (electrodes in black, dielectric in white, plasma in grey).*

Finally, a *coplanar* arrangement – used in plasma display panels - is a combination of the two aforementioned configurations. In this arrangement, pairs of coplanar electrodes are imbedded inside a dielectric (Figure 1.13b). The use of atmospheric pressure coplanar surface discharge for surface treatment was investigated by Simor *et al.* [31-33].

Microhollow cathode discharge

Microhollow cathode discharge is one of the examples of atmospheric plasma sources using a DC power supply. Starting from the DC glow discharge setup at low pressure (paragraph 1.2), one of the major tasks in operating the discharge at higher pressure is that instabilities will be formed near the cathode, more specific in the *cathode fall*. This region of high electric field is responsible for the emission of high energetic electrons. Stable operation would be possible by eliminating

the cathode fall, but the plasma could not be initiated and sustained without any alternative electron supplier. Stark *et al.* introduced a *microhollow cathode discharge* as electron emitter in their DC high pressure glow discharge [34]. The cathode is replaced by a microhollow electrode system, as shown in Figure 1.14.

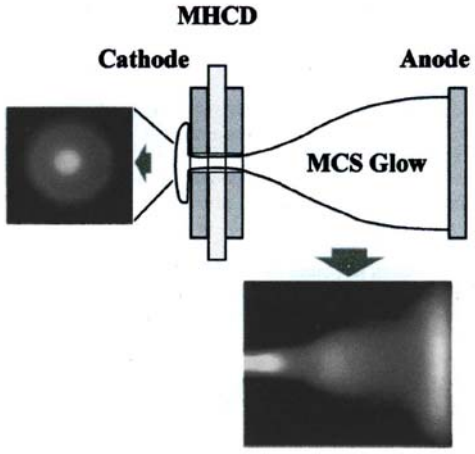

Figure 1.14 *Basic geometry of the microhollow electrode system with a third electrode and the appearance of the plasma is shown end-on and side-on [34].*

This system contains a DC glow discharge at atmospheric pressure between closely spaced plane-parallel electrodes with a central borehole of approximately 100 µm in each electrode. A dielectric with a thickness of about 200 µm is used as a spacer between the electrodes. The anode of the microhollow cathode geometry is grounded and the third electrode is biased positively with respect to the microhollow anode.

Atmospheric DC glow discharge

Besides the microhollow cathode discharge, another successful method to prevent glow to arc transition in a DC glow discharge at atmospheric pressure was developed. The current density in the bulk of the glow discharge is known to increase linearly with pressure ($j \propto p$), while there is a quadratically dependence on pressure in the cathode layer ($j \propto p^2$). If there is a method to reduce the current cross section at the cathode, the conditions near the cathode could be brought into line with the conditions in the bulk. A possible method consists of using pins as individual cathodes with small cross sections compared to the total area of the cathode segment. Moreover, bulk instabilities are prevented by a fast gas flow that "blows" away any species accumulation that would cause transition to an arc. This *DC glow discharge at atmospheric pressure* can be considered as an extension of the low pressure glow discharge discussed in paragraph 1.2. The combination of a specific electrode geometry, appropriate gas flow and ballast resistors make it possible to develop a stable and workable discharge type. This type of discharge will be described and investigated in more detail in chapter 4.

Atmospheric microwave reactor

Microwave plasma systems, discussed in paragraph 1.5.1.2, can also be operated at atmospheric pressure and both in remote and direct regime, depending on the application. One example of such a source which is already implemented in industrial applications such as cleaning, etching, functionalisation, sterilisation and deposition is CYRANNUS® [35].

1.5.2.2 Remote plasma treatment

As mentioned before, plasma treatment in a remote setup ensures that the plasma chamber and the application zone are separated in space so that the mutual influence is minimized.

The *plasma torch* configuration is a remote plasma source which already found its way to industry for cutting and welding applications. Although this technique usually starts from a thermal discharge, the more gentle characteristics in the “afterglow” also allow the use of this technique for deposition purposes. The majority of commercially available plasma torches use a *thermal DC arc discharge* as plasma source. *Arc discharges* are characterized by high currents (5-2000 A) and current densities (> 1 A cm^{-2}) (see Figure 1.3). A typical configuration for a plasma torch is given in Figure 1.15. The torch consists of an axial cathode and a water-cooled axisymmetric anode, with a conical gap across which an arc forms. The working gas is heated by passage through the arc region and forms a high temperature *arc jet* downstream the nozzle.

In applications where very clean plasmas are required, electrodeless RF plasma sources can also be used in a torch configuration. In the *inductive plasma torch* the plasma can be ignited by applying a pulsed high voltage to a starting rod and maintained by RF power applied to an axisymmetric coil wrapped around the plasma tube (Figure 1.16). The heating coil is not in contact with the plasma, which preserves the gas stream from contamination with vaporized or sputtered electrode material. As compared to the DC arc jet, the inductive plasma torch can treat a larger surface and can produce variable shapes of the plasma according to the shape of the heating coil.

A newly developed non-thermal plasma reactor for remote treatment at atmospheric pressure is described in chapter 4.

As mentioned before, the choice for one or another plasma source type depends on the particular application. Nevertheless, the dielectric barrier discharge and the DC glow discharge at atmospheric pressure, which will be discussed more in detail in the next chapters, attract the industrial attention because of their technical simplicity.

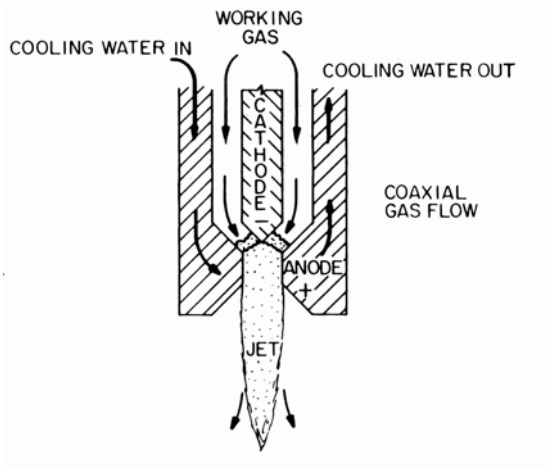

Figure 1.15 *A typical configuration of the DC arc jet plasma torch [14].*

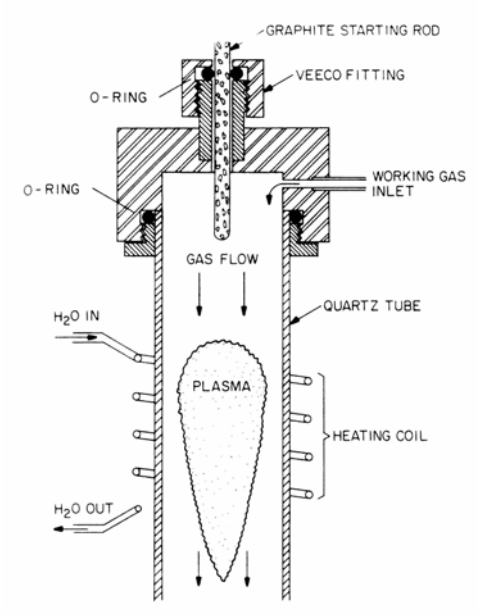

Figure 1.16 *Schematic drawing of the inductive plasma torch [14].*

2 PHYSICO-CHEMICAL SURFACE ANALYSIS

2.1 INTRODUCTION

After plasma treatment of the sample surface, the efficiency of the treatment is evaluated by quantification of the surface wettability. For samples with a closed structure (e.g. polymer foils), wettability is tested by contact angle measurements. Changes in the wettability of surfaces with a more open structure – such as woven and nonwoven fabrics – are measured by means of the liquid absorptive capacity (W_A). The hydrophilic behaviour of the treated yarn is quantified by the liquid wicking rate test.

Detailed characterization of the treated surface is performed by X-ray photoelectron spectroscopy (XPS) and static secondary ion mass spectrometry (S-SIMS). These analytical techniques provide an insight into the modification mechanism that is responsible for the increase in wettability.

In the following paragraphs the experimental details of the above mentioned characterization techniques will be discussed briefly.

2.2 CONTACT ANGLE

The surface energy, which is a measure for the wettability of the surface, can be derived from the static contact angle of small droplets of distilled water or other liquids on the treated surface [36]. The contact angle is defined as the angle between the liquid and solid interface at the three-phase line of contact. If the surface tension of the solid material is higher than the surface tension of water (72.8 mJ N^{-1}), a complete wetting of the solid surface is accomplished and the contact angle will be zero. A value of the surface energy lower

than the surface energy of water gives rise to a non-zero contact angle. In this thesis, the value of the static contact angle is obtained by graphic measurements of the contact angle on end-on photographs of 3 µl sessile droplets of distilled water deposited on the horizontal sample surface at mid-plane of the discharge. A tangent is drawn at the three-phase point, and its angle respective to the surface of the solid is defined as the contact angle (Figure 2.1). The contact angles shown in the graphs in chapters 3, 4 and 5 are always average values of at least 5 individual measurements. The error bars displayed on the graphs indicate the standard deviation.

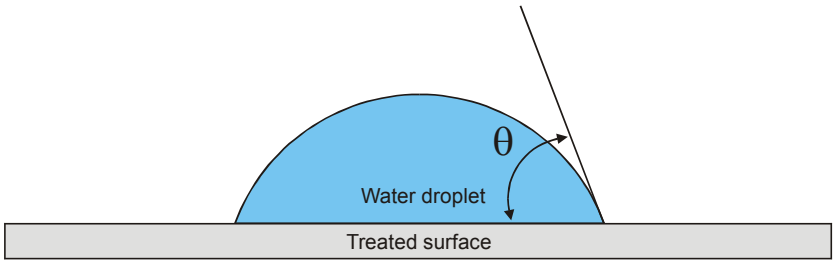

Figure 2.1 *Principle of contact angle measurement (θ = contact angle): the sessile drop method*

On graphically fitting the shape of the drop, difficulties are experienced with finding the baseline accurately, i.e. the line defining the interface between the liquid and the treated surface. This problem can be solved by adjusting the camera angle. The camera is tilted at an angle of 3°, so that it looks down at the surface. In this way, a reflection image of the drop can be seen below the baseline and thus the baseline can be found more accurately (Figure 2.2).

This method for measuring the contact angle differs from the more complex method used in commercially available contact angle goniometers. However, the obtained values of the contact angle are solely compared relatively within this work, where a consistency in the method is sustained.

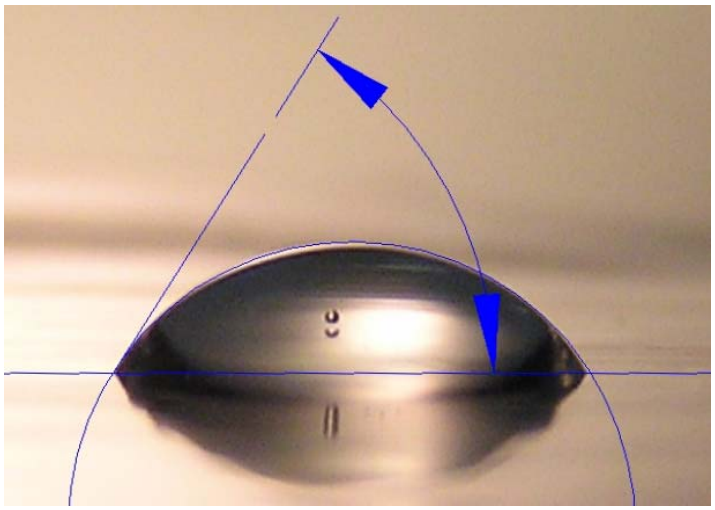

Figure 2.2 *Example of a photographic picture for contact angle measurement with a 3° tilted camera; accurate baseline determination by means of the reflection image.*

2.3 LIQUID ABSORPTIVE CAPACITY

As the contact angle can only be measured on smooth surfaces, the plasma induced changes in wettability of the woven and nonwoven fabrics are quantified by measuring the liquid absorptive capacity W_A [37], according to DIN 53 923 (EDANA 10.1-72). W_A is defined as the amount of water that a fabric has absorbed after one minute of immersion in water, relative to its own weight.

First, the dry sample is weighed (M_k). The sample is then immersed in pure water of 20°C for 60 s, 20 mm below liquid surface. After the wet sample is suspended to drain vertically for 120 s, it is weighed again (M_n). The liquid absorptive capacity is then given by:

$$W_A = \frac{M_n - M_k}{M_k}.100 \qquad (2.1)$$

The values of M_n and M_k are obtained by taking the average of 3 repetition measurements.

In the determination of W_A, the temperature of the distilled water strongly influences the value of the liquid absorptive capacity measured (see Figure 2.3). Therefore, the water temperature is kept constant (20°C) for all quantitative measurements of the values for W_A.

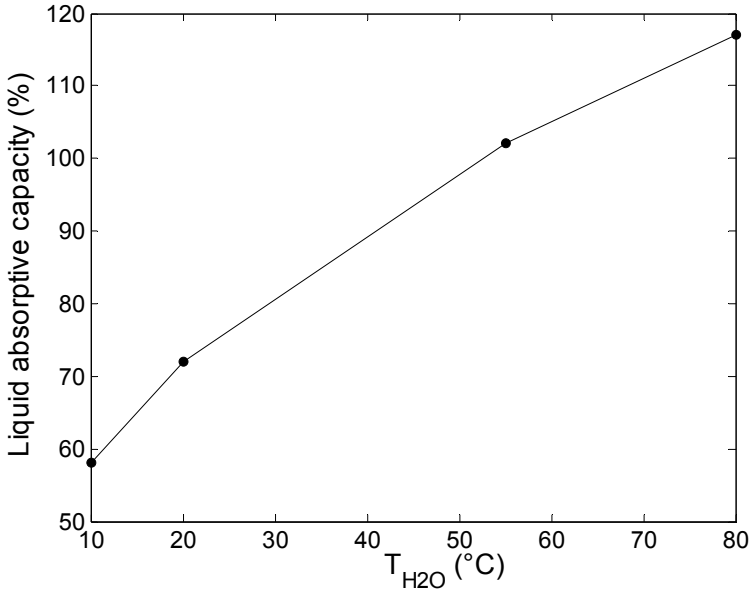

Figure 2.3 *Liquid absorptive capacity, W_A [%], of non-treated sample versus temperature T_{H2O} [°C].*

2.4 LIQUID WICKING RATE

As it is difficult to measure the contact angle at the surface of a yarn, the efficiency of the plasma treatment of the cotton yarn is quantified by measuring the liquid wicking rate, based on DIN 53 924 (EDANA 10.1-72). The rate of the vertical capillary rise is measured when the

yarn is suspended in coloured distilled water, in such a way that the lower sample edge is 15 mm below liquid surface (Figure 2.4). The height of the rising water boundary is recorded after 10, 30, 60, 100 and 300 seconds and is repeated 3 times for each sample.

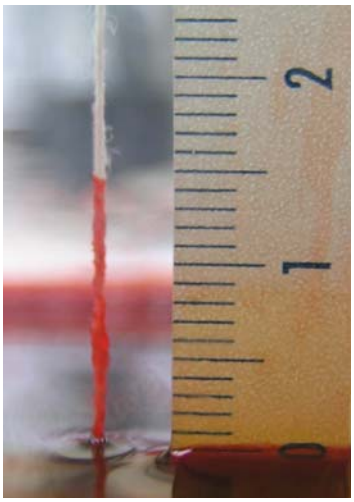

Figure 2.4 *On measuring the wicking rate, the height of the rising water boundary is recorded.*

2.5 XPS ANALYSIS

X-ray photoelectron spectroscopy (XPS) is a well-established characterization technique in surface research. This technique provides a quantitative analysis of the atomic surface composition and can resolve different types of chemical bonds at the surface [38].

Figure 2.5 shows the experimental setup for the XPS measurements. A monochromatic source of radiation is focused on the specimen. An X-ray photon with fixed energy ($h\nu$) is absorbed by an atom at the surface of the sample, leading to the removal and emission of a K or L electron from the inner electron shell of that atom. The kinetic energy of this emitted *photoelectron* is determined by a hemispherical

electron energy analyzer. The binding energy E_b of the electron to the atom can be calculated from the kinetic energy E_k of this emitted electron by the following equation:

$$E_b = h\nu - E_k - \phi \qquad (2.2)$$

where $h\nu$ is the energy of the monochromatic X-ray photons and ϕ is the work function of the sample surface. Figure 2.6 shows the energy diagram of a photoionization process.

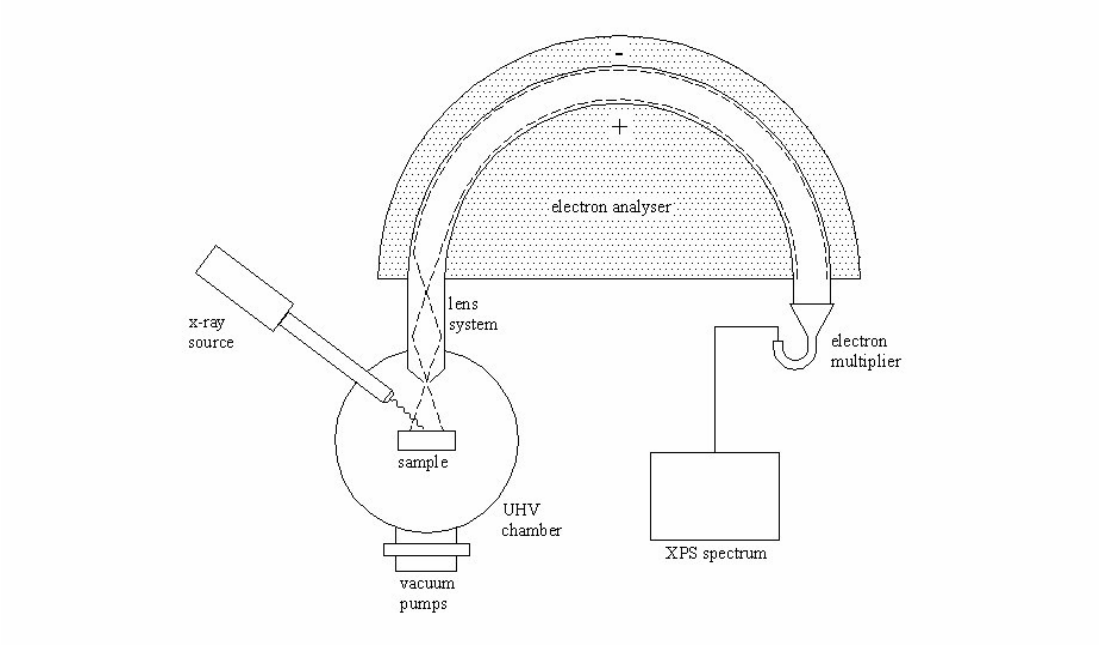

Figure 2.5 *Experimental setup for XPS measurements.*

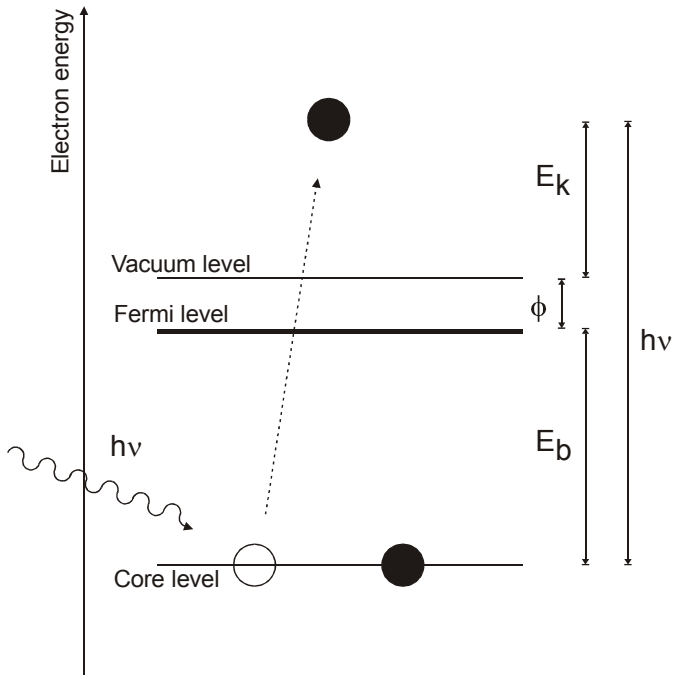

Figure 2.6 *General energy diagram of the photoionization process.*

For each atomic element, there will be a characteristic binding energy associated with each core atomic orbital i.e. each element will give rise to a characteristic set of peaks in the photoelectron spectrum at kinetic energies determined by the photon energy and the respective binding energies. The presence of peaks at particular energies therefore indicates the presence of a specific element in the sample under study. Furthermore, the intensity of the peaks (expressed by the peak area) is proportional to the relative abundance of the element within the analyzed region of the sample surface. A quantitative analysis of the atomic surface composition can be determined through a *survey scan*, i.e. an XPS spectrum with a wide energy frame and a relatively low resolution. The atomic concentration of an element relative to the other elements in the survey scan can be calculated as follows:

$$X_A = \frac{I_A / S_A}{\sum_k I_k / S_k} \tag{2.3}$$

where the sum includes all elements present in the same survey scan. X_A is the concentration of element A, I_A is the intensity of the XPS peak corresponding to A and S_A is the atomic sensitivity factor of the XPS detector for element A. The intensity is calculated by the area of the corresponding XPS peak.

The relative concentration ratio can then be given by:

$$\frac{X_A}{X_B} = \frac{I_A / S_A}{I_B / S_B} \tag{2.4}$$

The empirical sensitivity factors are published by Wagner *et al.* [39]. Table 2.1 gives the values used in this work.

S_{C1s}	0.296
S_{O1s}	0.711
S_{N1s}	0.477

Table 2.1 *Empirical sensitivity factors for C1s, O1s and N1s.*

The exact binding energy of an electron depends not only upon the electron shell from which photoemission is occurring, but also upon the formal oxidation state of the atom and the local chemical and physical environment. Changes in either of these give rise to small shifts in the peak positions in the spectrum – so-called *chemical shifts*. In this way, XPS can also provide information on the type of chemical bonds that are formed at the surface. For an accurate determination of the binding energy of a specific electron level, a narrow energy frame is placed around the corresponding XPS peak, where the measurement is performed with a high resolution and a small energy step. Such a measurement is called a *multiplex*. In this high resolution

spectrum, deconvolution of overlapping peaks is performed in order to resolve the different types of chemical bonds.

The intensity of an XPS peak is only determined by the photoelectrons that reach the detector without energy loss. The photoelectrons that lose energy through inelastic or elastic collisions within the sample surface contribute to the background or deviate from the detection line. Consequently, an XPS spectrum provides information only on the top atomic layers (up to 50 Å) of the sample surface. The effective information depth d_i is determined by the attenuation length λ_a of the photoelectrons and the measurement geometry:

$$d_i = 3\lambda_a \sin\theta \qquad (2.5)$$

where θ is the angle between the sample surface and the detection axis (Figure 2.7). The attenuation length λ_a depends on the kinetic energy of the photoelectron.

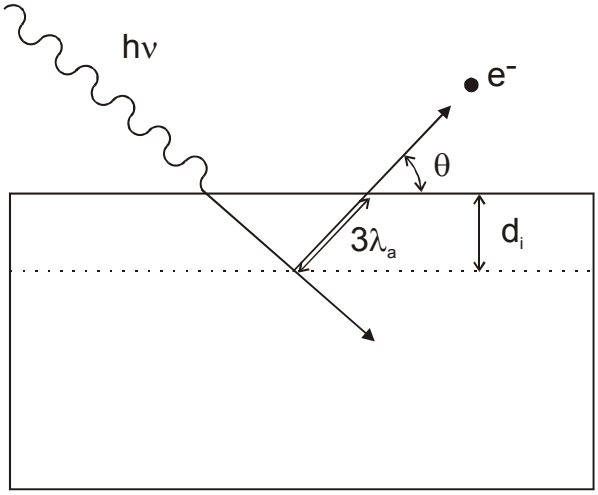

Figure 2.7 *The effective depth d_i is determined by the attenuation length λ_a and the angle θ between the sample surface and the detection line.*

The XPS system used for the characterization of the plasma treated samples is a Perkin-Elmer Phi ESCA 5500 system, with a Phi model 10-360 energy analyzer for the detection of the photoelectrons. The samples were irradiated with monoenergetic 450 W X-rays of Al-Kα (1486.6 eV). The base pressure in the ultra high vacuum (UHV) analyzing chamber was below 10^{-9} mbar. Experiments were recorded with 220 W source power and an angular acceptance of 7°. The analyser axis made an angle of 45° with the specimen surface. Wide scan spectra were measured over a binding energy range of 0-1400 eV and a pass energy of 187.85 eV. The C1s, O1s and N1s core levels were recorded with a pass energy of 58.7 eV.

3 ATMOSPHERIC AC BARRIER CORONA DISCHARGE

3.1 INTRODUCTION

The dielectric barrier discharge (DBD) is widely used as a source in plasma technology [28]. DBDs are characterized by the presence of an insulating layer on one or both plate electrodes and usually consist of many small current filaments (microdischarges). In material processing applications, the filamentary nature of the DBD results in a non-uniform treatment of the surface. Direct current (DC) corona discharges on the other hand are initiated in the non-uniform electrical field of a sharp electrode and feature a faint glow around this electrode [40]. As a rule, DC corona discharges are limited to low power densities. Increasing the discharge current leads to the formation of narrow sparks bridging the gap. We also investigate an alternative approach to generate an atmospheric pressure discharge, in which a corona electrode geometry is combined with a dielectric barrier. The resulting AC barrier corona discharge (BCD) is studied in both a pin-to-plate and a wedge-to-plate configuration. These geometries are compared to the classical DBD with regard to their electrical characteristics. From Lissajous figures the energy coupled into the plasma is measured and more details on the discharge regime are revealed.

To determine the characteristics of surfaces treated by DBD and BCD optical microscopy, UV spectroscopy and contact angle measurements are performed after various treatments.

3.2 EXPERIMENTAL SETUP

The electrodes are placed in a cylindrical enclosure with a volume of 13.25 dm^3. In the classical DBD (Figure 3.1(a)), the plasma is generated between two parallel copper disk electrodes. The upper one is variable in height in order to change the distance between the electrodes. This electrode is covered with an Al_2O_3 (Rubalit Alumina, CeramTec) or glass plate and connected to an AC power source. The other electrode is connected to earth and also covered with an insulating plate. The edges of both electrodes are smoothed in order to prevent parasitic corona discharges that would deteriorate the stability of the plasma. In the pin-to-plate configuration, the upper electrode is a stainless steel pin (diameter = 4 mm) with crenellated tip (Figure 3.1(b)), while the wedge-to-plate configuration has a stainless steel sharp blade as upper electrode (Figure 3.1(c)). Two different AC power sources were used. The AC power source with a frequency of 50 kHz has maximum rms output values of 30 kV and 100 mA (Bayerle, Germany). The power source with a frequency of 50 Hz is a transformer with maximum rms output values of 6 kV and 50 mA (Siet, Metalbox® transformers).

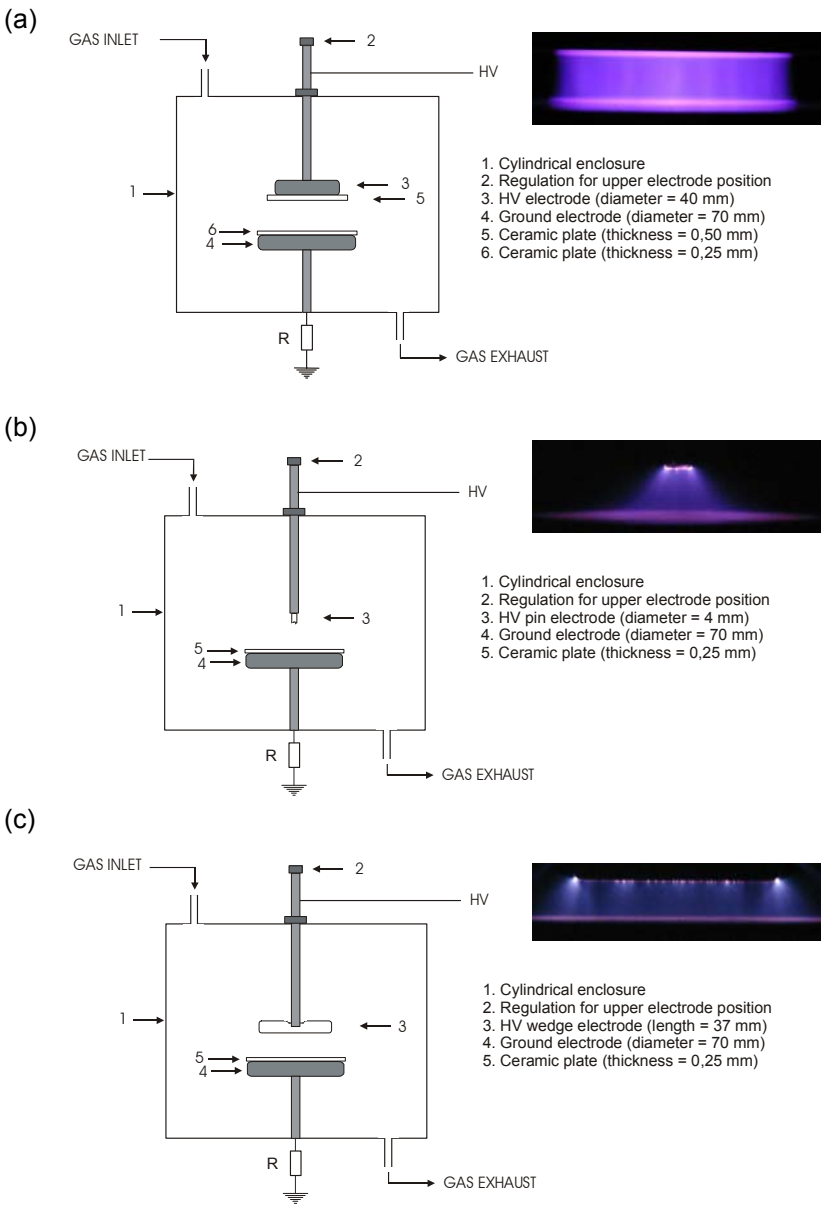

Figure 3.1 *Experimental setup and visual appearance of the dielectric barrier discharge with (a) parallel-plate, (b) pin-to-plate and (c) wedge-to-plate geometry.*

The gas mixture used in these experiments consists of helium and a small percentage of oxygen, unless stated otherwise. The gas inlet is controlled by mass-flow controllers (MKS Instruments, 2179AX52CS1BV) at 1 dm^3 min^{-1} for He, and the gas exhaust is controlled by a pump in such a way that the pressure is kept constant (Figure 3.2). Helium is chosen because it is easy to obtain a stable discharge in this gas. The small percentage of O_2 is added because of the aim to increase the hydrophilicity of the surfaces.

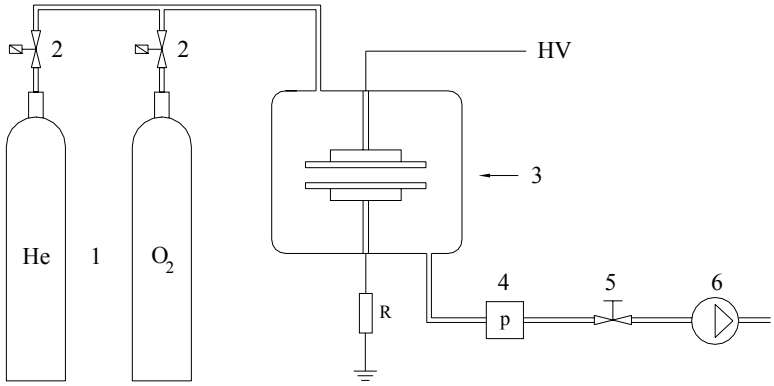

Figure 3.2 *Schematic diagram of the experimental setup; 1. gas cylinders, 2. mass-flow controller, 3. plasma chamber, 4. pressure gauge, 5. needle valve, 6. pump.*

Figure 3.3 shows a diagram of the electrical circuit for measuring the electrical characteristics. The time variation of the discharge current and the applied voltage during one cycle of the dielectric barrier discharge is monitored with a Tektronix TDS210 digital oscilloscope (60 MHz, 1 GS s^{-1}). The current is deduced from the voltage across a resistor *R* (100Ω) that is inserted in the current loop as shown in Figure 3.3. The applied voltage is measured with a high voltage probe (1:1000 voltage divider, Tektronix P6015A). The power consumed by the plasma during one cycle can be estimated by means of a Lissajous figure [41], which is displayed on the oscilloscope screen by

plotting the applied voltage on the X-axis and the accumulated charge on the plate(s) on the Y-axis. The accumulated charge is derived from the voltage across a measuring capacitor C_m (0.01 µF) in series with the discharge (Figure 3.3). This capacitor has a much larger value than that of the discharge cell (± 10 pF), in order not to influence the voltage across the cell significantly. The plasma input energy per cycle is equal to the area enclosed by the charge-voltage curve in the Lissajous figure. Multiplying this input energy by the frequency yields the consumed discharge power.

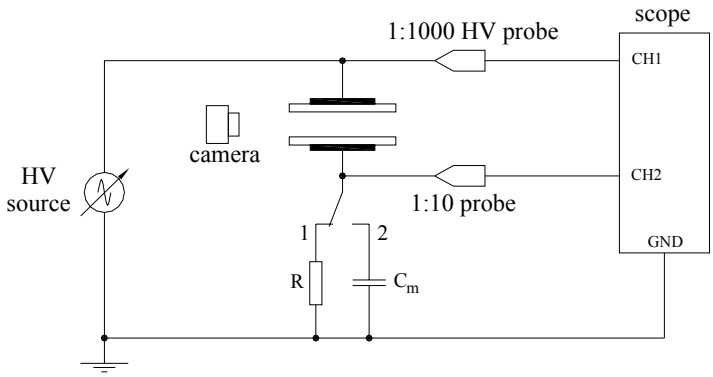

Figure 3.3 *Schematic diagram of the electrical circuit for measuring the electrical characteristics; switch in position 1: time variation of voltage and current (oscilloscope in X-T regime), switch in position 2: Lissajous figure (oscilloscope in X-Y regime).*

3.3 ELECTRICAL CHARACTERISTICS

Figure 3.4 gives the current for the parallel-plate (a), pin-to-plate (b) and the wedge-to-plate (c) configuration. The plasma is generated with a 50 Hz power source in He + 1 % O_2 at 1000 mbar and a gap distance of 4 mm. It can be seen that for each of the configurations the current essentially consists of many microdischarge pulses. This indicates that the plasma is built up by a large number of filaments in

parallel. The filaments are distributed randomly in the gas gap and are of short duration. The lifetime is governed by the capacitance of the dielectric “barrier” on the electrodes. This capacitance is locally charged by the filament. This charge build-up at the dielectric surface creates an opposite electric field in the gap and eventually terminates the discharge. Because of the alternating applied voltage this phenomenon is repeated every half cycle. By raising the applied voltage, the number of filaments increases.

The different electrode configurations also reveal some distinctions. In comparison with the parallel-plate geometry, the plasma of the pin-to-plate and wedge-to-plate geometry needs a lower applied voltage, due to the strong electric field at the sharp electrode.

The discharge current during one cycle is symmetrical in the parallel-plate configuration, which is expected on account of the symmetrical geometry of the electrodes. The other configurations show an asymmetry. Here, the positive discharge reaches higher current than the negative discharge. The difference in the shape of the current waveforms under positive and negative half cycle can be explained by the existence of different corona modes. If the sharp electrode is the cathode, during negative half cycle, secondary electrons are mainly originating from electron emission from the cathode and possibly photoionization in the bulk of the gas. In principle, the avalanche multiplication process does not differ from the Townsend breakdown. If the sharp electrode is the anode, during positive half cycle, the secondary electrons are produced by secondary photoprocesses in the gas around the sharp electrode edge. The plane cathode does not participate in multiplication on account of the weak field in its vicinity. In contrast to the more diffusive glow of the negative corona, the positive corona displays luminous streamer filaments running away from the sharp electrode [42].

(a)

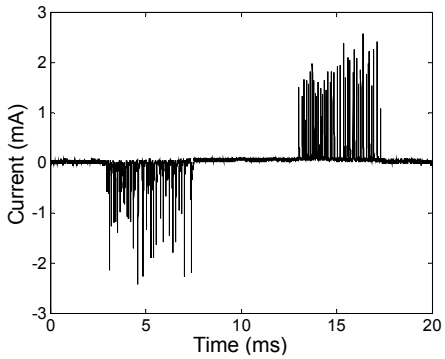

(b)

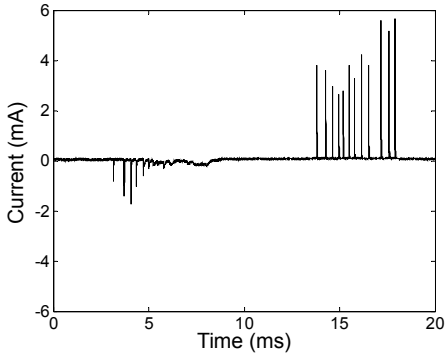

(c)

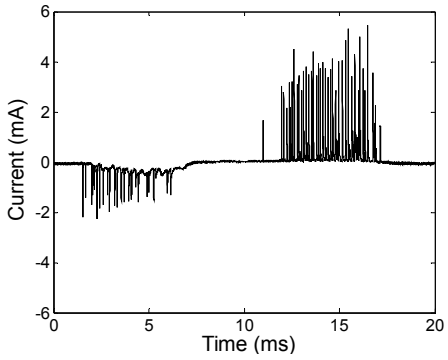

Figure 3.4 *Time variation of the discharge current during one cycle (50 Hz) for the (a) parallel-plate, (b) pin-to-plate and (c) wedge-to-plate configuration in 99 % He + 1 % O_2.*

The time variation of the wedge-to-plate configuration is similar to the pin-to-plate configuration, except for an increase of current peaks.

In the negative discharge current of the wedge-to-plate configuration, it can be seen that there is a non-filamentary current component. This can be attributed to the transition of a negative corona to a gap-filling glow [43].

When altering the frequency of the power supply from 50 Hz to 50 kHz, we see a remarkable change in the discharge current. Figure 3.5 gives the time variation of the current for the parallel-plate and wedge-to-plate configuration with a 50 kHz power supply. There are clearly less current peaks then with the 50 Hz power supply and there is one high current peak immediately after the breakdown voltage is reached. The discharge at higher frequency now reveals clear characteristics of the diffuse gap-filling glow discharge.

When generating the barrier discharge in pure He, the characteristics of the time variation of the current are even closer to the glow discharge (Figure 3.6). We can observe mainly one current peak per half cycle with a width of about 0.5 μs, which indicates that most of the charge is transferred at once.

This dependency of the discharge regime on the frequency and the gas composition can be explained by considering the discharge mechanism [5]. The main species controlling the breakdown mechanism are (i) electrons, created during one discharge and maintained in the gas till the next breakdown, and (ii) metastables which also create seed electrons after ionizing the gas by Penning ionization. Breakdown occurs easier (under lower electric field) when the densities of electrons and metastables are high. In glow discharge regime, the seed electron density just before the breakdown is high enough to allow the development of numerous small primary avalanches under a low electric field. If the number of these small avalanches is sufficiently large, they interfere and induce a wide positive space charge area. This wide space charge avoids the tendency of the electrons originating from the secondary avalanches to converge toward a single point, which would lead to a streamer and

thus to a filamentary regime. The excitation frequency determines the discharge regime because it acts on the density of both the electrons and metastables maintained in the gas gap from one discharge to the next. If the frequency is low, the time between two consecutive discharges is long enough for electron recombination and destruction of metastables to occur between two discharges. At high frequency, the seed electron density maintains high at the ignition of the next discharge and a glow regime can occur. Introducing other gases to the He environment can quench the He metastables after the discharge and consequently can induce a lower contribution of the metastables to the next breakdown. This explains the difference in regime between Figures 3.5 and 3.6.

(a)

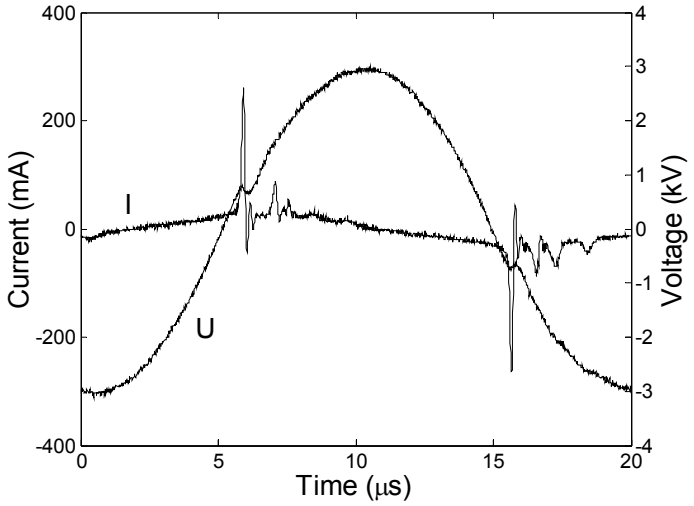

(b)

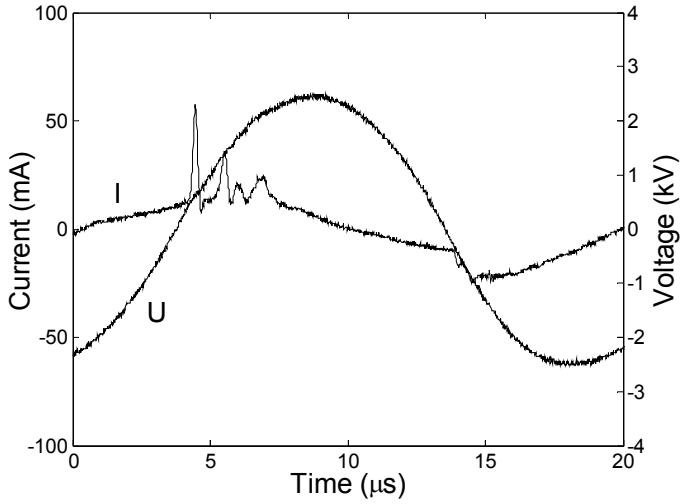

Figure 3.5 *Time and voltage variation of the discharge current during one cycle (50 kHz) for the (a) parallel-plate and (b) wedge-to-plate configuration in 99 % He + 1 % O_2.*

(a)

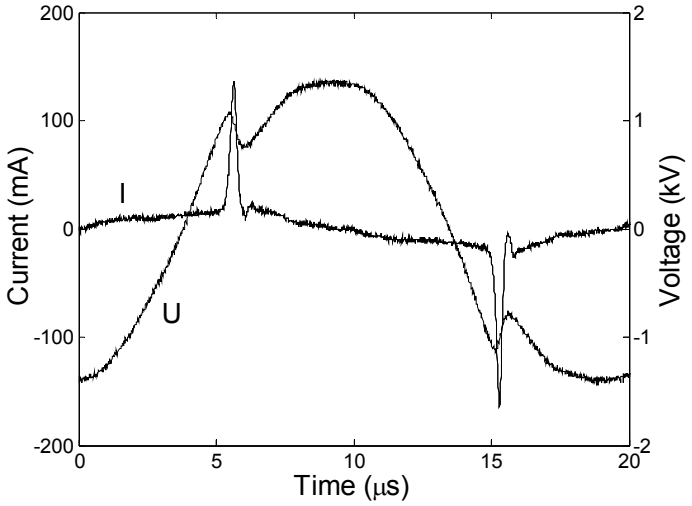

(b)

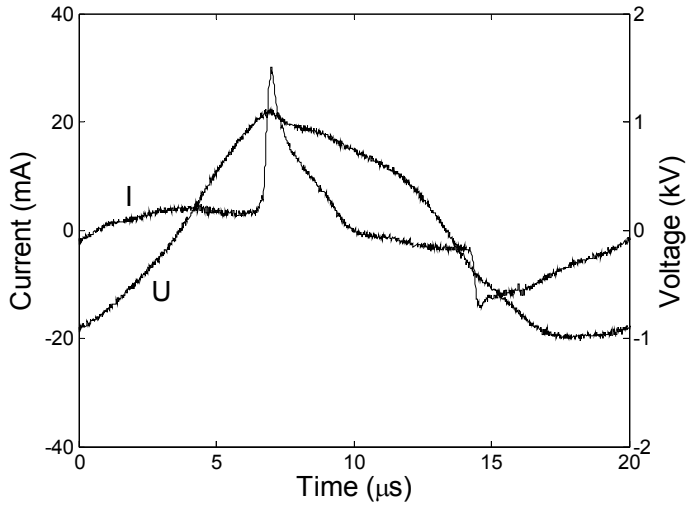

Figure 3.6 *Time and voltage variation of the discharge current during one cycle (50 kHz) for the (a) parallel-plate and (b) wedge-to-plate configuration in He.*

The energy coupled into the gas discharge can be derived from the Lissajous figures (*Q*-*U* plot) by means of the Manley equations [44]. The notations used in the derivation of the Manley equations are:

u_{cell} = total applied sinusoidal voltage

u_{peak} = peak value of the applied sinusoidal voltage

u_{gas} = voltage across the gas

u_b = effective gas breakdown voltage

Q_{cell} = total charge

Q_{die} = charge on the dielectric

C_{cell} = total capacitance

C_{die} = capacitance of the dielectric(s)

C_{gas} = capacitance of the gas

As long as u_{gas} is below the breakdown voltage, there is no discharge between the electrodes so the cell is purely capacitive and behaves like two capacitors in series. The total capacitance of the cell C_{cell} can thus be represented by the equivalent capacitor of two capacitors in series, C_{die} and C_{gas}:

$$C_{cell} = \frac{C_{die}C_{gas}}{C_{die} + C_{gas}} \tag{3.1}$$

The *Q*-*U* plot is now described by a straight line: $Q_{cell} = C_{cell}u_{cell}$, which intercepts the origin. By increasing the voltage above the breakdown voltage, resistive losses in the discharge causes *Q* to shift in phase, so that the straight line changes into a parallelogram (Figure 3.7).

$$u_{cell} = u_{die} + u_{gas} \tag{3.2}$$

$$u_{die} = \frac{Q_{die}}{C_{die}} = \frac{Q_{cell}}{C_{die}} \tag{3.3}$$

$$u_{gas} = \frac{Q_{gas}}{C_{gas}} = u_b \tag{3.4}$$

Equation (3.3) relies on the fact that the charge on the dielectric Q_{die} consists of the charge both capacitively and resistively coupled through the gas onto the dielectric, thus is equal to the total charge Q_{cell}. Once the discharge is initiated, the voltage over the gas u_{gas} remains constant at the breakdown voltage u_b, as expressed in equation (3.4). This breakdown voltage depends mainly on the gas composition, the pressure and the electrode spacing. Combining these three equations leads to:

$$Q_{cell} = C_{die}(u_{cell} - u_b) \tag{3.5}$$

This straight line describes the discharge transitions 2-3 and 4-1 in Figure 3.7. Therefore, C_{die} can be directly measured from the Lissajous figure as the slope of these straight lines. For the peak values we can write:

$$Q_{peak} = C_{die}(u_{peak} - u_b) \tag{3.6}$$

The charge ΔQ_c required for a voltage reversal across the gap during the capacitive transition 1-2 from $u_{gas} = u_b$ to $u_{gas} = -u_b$ is:

$$\Delta Q_c = 2C_{gas}u_b \tag{3.7}$$

and as can be seen from Figure 3.7:

$$2Q_{peak} = \Delta Q_c + \Delta Q_d \tag{3.8}$$

Using equations (3.6) and (3.7) in equation (3.8) we get the expression for ΔQ_d, the charge transferred across the gap during the discharge transitions 2-3 and 4-1:

$$\Delta Q_d = 2C_{die}\{u_{peak} - [(C_{die} + C_{gas})/C_{die}]u_b\} \tag{3.9}$$

As each charge deposits eu_b of energy into the gas discharge, the mean energy deposited into the plasma during a full cycle (two discharges with opposite sign) is given by:

$$W_{plasma} = 2\Delta Q_d u_b \tag{3.10}$$

Inserting equation (3.9) gives:

$$W_{plasma} = 4u_b C_{die}\{u_{peak} - [(C_{die} + C_{gas})/C_{die}]u_b\} \tag{3.11}$$

The mean power dissipated by the plasma P_{plasma} can be obtained by multiplying W_{plasma} with the frequency. Equation (3.9) and (3.11) are known as Manley's equations.

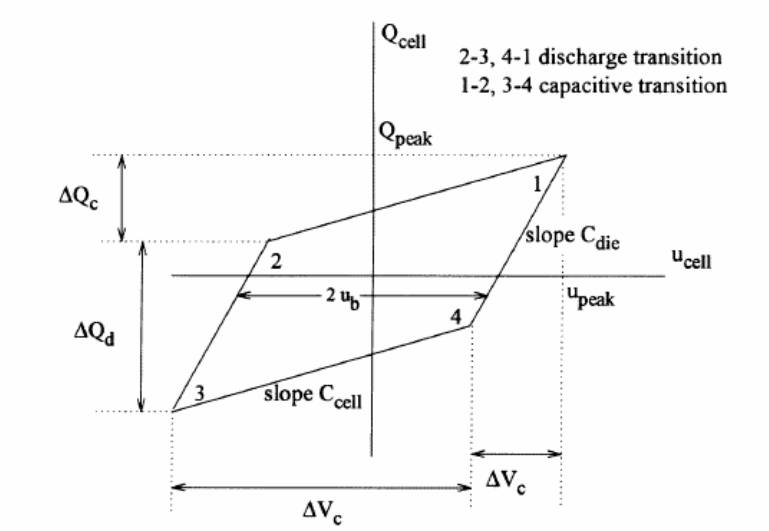

Figure 3.7 *Theoretical Lissajous figure to illustrate the derivation of the Manley equations [41].*

A numerical method to measure the power consumed by the discharge, is based on the definition of power:

$$P_{plasma} = \frac{1}{T}\int_{t_0-\frac{T}{2}}^{t_0+\frac{T}{2}} u_{cell}(t)i(t)dt \qquad (3.12)$$

with T the period, $u_{cell}(t)$ and $i(t)$ the instantaneous voltage and current.

The energy per cycle is then given by:

$$W_{plasma} = \int_{t_0-\frac{T}{2}}^{t_0+\frac{T}{2}} u_{cell}(t)i(t)dt \qquad (3.13)$$

When recording the Lissajous figure, the current flows through the measuring capacitor C_m and the charge on C_m is equal to Q_{cell} so we can write:

$$i(t) = \frac{dQ_{cell}}{dt} \tag{3.14}$$

Inserting (3.14) in (3.13) gives:

$$W_{plasma} = \int_{t_0-\frac{T}{2}}^{t_0+\frac{T}{2}} u_{cell}(t) dQ_{cell}(t) \tag{3.15}$$

This integration represents the total area enclosed by the *Q*-*U* plot. The values u_{cell} and Q_{cell} are measured via the oscilloscope and are transferred to the computer as values Q_k and u_k. The computer calculates the energy dissipated per cycle by the following approximation of (3.15):

$$W_{plasma} \approx \sum_{k=1}^{n} (Q_{k+1} - Q_k) \frac{u_{k+1} + u_k}{2} \tag{3.16}$$

where *n* is the number of samples in one cycle. The power dissipated by the discharge can then easily be obtained by:

$$P_{plasma} = f\, W_{plasma} \tag{3.17}$$

By means of the Lissajous figures we can again compare the differences in regime between the discharges at 50 Hz and at 50 kHz. Figure 3.8 shows the Lissajous figure and corresponding voltage and current time variation of a parallel-plate DBD discharge in He + O_2 at 50 Hz. Figure 3.9 shows the same features for the discharge at 50 kHz.

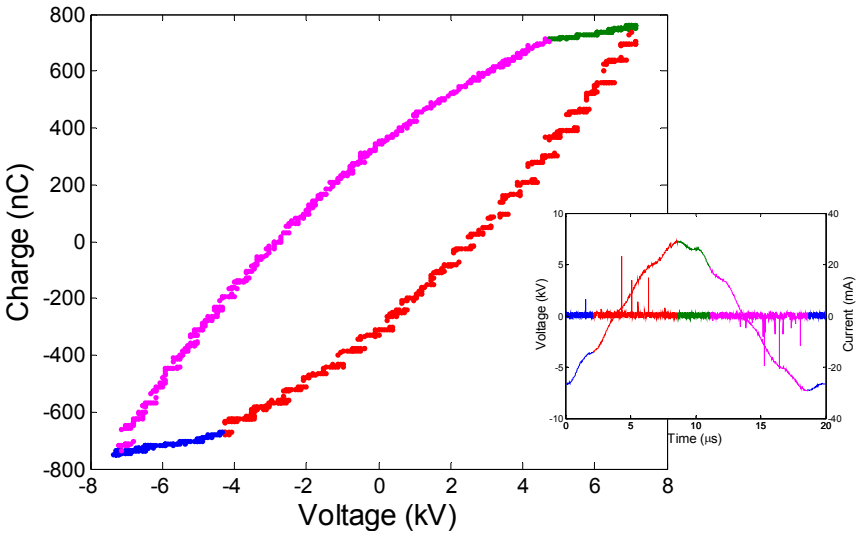

Figure 3.8 *Electrical characteristics for the parallel-plate DBD discharge in He + 1% O_2 with p = 1000 mbar and f = 50 Hz; P_{plasma} = 300 mW.*

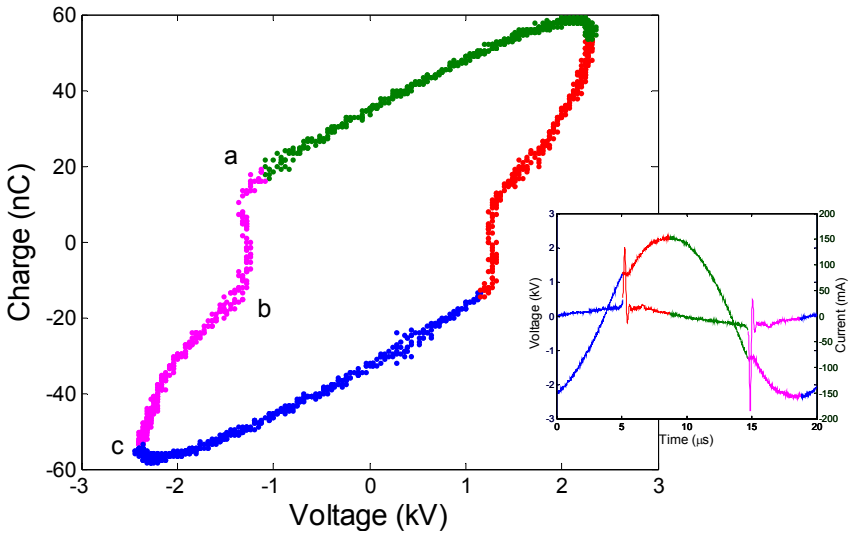

Figure 3.9 *Electrical characteristics for the parallel-plate DBD discharge in He + 1% O_2 with p = 1000 mbar and f = 50 kHz; P_{plasma} = 11.5 W.*

At the 50Hz Lissajous figure, the short current pulses can be noticed by the stair-like lines during discharge transition (corresponding to the transitions 2-3 and 4-1 in Figure 3.7). The shape of the 50 kHz Lissajous figure looks different. In a pure glow regime, the discharge transition would occur in only one current pulse, so within the time duration of about 200 ns. Okazaki *et al.* [45] observed in the Lissajous figure for the pure glow discharge only the two capacitive transition lines. The discharge transition lines were not displayed as the discharge transitions were too fast to be seen for their oscilloscope. The discharge transitions (red and pink) in Figure 3.9 show a small region where the data points form a vertical line (from a to b in the pink trace). The transition from b to c is a line with a slope corresponding to C_{die}. The transition region from a to b corresponds to the high peak in the current time variation. If we look at the time variation graph, we notice that the applied voltage deviates from the sinus wave during this short instant. The small current spikes following the high current peak correspond to the b-c transition. It is therefore suggested that the discharge is possibly no pure glow discharge, but a mixture of glow and filamentary discharge.

Figure 3.10 compares Lissajous figures of the parallel plate setup recorded for different applied voltages with constant frequency and pressure. We can see that the width of the Lissajous figures in horizontal direction, confined by the intersections with the X-axis, does not change. According to Figure 3.7 this length is two times the breakdown voltage ($u_b \approx 1.2$ kV), so we indeed do not expect this value to change while changing the input power. Table 3.1 resumes the numerical calculated values of the dissipated power P_{plasma} (equation (3.16) and (3.17)) and the values of the capacitance deduced from the slopes of the Lissajous figures in Figure 3.10. For the lowest applied voltage, the discharge is probably not filling the whole electrode surface which explains the low value of P_{plasma} and also the lower value of C_{die}.

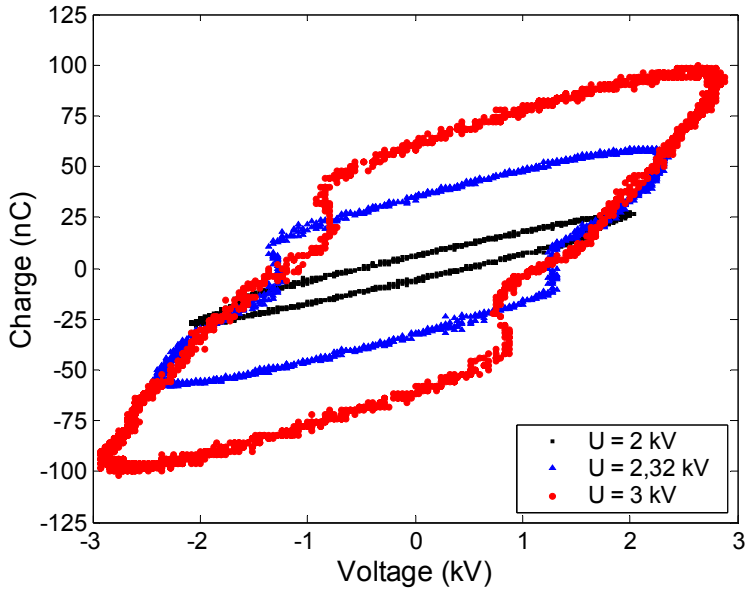

Figure 3.10 *Lissajous figures for various applied voltages in a parallel-plate DBD gas discharge in He + 1 % O_2 with p = 1000 mbar and f = 50 kHz.*

U_{max} (kV)	P_{plasma} (W)	C_{cell} (pF)	C_{gas} (pF)	C_{die} (pF)
2	1.9	11.7	19.4	29.5
2.32	11.5	12.5	15.5	63.9
3	21.3	14.1	17.7	67.3

Table 3.1 *Characteristic values of the Lissajous figures in Figure 3.10.*

3.4 SURFACE TREATMENT CHARACTERISTICS

In order to have a first view on the treatment characteristics for the DBD setup, the surface of a poly(ethylene terephtalate) foil (PET-foil) was treated in the active plasma volume with a treatment time of 2 minutes. The objective is to have a clear insight on the spatial extension and the homogeneity of the plasma effect which is more

easily detected with long treatment times. The sample was placed on top of the dielectric plate at the grounded electrode. The biaxially oriented PET-foil (Goodfellow), with a thickness of 50 µm, is first treated by the plasma of a wedge-to-plate configuration (Figure 3.2c) in a gas mixture of 2 % O_2 in He and at atmospheric pressure. The voltage amplitude during the treatment is 2.2 kV and the distance *d* between the electrodes is 5 mm. First, plasma treatment is performed during 2 minutes with a power frequency of 50 kHz. The long treatment time is chosen to cause an overtreatment and magnify the plasma effect. Figure 3.11 shows a photograph of the discharge and Figure 3.12 shows the PET surface after treatment. We can see that the treated zone is not homogeneous but consists of different separated opaque imprints with a visible size between 3 mm (near the centre of the blade's length) and 7 mm (near its edges). Their shape and distribution clearly correspond to the different plasma filaments formed between blade and plate. These filaments are more intensive at the blade ends due to a higher electric field strength near the edges.

Brightfield microscopic images provide a better view on how the plasma treatment affects the sample surface within such an opaque imprint (Figure 3.13). The microscopic image reveals the presence of pits on the treated foil surface, which is caused by an overtreatment. The pits have regular size and circular shape, not more than 1 µm in diameter. This effect causes the foil to become non-transparent. Cleaning has no visible influence on size or distribution of the pits. It is suggested that these pits are caused by a selective etching of amorphous polymer around polymer spherulites [46].

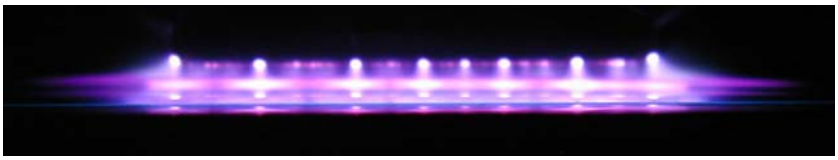

Figure 3.11 *Photograph of the wedge-to-plate DBD in He + 2% O_2 at atmospheric pressure with f = 50 kHz and d = 2 mm.*

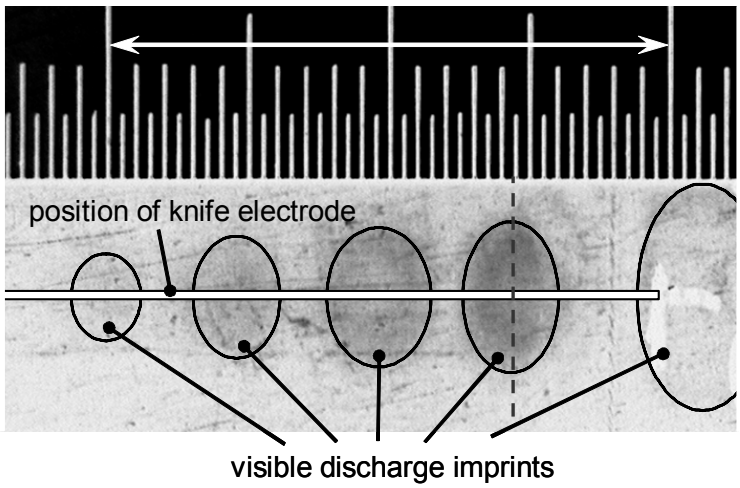

Figure 3.12 *Image of the PET-foil after 2 minutes of treatment in the wedge-to-plate DBD in He + 2 % O_2 at atmospheric pressure with f = 50 kHz and d = 5 mm. The original image was inverted and enhanced for clarity. The arrow represents a length of 20 mm.*

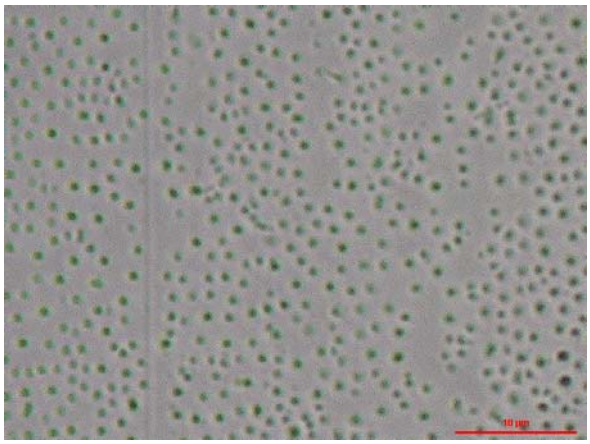

Figure 3.13 *Brightfield microscopic image of AC corona treated PET-foil, near the centre of the discharge.*

The spatial extension of the surface modification is examined more in detail by UV-VIS spectroscopy. The effect of the plasma treatment is manifested by differences in the transmission and reflection spectra at a specific wavelength before and after the treatment [46]. At selected wavelengths, transmission spectra across a discharge imprint on the surface are measured by focusing the beam to a light spot on the foil that is 1 mm in width and 5 mm in height. By using a translation stage, a spectrum can be recorded at 1 mm interval through the width of the discharge imprint (cross section along the dashed line in Figure 3.12).

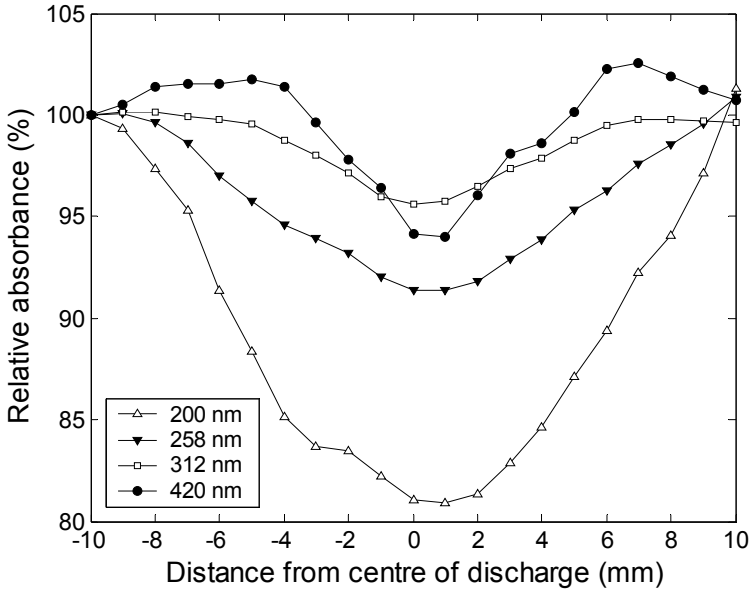

Figure 3.14 *Spectral profiles throughout a discharge imprint along the dashed line in Figure 3.12; the ordinate expresses the absorbance relative to the absorbance at one of the edges of the profile.*

Figure 3.14 shows profiles at wavelengths of 200, 258 and 312 nm. The profile at 420 nm is included as a reference for the visual part of the spectrum. To enable a direct comparison of profiles at different wavelengths, the absorbance relative to the value at one of the edges

of the profile is determined. Several features of the discharge effect are visualized. First of all, we can see that there is a gradual decrease of the absorption from the edge to the centre of the imprint, which indicates also an additional non-uniform intensity of the treatment within the opaque imprints. The profiles are 21 mm wide, which is considerably larger than the visible plasma treatment effect (5 mm). In this way, the profiles at 200 and 258 nm show that the plasma effect is much wider than can be seen with the naked eye and even beyond the scanned area. These two profiles have a similar shape and are believed to be related to the same chromophoric polymer structural entity [46]. The profile at 312 nm (which is related to the therephtalic group) is complete and has a Gaussian-type shape, while the one at 420 nm has an (unexplained) bird-shape. The spectral changes are too large to be due to surface modification only. Of course, the plasma parameters used in this experiment were too strong and caused an overtreatment. However, these results give a good idea on the spatial extension of the modification activity of the plasma along the surface. More details on the spectroscopic analysis can be found in [46].

In a second series of experiments, more gentle treatment conditions are used. The AC power frequency is changed to 50 Hz and the treatment time is reduced up to 10 seconds. Here, the treated PET-foil surface shows no visible transformation. In order to quantify roughly the treatment effect, the changes in wettability of the samples are derived from the diameter of 10 µl water droplets deposited on the surface (Figure 3.15). After the plasma treatment the diameter of the water droplet is 56 % larger at the position under the knife electrode. The spreading of the water droplets is enhanced by the plasma treatment due to the introduction of oxygen-containing polar molecular groups. The diameters of the droplets deposited further away from the knife are gradually lower.

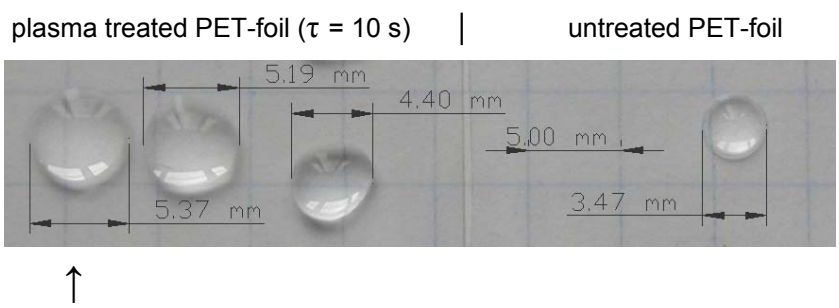

Figure 3.15 *Diameter of 10 µl droplets deposited on the PET-foil surface. Left side: plasma treated during 10 s with wedge-to-plate configuration; right side: untreated.*

More systematic measurements on the treatment effect are done on samples treated with the parallel-plate configuration in air in order to approach treatment conditions more convenient for industrial applications. However, the discharge is unstable in air at atmospheric pressure. Therefore, we work at medium pressure (p = 50 mbar). The frequency is fixed at 50 kHz, the source power P at 15 W and the distance d between the plates at 4 mm. The treatment time is varied between 0 and 1 s. Figure 3.16 gives the water contact angle as a function of treatment time. The water contact angle of the PET-foil decreases with increasing treatment time, i.e. the surface energy of the treated polymer increases with the dose of energy delivered onto the surface. The active plasma treatment in the DBD causes a steep decrease in contact angle already after 0.1 s. The contact angle continues to decrease for treatment times up to 0.5 s, corresponding to an energy dose D of 0.60 J cm^{-2}. For longer treatment times, the contact angle levels off at a value of 33°. This behaviour of the contact angle is also found for treatment with the remote DC discharge and will be discussed more in detail in chapter 4.

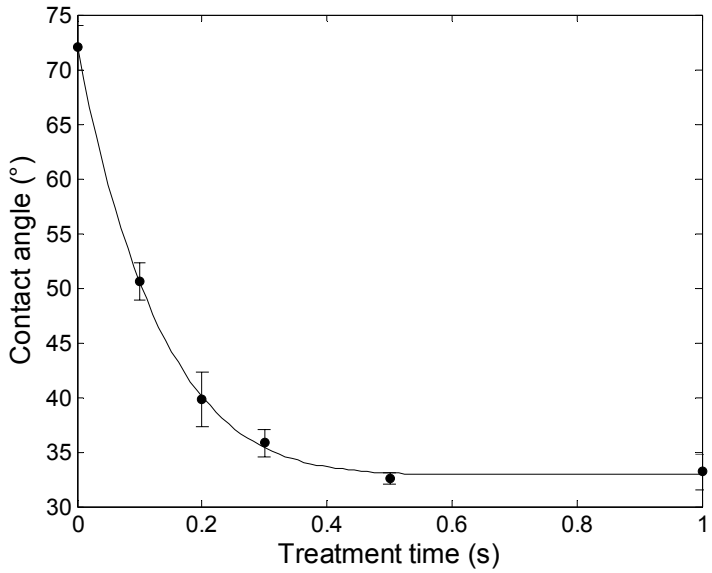

Figure 3.16 *Water contact angle as a function of treatment time for PET-foil, treated in the parallel-plate DBD in air with f = 50 kHz, P = 15 W, p = 50 mbar and d = 4 mm.*

3.5 CONCLUSION

The Lissajous figures, together with the current time variation, point out that the parallel-plate DBD in He + 1 % O_2 is filamentary at 50 Hz, while at 50 kHz a mixture of filamentary and glow discharge occurs. The discharge regime of a DBD depends on the excitation frequency and the chemical gas composition.

The dielectric barrier discharge can be used for active surface treatment with different kind of electrode geometries. First treatment experiments were performed on PET-foil in the wedge-to-plate discharge with long treatment time, so that the sample was deliberately overtreated. In this way, the plasma effect is enlarged and the inhomogeneous nature of the treatment is made visible. The characterization results show the potential of UV transmission

spectroscopy to determine the spatial extension of the atmospheric treatment effect. Contact angle measurements for treatment with more gentle parameters indicate a steep decrease of the contact angle for treatment time in the first 0.5 s. The angle decreases exponentially from 72° (untreated) to 33° (for τ = 0.5 s). Longer treatment time gives no further improvement of the surface wettability.

Although the dielectric barrier discharge has already proven its feasibility regarding surface modification, this technology still has to deal with disadvantages that prevent the industrial use for certain applications. Mainly on account of the inhomogeneity of the filamentary treatment and the restrictions on thickness and geometry of the treated samples, the search for new kinds of technology arose.

4 ATMOSPHERIC DC GLOW DISCHARGE

4.1 INTRODUCTION

Due to the shortcomings of the DBD treatment and the great advantages of atmospheric pressure compared to low pressure treatment, the research is focused on developing a new remote surface treatment device at atmospheric pressure. The core of the plasma source is a simple DC electrode system and can therefore easily be upgraded to industrial dimensions. As already mentioned in chapter 1, working in remote treatment mode has the advantage of preventing damages from the discharge like pin holing and undesired backside treatment. It also ensures the possibility to treat samples of any thickness and geometry.

This chapter gives an overview of the performance of the remote surface treatment with the atmospheric DC glow discharge. The remote treatment characteristics of the glow regime are first investigated, more particularly the dependency on treatment time, homogeneity, extension and permanency of the treatment effect. Furthermore, the active treatment of a cotton yarn in the DC glow discharge plasma source gives us an idea of the local influence of different parameters on the plasma effect.

4.2 EXPERIMENTAL SETUP

The experimental setup used for the remote plasma treatment at atmospheric pressure is similar to that reported in [47] and is shown in Figure 4.1. The non-thermal plasma is generated between two electrodes that are connected to a DC high voltage power supply with output voltage up to 30 kV and current up to 20 mA (Bayerle,

Germany). A fast airflow transports the plasma-produced reactive particles towards the sample to be treated. To diminish any losses in reactive species during their transportation to the treated surface, the distance *G* between the output of the plasma source and a sample is shorter than 10 mm. The sample is mounted on a rotating drum of about 0.40 m in diameter, in order to simulate in-line processing at variable line speeds. The results presented below are for so called cyclical treatment. This means that the sample passes once or a number of times through the exit region of the plasma source, where it is exposed to the flowing afterglow.

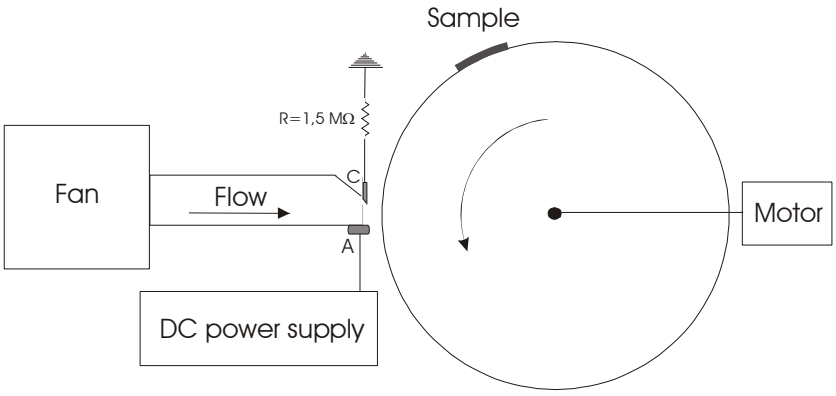

Figure 4.1 *Schematic diagram of the experimental setup; C = cathode pins, A = anode plate, G = distance between cathodes and sample.*

The glow regime is characterized by quiet operation with steady discharge current and corresponds to the existence of diffusive plasma in the interelectrode gap. A typical range of power density $\mathcal{P}$ in the bulk of the diffusive glow discharge is 20-100 W cm^{-3}.

The atmospheric pressure plasma source consists of an aluminium plate anode and a single row of 7 cathode electrode elements oriented in parallel to the treated surface (Figure 4.2). Each of these electrode elements is a stainless steel pin, ballasted with a resistor of 1.5 MΩ (Caddock, MX440, 2% accuracy). The electrode gap is 10 mm. The discharge is stabilized by a transverse airflow with a velocity

of 40 m s^{-1} produced by a fan (Ventomatic, CMT31M). The glow regime of the diffusive discharge has a maximum linear current density of about 4.5 mA cm^{-1} at the discharge voltage of 24 kV. Figure 4.3 shows how the discharge in glow regime looks like. The plasma length for 7 pins is about 3.5 cm. With a view to industrial implementation, the plasma length can easily be scaled up to any roll width by putting more electrode elements in parallel.

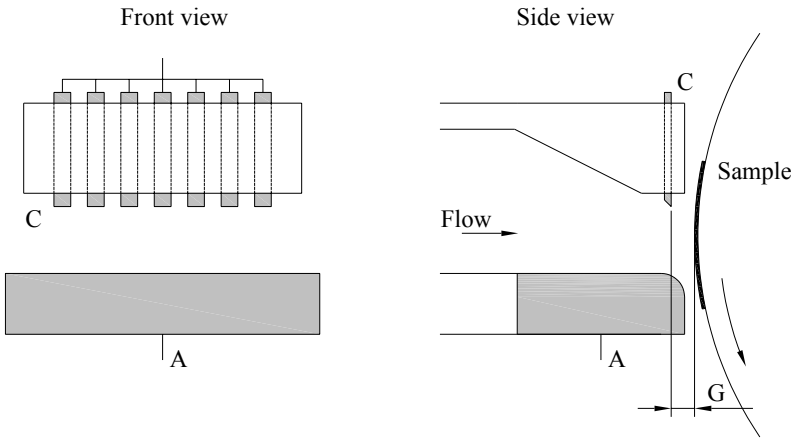

Figure 4.2 *Schematic diagram of the electrode system, used to generate the plasma in the remote system of Figure 4.1.*

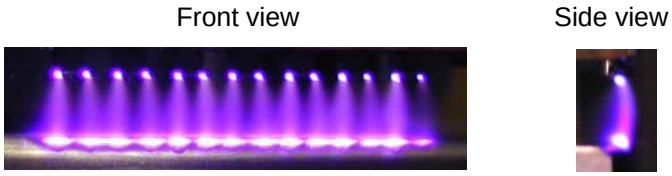

Figure 4.3 *Photographs of the atmospheric glow discharge; direction of the airflow is out of the paper in the front view picture and from left to right in the side view picture. Each cathode pin generates two plasma cones, at its sharp edges.*

The voltage-current characteristic for this electrode system is shown in Figure 4.4. The voltage applied to the electrodes is shown as a function of the current divided by the length of the plasma. On changing the discharge current, we can distinguish 3 different regimes: corona, glow and spark regime (Figure 4.4). For initial values of the current (between 0 and 0.15 mA cm-1), the discharge voltage increases fast, which indicates the corona regime. The region of slow increase in discharge voltage corresponds to the regime of the glow discharge [40]. At a critical voltage plasma instabilities (sparks) occur due to charge accumulation. However, the fast gas flow removes charge carriers from the plasma zone so that the critical voltage and the corresponding critical current are shifted towards higher values. For the air flow of 40 m s-1, currents higher than 4.5 mA cm-1 cause the plasma to be unstable and sparking to occur.

In the reduced current-voltage characteristic (Figure 4.5), the corona regime is characterized by a linear dependency of the reduced current (I/U) on the discharge voltage, according to the semi-empirical relation, found by Townsend [48]:

$$I = kU(U - U_0) \tag{4.1}$$

U_0 is the corona inception voltage. The slope factor k is inversely proportional to the gas density n and dependent on the interelectrode distance. At the transition to the glow regime, this linear dependence changes into an exponential dependence, as also observed in [49].

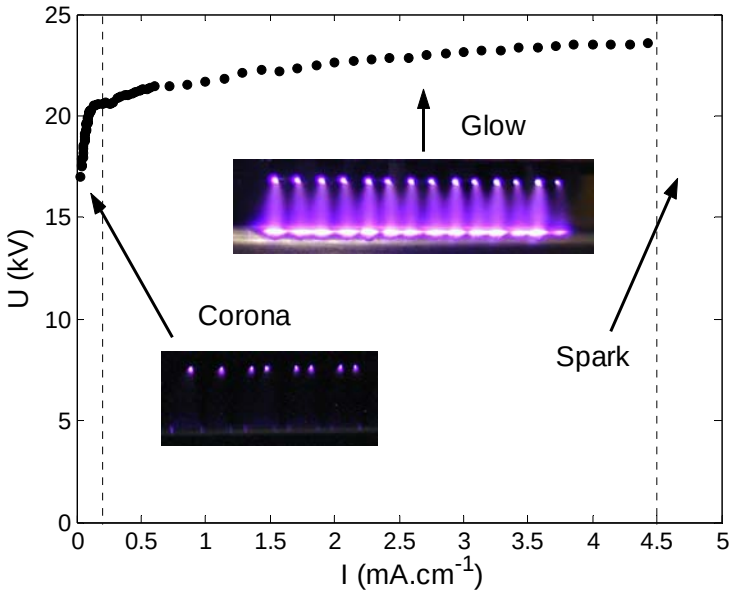

Figure 4.4 *Voltage-current characteristic of the DC atmospheric discharge used for the remote surface treatment.*

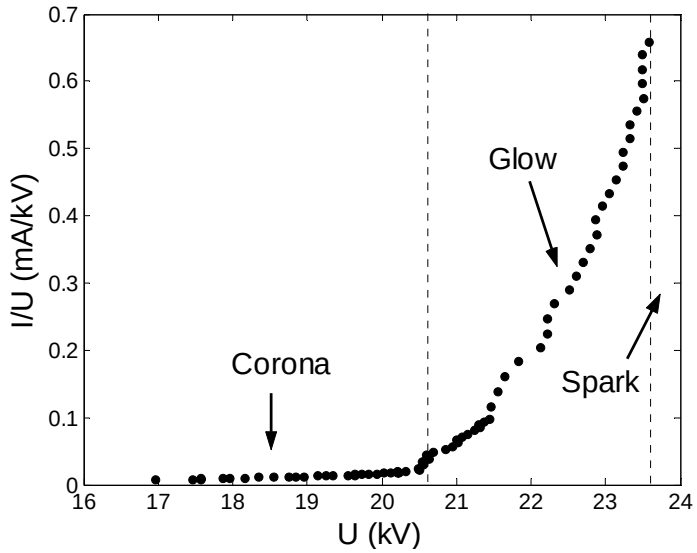

Figure 4.5 *Reduced current-voltage characteristic of the DC atmospheric discharge used for the remote surface treatment.*

In Figure 4.6, the voltage-current characteristics are shown for different distances *d* between the cathode pins and the plate anode. The working voltage increases with the interelectrode distance. The maximum current which can be obtained before sparking occurs, is also influenced by the interelectrode distance. By decreasing the interelectrode distance the flow channel opening is reduced as well. This causes an increase in the local gas flow velocity and consequently improves the stability. On the other hand, the decrease in interelectrode distance causes a decrease in the cross section of the plasma cones at the anode (see Figure 4.3). This, in turn, causes the current density to increase at the anode. As instabilities arise at the anode, the maximum current of the glow regime tends to be lower at small interelectrode distances. These two opposing mechanisms reach an equilibrium at an interelectrode distance of 10 mm. Here, a clear maximum in the threshold current is observed. The interelectrode distance *d* will be fixed at 10 mm for all further measurements.

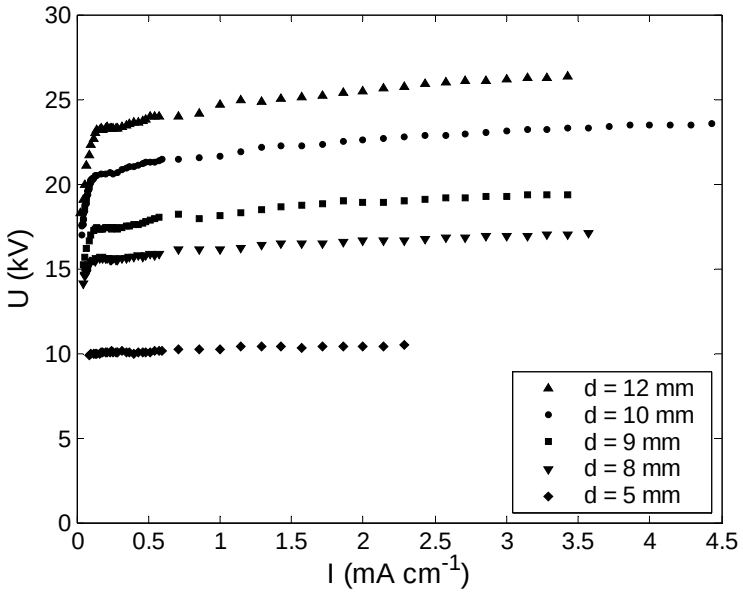

Figure 4.6 *Voltage-current characteristics of the DC atmospheric discharge used for the remote surface treatment, for different values of the interelectrode distance d.*

Finally, the glow-to-spark threshold current is also influenced by the position of the drum, more specifically by the distance *G* between the sample and the cathode pins as was shown in Figure 4.2. The maximum current of the glow regime decreases with *G* (Figure 4.7). The main reason is the change in the gas flow pattern when the drum is moved. A maximum is observed at *G* = 4 mm. This distance between sample and cathode pins will be preserved for all measurements, unless stated otherwise.

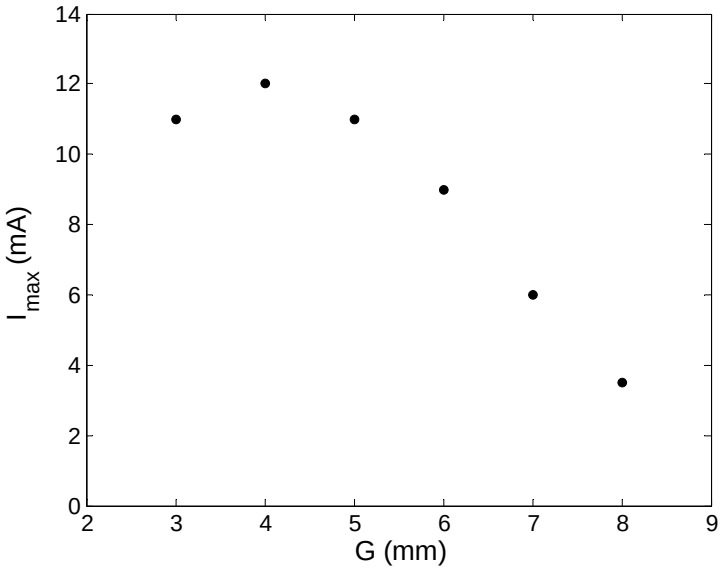

Figure 4.7 *Maximum total current of the glow regime as a function of the distance G between the sample and the 7 cathode pins.*

4.3 SURFACE TREATMENT CHARACTERISTICS

The atmospheric DC discharge for remote surface treatment is examined in the glow regime. We started with treating samples of PET-foil. The remote plasma treatment is investigated by measuring the dependence on treatment time, the homogeneity of the plasma effect on the surface energy and the stability in time after treatment.

The treated PET-foils are characterized by contact angle measurements and XPS analysis. Finally, contact angle measurements are also performed on samples of PP-foil, silicone, PET nonwoven and PP nonwoven.

4.3.1 DEPENDENCE ON TREATMENT TIME

Contact angles are measured immediately after treatment for different treatment times. The variation in treatment time τ is determined by the number of passes through the flowing afterglow. The treatment time is proportional to the energy dose D delivered onto the surface (see paragraph 1.4, $D = L\tau$). Experimental results were obtained at power loadings L ranging between 10 and 80 W cm^{-2} (The power loading L was defined in paragraph 1.4 as the discharge power per exposed area of the sample surface). The total area of the treated sample is 35 mm x 100 mm.

4.3.1.1 Poly(ethylene terephtalate) foil (PET-foil)

Poly(ethylene terephtalate) is frequently used in industrial applications because of its desirable bulk properties (strength, transparency, thermal resistance, …). PET is for example used in the production of containers for food, beverages and other liquids. It is also one of the most important raw materials used in man-made fibres. The main disadvantage of this material is its low surface energy. Consequently, there is a great demand for ecological and efficient pre-treatment that facilitates the processing of PET.

Figure 4.8 presents the results on plasma processing of 50 µm thick PET-films using a DC discharge at atmospheric pressure in the glow regime. According to optical microscopic observations, no physical changes can be seen on the treated surface. There is a sharp drop of the contact angle value. This can be attributed to the introduction of oxygen containing polar groups (explained further in this paragraph). For a treatment time more than 1 s the contact angle stabilizes at a

value of about 33°. This suggests that the physical and chemical changes induced by the plasma saturate once a critical value of the energy dose is reached. The binding of oxygen atoms is possibly compensated by the process of breaking up polymer chains into low molecular weight fragments, resulting in a saturation of the contact angle. One may conclude based on this dependence that from energy saving point of view, it is not effective to treat the PET-foil with atmospheric plasma longer than 1 s, corresponding to a minimum energy dose of 58 J cm^{-2}. A higher power loading will reduce the required treatment time, which allows a higher roll velocity. A limit is posed here by the sparking threshold current. A better solution to reach the same effect could be found in placing several plasma sources in series in the direction of the moving PET-foil. Each plasma section contributes to the overall treatment time. In this way, the required treatment time is reached without a decrease in roll velocity or an increase in power loading per discharge.

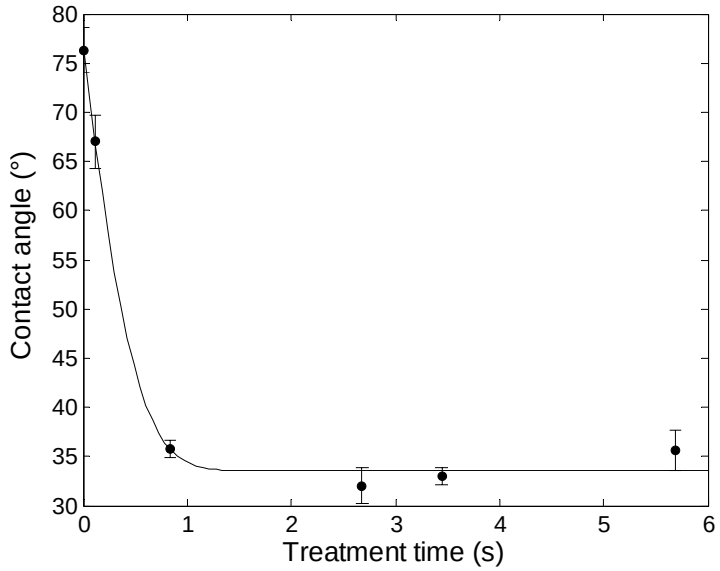

Figure 4.8 *Water contact angle as a function of treatment time for cyclically treated PET-foil (L = 58 W cm^{-2}).*

The chemical surface modification of the plasma treated PET-foils is characterized by X-ray photoelectron spectroscopy (XPS) measurements. A detailed description of the XPS measurement device is given in chapter 2 (paragraph 2.5). The composition of the PET surface is revealed by analyzing the high-resolution XPS spectra by deconvolution of the C1s and O1s peaks using the XPSPEAK41 software. Curve-fitting is performed using mixed Gaussian-Lorentzian component profile, after subtraction of a Shirley-type background. The peak areas together with the sensitivity factors allow us to make quantitative analyses of the surface composition.

The survey scan gives a first overview of the different composing elements at the surface. Figure 4.9 shows the presence of oxygen and carbon atoms at the surface of the untreated PET-foil. Due to the non-conducting character of the PET sample, charging occurs during XPS recording. This charging effect causes the spectra to shift towards lower binding energies. The spectra were corrected so that the peak corresponding to the aromatic ring carbons (C1s) is located at 284.7 eV [50]. The small peaks at very low binding energy are identified as valence band peaks. The remaining peaks at high binding energy are no XPS peaks but result from Auger transitions following ionisation [38]. After an inner shell electron is removed by an incident X-ray photon, the atom can rearrange by dropping an electron from a higher energy level to the vacant core hole. The released energy is transferred to an electron in an outer electron shell. If this electron has enough energy to overcome the binding energy and work function of the surface, it may be ejected. This ejected electron is referred to as an Auger electron. It is also observed that the background intensity increases to the low kinetic energy side of a peak (high binding energy side). This is caused by electrons ejected from depths several mean free path lengths below the surface. On passing through the upper surface layers, those electrons lose energy due to inelastic scattering before they leave the sample [38].

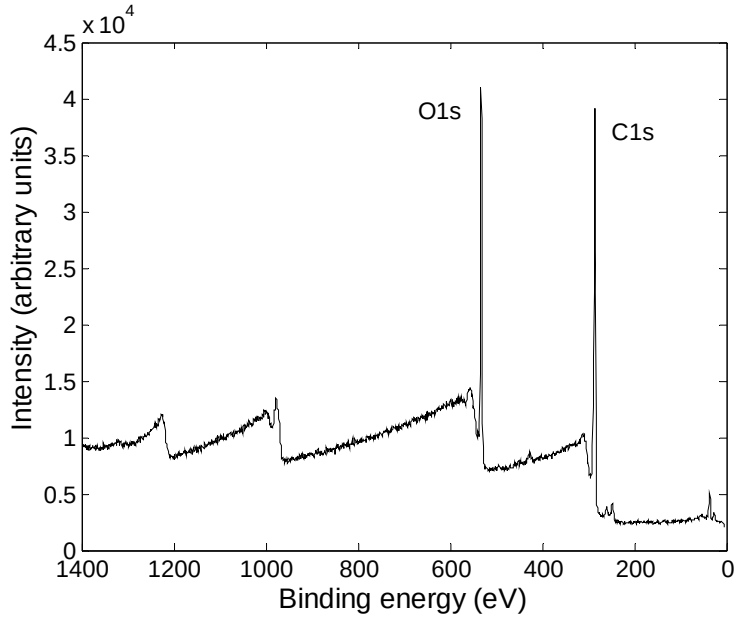

Figure 4.9 *XPS survey scan of the untreated PET-foil.*

Figure 4.10 shows the chemical structure of the PET repeat unit. The C and O atoms will have different binding energies depending on their local chemical environment. The label numbers correspond to the labels in the XPS spectra of Figures 4.11 and 4.12.

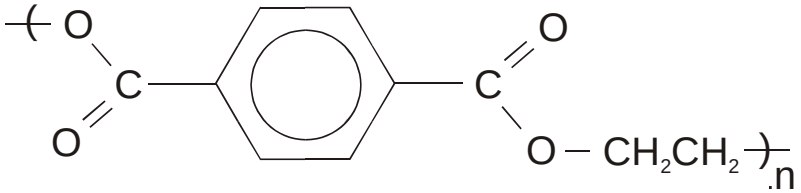

Figure 4.10 *The PET repeat unit. The numbers refer to the peak locations of Figures 4.10 and 4.11.*

The XPS spectra for untreated PET-foil are displayed in Figures 4.11 and 4.12. The C1s envelope is fitted with three component peaks, in agreement with literature [50]. The peak at 284.7 ± 0.2 eV corresponds to carbon atoms bound to carbon or hydrogen in the benzene ring (C1). The peak at 286.2 ± 0.2 eV corresponds to methylene carbon atoms singly bound to oxygen (C2). The peak at 288.7 ± 0.2 eV corresponds to ester carbon atoms (C3). The O1s envelope is fitted with a peak centered at 531.7 ± 0.2 eV (O1) and a peak centered at 533.3 ± 0.2 eV (O2), corresponding respectively to the ester oxygen (O=C) and the carbonyl oxygen (O-C). The component peak separations are constrained relative to the position of the dominant C1-peak (284.7 ± 0.2 eV). In Table 4.1 the resulting data of the curve-fitting procedure are listed.

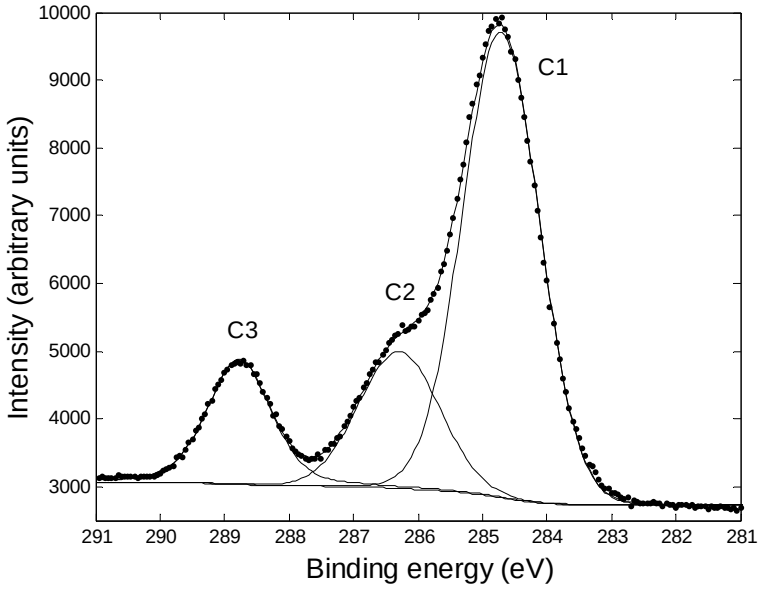

Figure 4.11 *Deconvolution of the C1s peak for untreated PET-foil.*

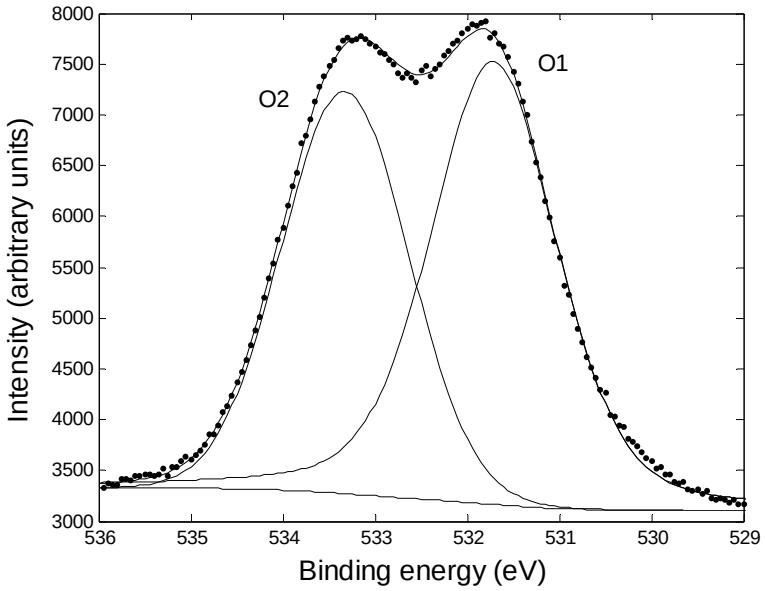

Figure 4.12 *Deconvolution of the O1s peak for untreated PET-foil.*

Functional group	E_b (eV)	ΔE_b comp. to C1	FWHM (eV)	Area (%)
C1	284.70	0.00	1.40	64.01
C2	286.30	1.58	1.48	19.76
C3	288.77	4.06	1.16	16.23
O1	531.71	247.00	1.61	55.71
O2	533.32	248.61	1.62	44.29

Table 4.1 *XPS data for curve-fitting of untreated PET-foil: binding energy (E_b), difference in binding energy compared to the C1-peak, full width at half-maximum (FWHM) and area of the peak.*

XPS spectra of plasma treated PET-foils are recorded as a function of treatment time and the changes with respect to the untreated sample are analyzed. Figure 4.13 shows the XPS survey scan of the PET-foil treated during 1.49 s. The most important change in the XPS spectrum compared to Figure 4.9 is the remarkable increase of the O1s peak intensity.

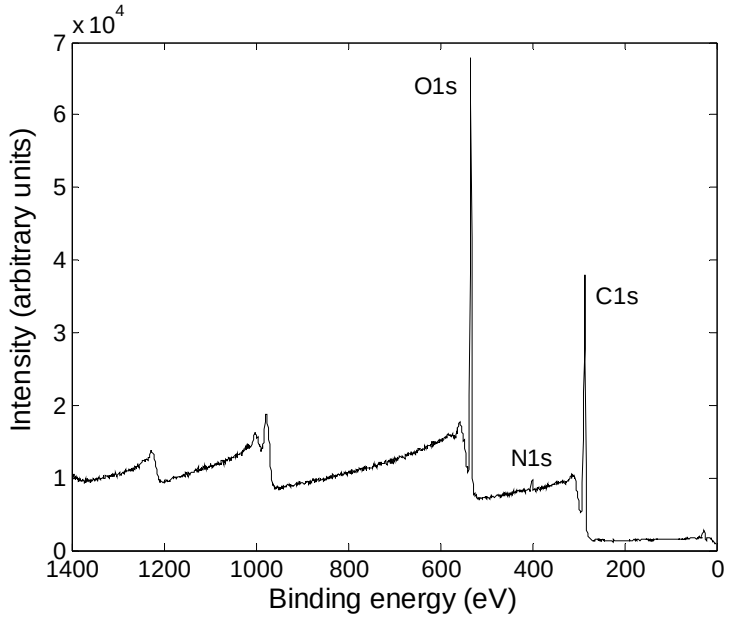

Figure 4.13 *XPS survey scan of a cyclically treated PET-foil (τ = 1.49 s, L = 58 W cm^{-2})*

The oxygen-to-carbon content ratio (O/C) can be calculated from the ratio of the total area of the O1s peak and the C1s peak, corrected with their corresponding sensitivity factor (see paragraph 2.5). For pure untreated PET this ratio is 0.40, which is in agreement with the theoretical composition (sum formula: $(C_{10}H_8O_4)_n$). Figure 4.14 shows the oxygen-to-carbon content ratio as a function of the treatment time. The level of oxidation increases with treatment time towards an O/C ratio higher than 0.5. This behaviour correlates well with the

continuous increase in surface wettability as a function of treatment time, deduced from the contact angle measurements of Figure 4.8. The O/C ratio increase seems to level off for treatment times longer than 1.5 s, which is again consistent with the saturation trend in the contact angle.

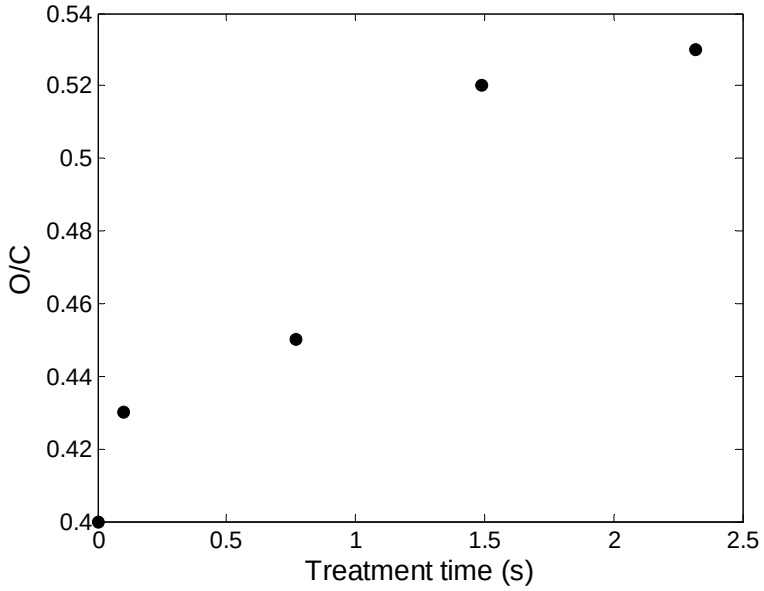

Figure 4.14 *Oxygen-to-carbon content ratio as a function of treatment time for cyclically treated PET-foil (L = 58 W cm^{-2}).*

Table 4.2 shows the changes in the relative concentrations of the carbon, oxygen and nitrogen atoms as a function of the treatment time. As already concluded from Figure 4.14 the oxygen concentration increases after the air plasma treatment. We can see also small nitrogen incorporation at the PET surface (peak at E_b = 399.6 $\pm$ 0.2 eV in Figure 4.13).

Core level	Treatment time				
	0 s	0.1 s	0.77 s	1.49 s	2.32 s
C 1s	71.48	69.70	68.97	65.52	65.01
O 1s	28.52	30.14	30.86	34.19	34.64
N 1s	0.00	0.16	0.17	0.29	0.35

Table 4.2 *Relative element concentration for carbon, oxygen and nitrogen at the PET-foil surface (at.%) as a function of the treatment time.*

Deconvolution of the XPS spectra for different treatment times gives more detailed information on the changes in chemical composition. Figures 4.15 and 4.16 show the spectra for the PET surface treated during 1.49 s. Table 4.3 summarizes the obtained results on the relative atomic compositions for different treatment times. The relative atomic concentrations of the three carbon composing elements (C1, C2 and C3) are compared with each other in Figure 4.17. The concentrations of the two different oxygen species (O1 and O2) are compared in Figure 4.18.

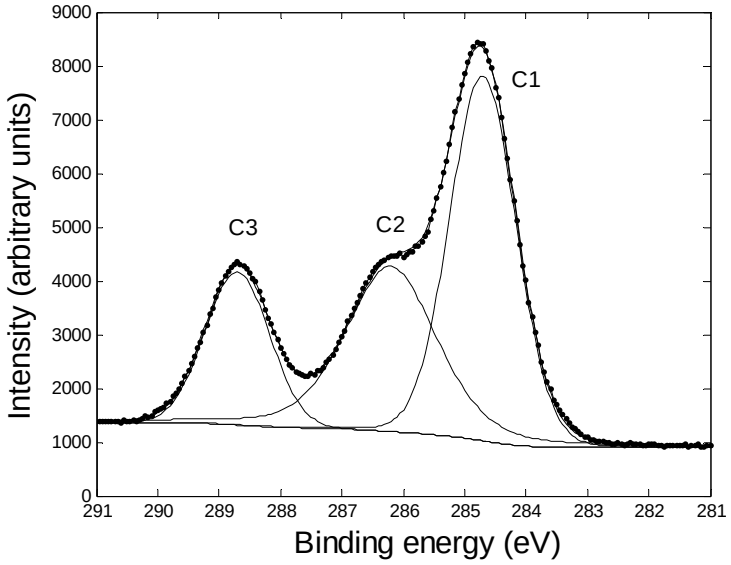

Figure 4.15 *Deconvolution of the C1s peak for plasma treated PET-foil (τ = 1.49 s).*

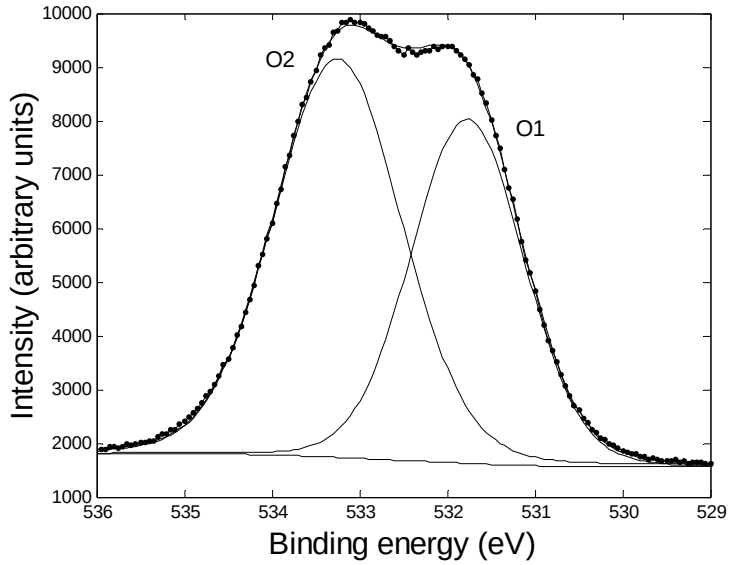

Figure 4.16 *Deconvolution of the O1s peak for plasma treated PET-foil (τ = 1.49 s).*

Ratio	Treatment time				
	0 s	0.1 s	0.77 s	1.49 s	2.32 s
C1/C	64.01	55.96	54.54	47.48	49.72
C2/C	19.76	25.03	25.91	33.64	28.71
C3/C	16.23	19.01	19.55	18.88	21.56
O1/O	55.71	49.40	43.88	42.79	40.15
O2/O	44.29	50.60	56.12	57.21	59.85

Table 4.3 *Relative atomic concentrations of the carbon and oxygen species on the PET-foil surface (in %) as a function of the treatment time.*

We can see a reduction of the benzene ring carbons (C1), while the concentration of the oxidized -C-O- groups (C2) increases simultaneously. This indicates that a fraction of the hydrogen atoms bound to carbon atoms in the benzene ring will be replaced by hydroxyl groups after the plasma treatment. The C2 peak can also include possible -C-N- groups, as a small concentration of nitrogen was observed in the XPS spectra (Table 4.2). There is also a slight increase in the concentration of the O=C-O- groups (C3).

For the oxygen species, an increase in the O2 peak (O-C) with respect to the O1 peak (O=C) is observed, which is in agreement with the observation that the C2 group increases faster than the C3 group.

These observations show once again that the decrease in contact angle can be related to the formation of oxygen (and nitrogen) containing functional groups.

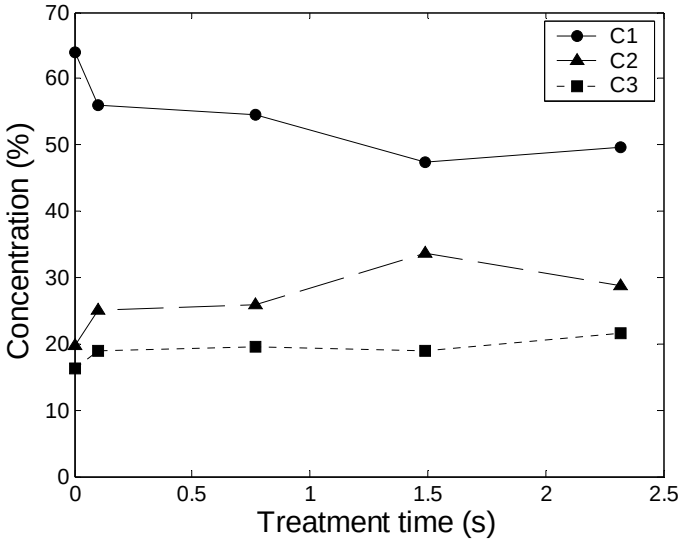

Figure 4.17 *Atomic composition of the carbon species on the PET-foil surface as a function of the treatment time.*

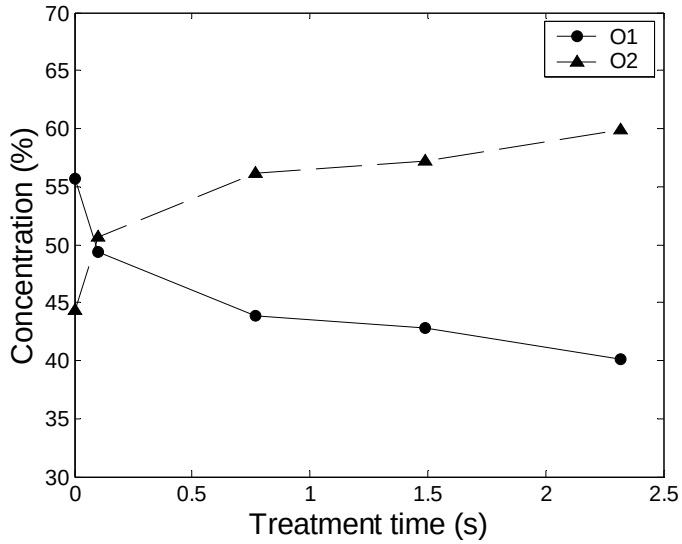

Figure 4.18 *Atomic composition of the oxygen species on the PET-foil surface as a function of the treatment time.*

4.3.1.2 Polypropylene foil (PP-foil)

Polypropylene (PP) represents an important part of textile industry but is generally known as a chemically inert material. Due to its low surface energy, an improved wicking behaviour is desirable for technical applications (e.g. geo and agro textiles) as well as for better comfort properties (e.g. for clothing or mattresses).

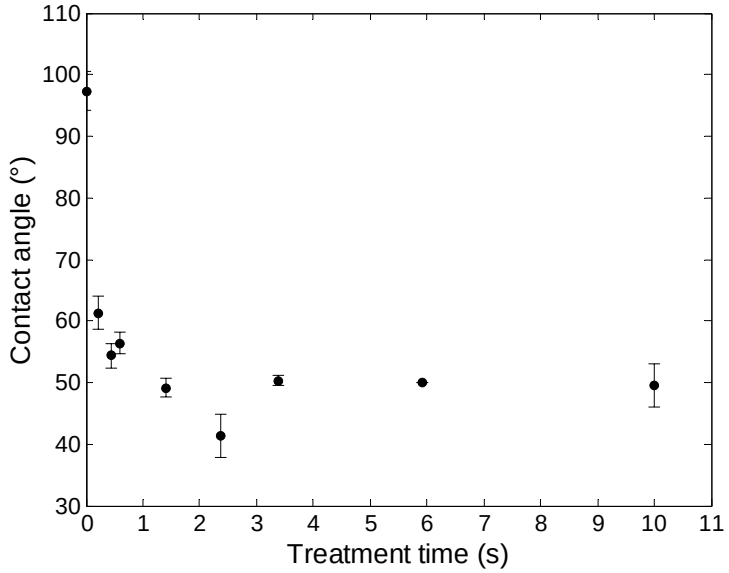

Figure 4.19 *Water contact angle as a function of treatment time for cyclically treated PP-foil (L = 53 W cm^{-2}).*

PP-foils with a thickness of 30 µm are treated with the remote glow discharge. The results on the contact angle are presented in Figure 4.19. A steep decrease with increasing treatment time is seen predominantly within the first second, similar to the results of PET-foil. It takes at least an energy dose of 80 J cm^{-2} to reach the saturation value of the contact angle of about 50°.

4.3.1.3 Silicone

Figure 4.20 contains data on plasma treatment of a 3 mm thick silicone sample (polydimethylsiloxane) with a textured surface. The thickness of the sample makes it impossible to treat the surface by an active DBD, because of the limitations imposed by the interelectrode distance. In this case, treatment in a remote regime is the obvious solution. The silicone material is used in automotive industry as mould in the production of dashboard covers. The motive for treatment is an enhancement of the adhesion between the silicone mould and the sprayed polyurethane material of the dashboard in order to prevent air bubbles at the interface.

Similar to the PET-foil, the static contact angle of water droplets on the silicone surface decreases with increasing the treatment time (i.e. with the energy dose). However, the decrease is slower and after 6 s of treatment, still no saturation occurs.

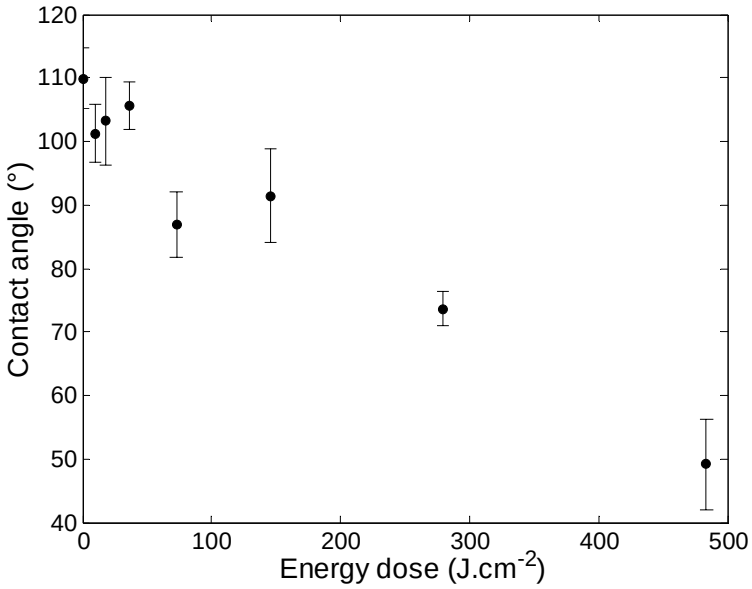

Figure 4.20 *Water contact angle as a function of treatment time for cyclically treated silicone (L = 80 W cm^{-2}).*

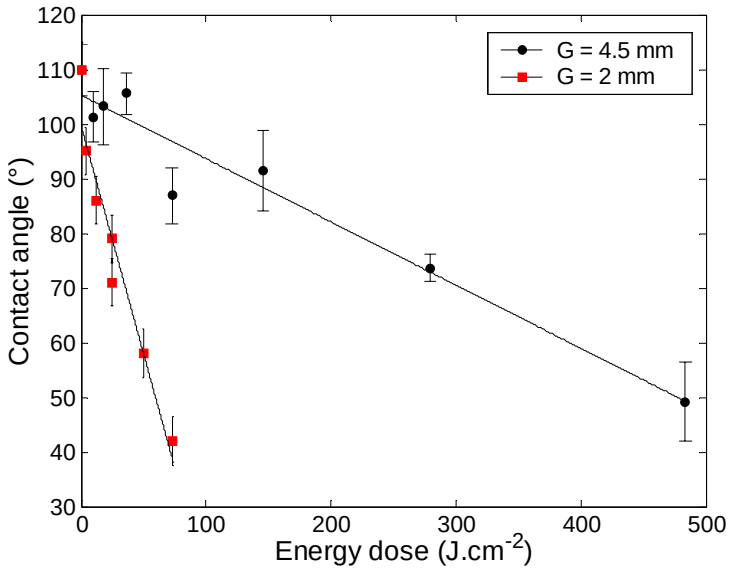

Figure 4.21 *Water contact angle as a function of energy dose for cyclically treated silicone; comparison for different distances G between sample and cathode pins.*

For the results with a power loading of 80 W cm^{-2} (Figure 4.20), the distance *G* between cathode pins and sample is 4.5 mm. In this case the energy dose ensuring a decrease of the contact angle from 110° down to 50° is nearly 480 J cm^{-2}, which is much higher than for the other treated materials. In order to increase the plasma effect, the distance *G* is decreased by putting the drum closer to the plasma source. However, instabilities (sparks) in the plasma arise if the distance between pins and sample is lower than 4.5 mm due to changes in the gas flow pattern (see paragraph 4.2). Therefore, it was necessary to lower the power loading simultaneously. In Figure 4.21, the results of Figure 4.20 are compared with results of a measurement where *G* is 2 mm and the power loading *L* is 11 W cm^{-2}. Both curves are recorded in the same treatment time range but as the power loading is different, the contact angle is given as a function of the energy dose instead of the treatment time. The curves show that the

decrease in contact angle with energy dose is much steeper when the sample is closer to the plasma. The increase in plasma effect due to the decrease in the distance *G* between pin and sample outweighs the decrease in plasma effect due to the decrease in power loading. The higher treatment effect with a smaller distance to the plasma is caused by a higher concentration of the active species. This will be further investigated in paragraph 4.3.2.

We can conclude that working with smaller distances between pins and treated sample is much more efficient, although in this case the power loading is limited by plasma disturbances caused by the nearness of the moving drum and by changes in the gas flow.

4.3.1.4 PET nonwoven

Nonwoven fabrics are characterized by a low-cost manufacturing process with a fast production rate. Therefore, this material is often used in disposable products (e.g. hygienic disposables, filters, dust cloths). In a lot of these applications the nonwoven material needs to be wettable to water or aqueous-based liquids. As this is not an inherent characteristic of the material, the wettability is usually obtained by coating the fabric with a surfactant solution and subsequent drying. However, these surfactants are liable to degradation which limits the product's utility life [33]. Therefore, a plasma treatment is investigated as an alternative to improve the surface properties of PET and PP nonwovens.

Experimental results on plasma treatment of a PET nonwoven are shown in Figure 4.22. As contact angles are difficult to measure, wettability is here quantified by the liquid absorptive capacity W_A. Again, we can see that the wettability improves mainly in the first second of treatment. A treatment time of 0.7 s (corresponding to an energy dose of 80 J cm^{-2}) seems to be a minimum when aiming at an improvement of the hydrophilic behaviour of the PET nonwoven.

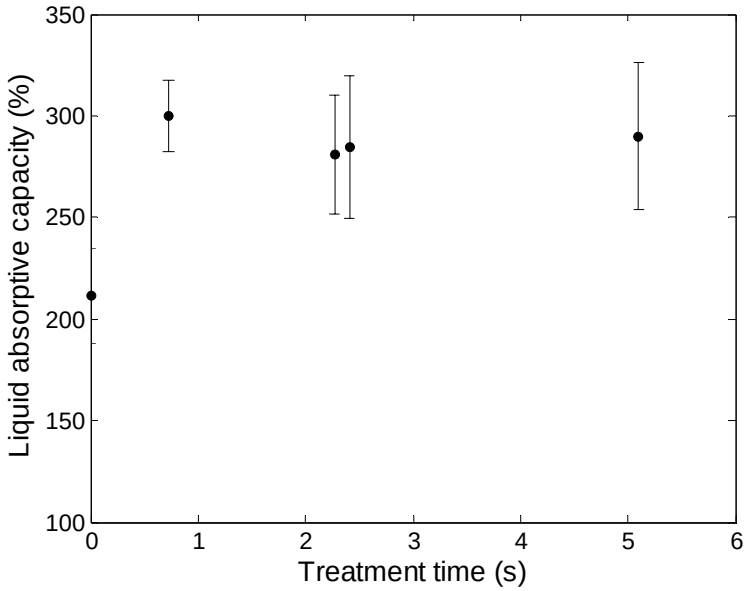

Figure 4.22 *Increase in liquid absorptive capacity as a function of treatment time for cyclically treated PET nonwoven (L = 80 W cm^{-2}).*

4.3.1.5 PP nonwoven

Due to the more closed structure and very low surface energy, it is possible to measure the contact angle on the PP nonwoven surface. The data is presented in Figure 4.23. Once again the same trend of the contact angle as a function of the treatment time is observed: a decrease in the first 0.2 seconds followed by a saturation for longer treatment times. However, the decrease of the contact angle is small in this case. If a higher wettability is desired, optimalisation of the plasma treatment for this material should be considered.

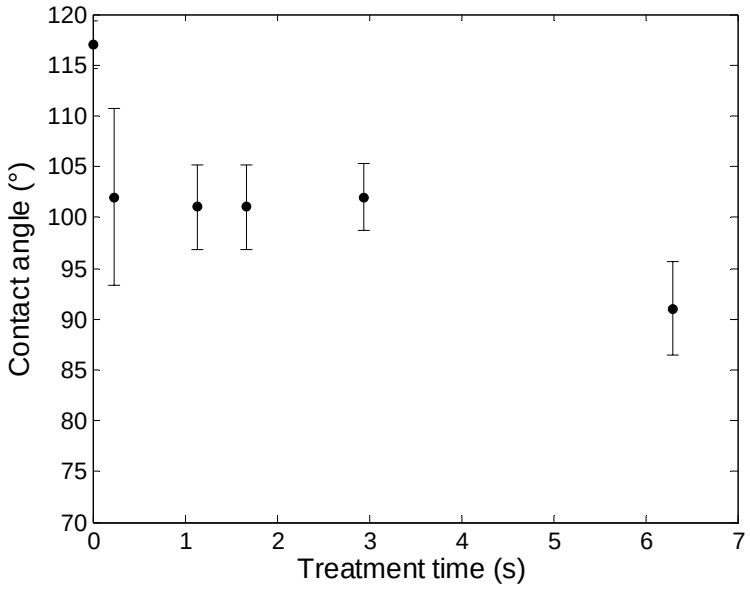

Figure 4.23 *Water contact angle as a function of treatment time for cyclically treated PP nonwoven (L = 80 W cm^{-2}).*

4.3.1.6 Overview

To conclude this paragraph about dependence on treatment time an overview is given of the different materials when treated with the same energy dose *D* (Table 4.4). This energy dose was fixed at 60 J cm^{-2}. The table gives successively the contact angle of the untreated surface ($\theta_{untreated}$), the contact angle of the surface treated with an energy dose of 60 J cm^{-2}, the power loading *L* and the treatment time τ for reaching the energy dose.

Sample	$\theta_{untreated}$ (°)	$\theta_{D = 60\ J\ cm^{-2}}$ (°)	L (W cm^{-2})	$\tau_{D = 60\ J\ cm^{-2}}$ (s)
PET-foil	76	35	58	0.97
PP-foil	97	50	53	1.13
Silicone	110	50	11	5.45
PP nonwoven	117	102	80	0.75

Table 4.4 *Overview of the contact angles for various materials treated by remote DC glow plasma treatment with an energy dose D of 60 J cm^{-2}.*

4.3.2 HOMOGENEITY OF PLASMA EFFECT

As the cathode consists of multiple pins in parallel, it is important to investigate the homogeneity of the discharge and of the resulting plasma effect along the treated surface in the direction of the pins, i.e. transverse to the flow. The contact angle is measured as a function of the transverse position on the treated PET sample, along the dashed line in Figure 4.24.

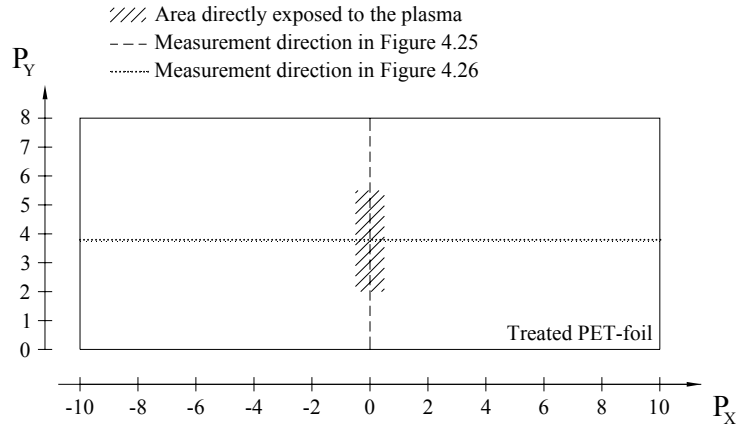

Figure 4.24 *Schematic view on the treated sample with indication of the directly exposed area and the lines along which contact angles are measured in the following graphs.*

The result is shown in Figure 4.25. In addition, the current through the individual cathode pins is shown in the graph, which also indicates the spacing of the cathodes. The profile of the contact angle indicates that the plasma effect is homogeneous in the region where the sample is directly exposed to the flowing afterglow, in spite of the observed transverse non-uniformity in luminosity of the discharge. Apparently, intensive turbulence in the gas flow is responsible for an efficient mixing of any inhomogeneities in the density of the plasma-borne reactive species. The graph also shows that the variations in the current through the individual pins are sufficiently small to have no impact on the homogeneity of the treatment.

The contact angle increases with the distance outside the plasma region, as the density of the reactive species rapidly decreases. The asymmetry in the increase is due to the experimental arrangement, which caused a net flow from left to right in Figure 4.25. The transport of the reactive species is reflected in the right part of the profile by a slower increase in contact angle.

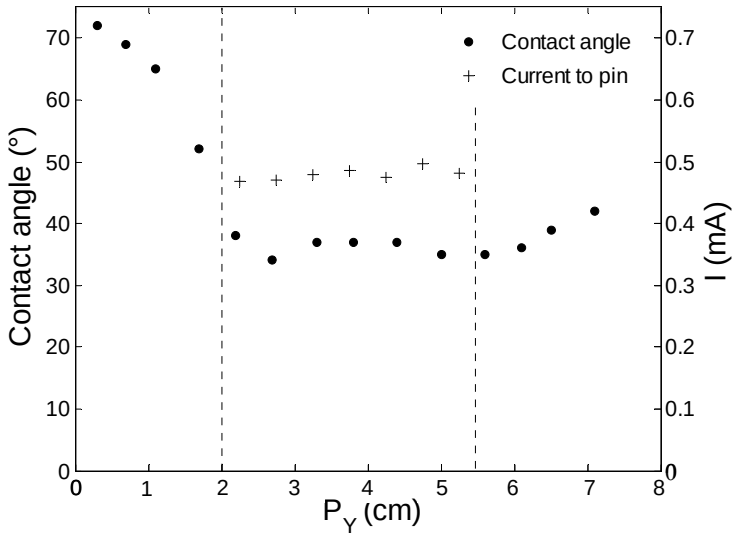

Figure 4.25 *Contact angle as a function of the transverse position on the sample and current to the individual cathode pins (cyclical treatment with τ = 1 s, L = 70 W cm^{-2}). The region between the dashed lines indicates the plasma zone.*

The extension of the active species is also examined in the direction perpendicular to the pin alignment, along the dotted line in Figure 4.24. A PET-foil surrounding the cylindrical drum was treated stationary during 2 seconds and the contact angle measurements after treatment are displayed in Figure 4.26. As expected, the lowest values are measured at the position on the sample which is directly exposed to the plasma zone (1 cm around zero). The larger fluctuations in the contact angle are related to the fact that this sample was treated stationary. In this case, there is no averaging in the direction of the movement. However, the average value of the contact angle below the plasma zone seems to be lower than the average value above the plasma zone, which is attributed to an unequal gas flow with a favourable downward direction. Generally, we can conclude that the extension of active species along the non-exposed area of the surface is limited, but depends on the local velocity of the gas flow.

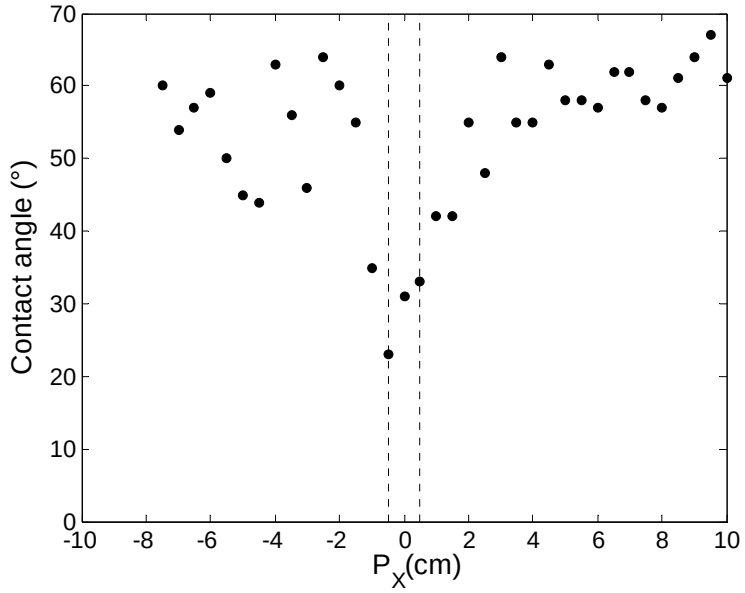

Figure 4.26 *Contact angle as a function of the position on the sample in the direction perpendicular to the pin alignment (stationary treatment with τ = 2 s and L = 70 W cm^{-2}). The region between the dashed lines indicates the plasma zone.*

Finally, the change in contact angle is examined while the distance *G* between the sample and the cathode pins is enlarged. At atmospheric pressure, the mean free paths of the excited species are short. A part of them returns to the fundamental level before reaching the surface and consequently do not contribute to the surface modification [51]. Due to growing losses in reactive species during their prolonged transportation towards the treated surface, the contact angle increases linearly with increasing distance from the active plasma zone. Nevertheless, Figure 4.27 demonstrates that the plasma afterglow still maintains sufficient reactivity to enhance the wettability of the PET surface up to 14 mm from the plasma zone, due to the intensive gas flow straight ahead towards the surface. Changing the distance between the discharge zone and the PET-foil however affects the gas flow pattern and this in turn, influences the plasma stability. For *G* longer than 14 mm the threshold current for sparking is too low to sustain a stable glow discharge.

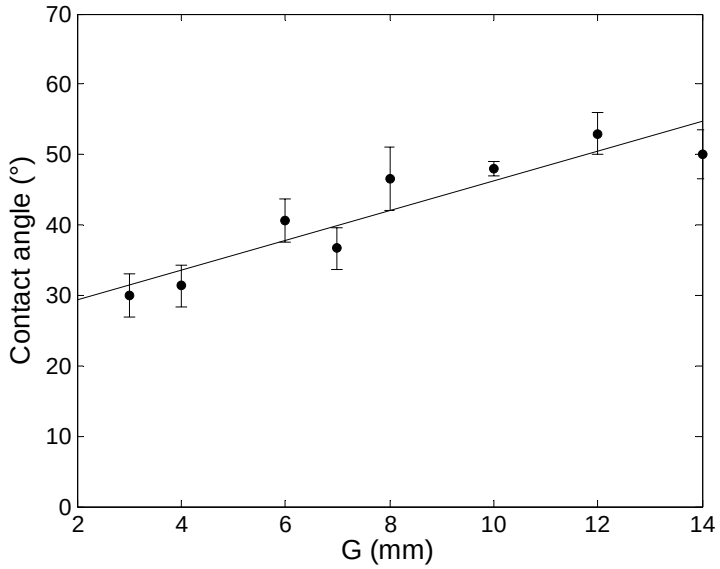

Figure 4.27 *Contact angle as a function of the distance G between the treated surface and the plasma (τ = 0.7 s, L = 15 W cm^{-2}).*

4.3.3 STABILITY OF PLASMA EFFECT IN TIME

For the treated surface, an ageing effect was observed during storage in air, i.e. the contact angle increased with the time after treatment. This can be explained by a reorientation of the plasma-created polar groups from the surface into the subsurface layer by thermodynamic relaxation [52]. As demonstrated in Figure 4.28, the initial contact angle after a treatment time τ of 2.7 s is 32°. After 5 hours of ageing, the contact angle increases to about 50° and then stabilizes at this value. This is still considerably lower than the 76° for an untreated surface and results in a wettability that is sufficient for many practical purposes. Moreover, there is no need for a long-lasting plasma effect in a production line, where plasma activation is followed by other processing steps.

It should be noted that this experiment is performed at room temperature of 20°C and a relative humidity of 40 %. It is known that the permanency of the plasma effect is influenced by the storage conditions as high temperature and high moisture result in a faster migration of the polar groups from the surface towards the bulk [53].

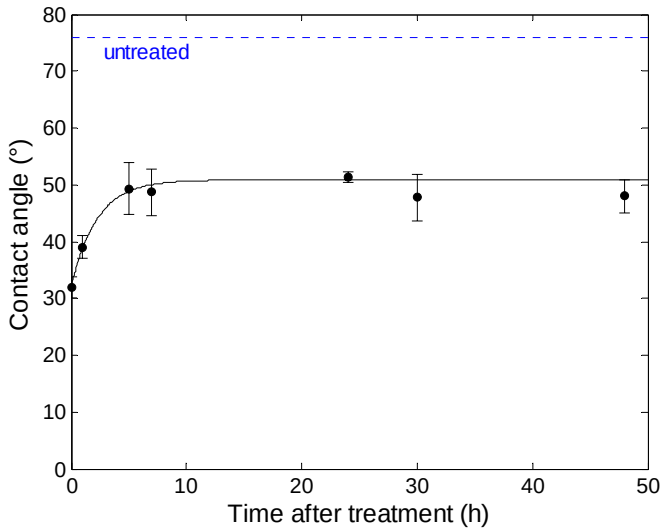

Figure 4.28 *Increase with ageing time after treatment of contact angle on cyclically treated PET-foil (τ = 2.7 s, L = 58 W cm^{-2}).*

4.4 ACTIVE SURFACE TREATMENT OF YARN

To have a better view on the efficiency and uniformity of the plasma treatment and on the optimal conditions for maximal increase in hydrophilic behaviour, cotton yarn was treated with variable power, treatment time and yarn position in the active plasma region. The aim of this paragraph is not to optimise the setup in order to reach an efficient treatment for the yarn. The main objective is to scan the plasma zone and to characterize the plasma activity as a function of the changed parameters. This is also the reason why this treatment is performed in an active regime, although the setup is optimised for remote treatment. Due to its dimensions, its easy handling and the small disturbance of the discharge while present in the plasma, a yarn is well suited for this characterisation.

The liquid wicking rate is measured immediately after treatment. For the untreated cotton yarn, the water boundary does not rise, so the wicking rate is zero for the untreated state. The reason for this hydrophobic nature of the surface is the waxy, inert outermost layer of the cotton fibre or the “cuticle” which protects the fibre from external agents. Finally, the stability of the plasma effect in time after treatment is investigated.

For clarity’s sake, error bars on the wicking rate are not displayed in the following graphs. The standard deviation for all measurements is about 3 mm.

4.4.1 EXPERIMENTAL SETUP

The experimental setup used for the active plasma treatment of yarn is given schematically in Figure 4.29. Basically, it is the same setup as in paragraph 4.3, but the number of connected pins is extended to 21, which makes that the discharge length is enlarged to 10.5 cm. The cathode pins near the yarn leads are disconnected to avoid discharge instabilities. As we work in an active regime and the yarn moves

through the plasma zone in the direction of the pins, an increase in the number of pins means an increase in treatment time. The treatment time can be controlled by the line speed. The position of the yarn, relative to the cathode and anode, can be changed.

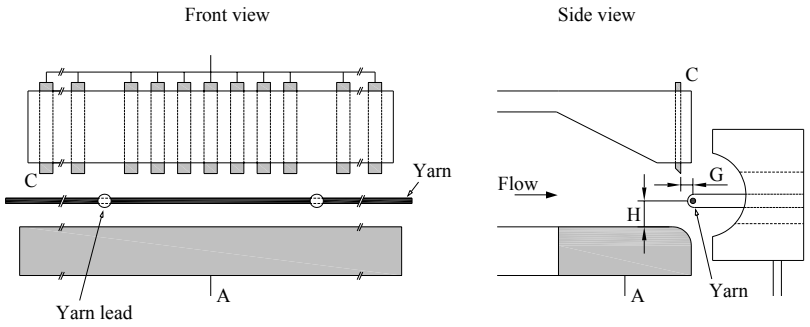

Figure 4.29 *Schematic diagram of the experimental setup for treatment of yarn. G and H give the position of the yarn, C = cathode pins, A = anode plate.*

4.4.2 INFLUENCE OF TREATMENT TIME ON PLASMA EFFECT

The treatment time τ is determined by the line speed of the yarn when passing through the plasma. Five samples of cotton yarn are treated with different line speed, i.e. different treatment time. The discharge power *P* is held constant at a value of 204 W and the yarn is positioned at a height *H* of 4 mm from the anode and at a distance *G* of 1 mm. At this position of the yarn, the efficiency of the plasma effect is optimal as will be discussed in paragraphs 4.4.4 and 4.4.5. Figure 4.30 shows the evolution of the rising water front on treated cotton yarn. The vertical wicking rate increases with higher treatment times. This can be attributed to the increasing number of plasma-created polar groups on the surface, due to oxidation and other chemical changes of the surface. Possibly, a physical etching effect which causes some erosion of the outer wax layer on the cotton fibres can also play a part in the increase of the surface wettability [54]. When the cotton yarn is treated during more than 15 seconds, the evolution

in height of the water front doesn't seem to change much anymore as a function of treatment time. This shows that there is saturation in the plasma effect on the surface of the cotton yarn.

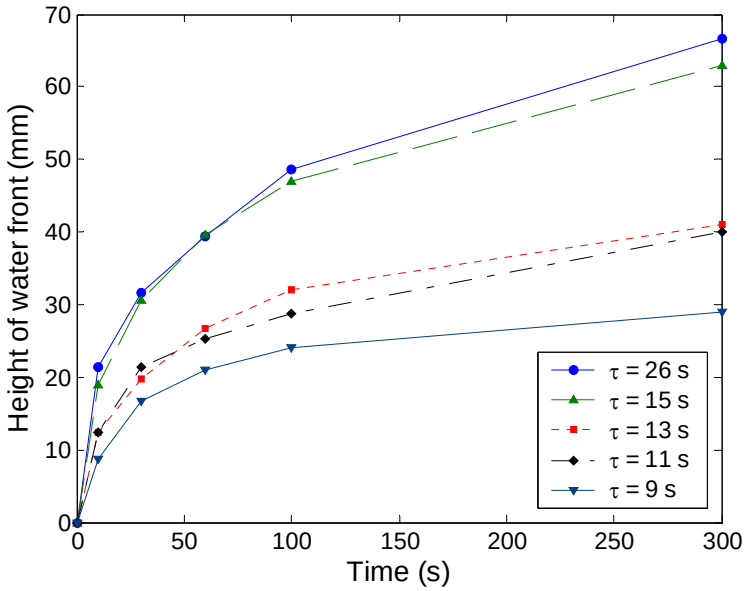

Figure 4.30 *Wicking rate for different treatment times τ (P = 204 W, H = 4 mm, G = 1 mm).*

4.4.3 INFLUENCE OF DISCHARGE POWER ON PLASMA EFFECT

The power *P* in the discharge is changed by varying the current. The wicking rate increases with power (Figure 4.31). However, for values of the discharge power higher than 200 W the plasma effect saturates. Higher power increases the amount of active species in the plasma, thus an increase in the formation of polar groups on the surface.

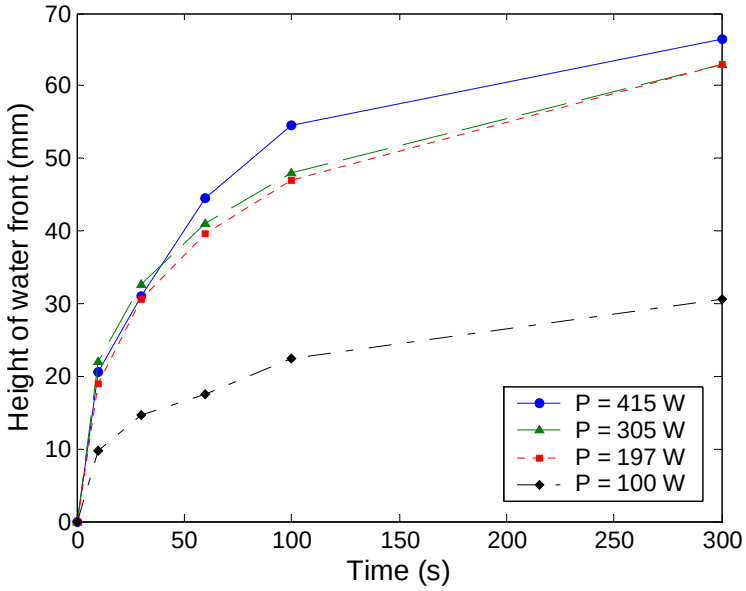

Figure 4.31 *Wicking rate for different values of the discharge power (τ = 15 s, H = 4 mm, G = 1 mm).*

4.4.4 INFLUENCE OF YARN POSITION ON PLASMA EFFECT

Another parameter that can influence the efficiency of the plasma treatment is the position of the yarn in the plasma region. The position of the yarn is changed in horizontal and vertical direction (see Figure 4.29). Figure 4.32 gives the wicking rate as a function of the height of the yarn relative to the height of the anode. This parameter *H* could be changed between 4 and 8 mm. Higher and lower positions could not be reached due to the mechanic limitations of the yarn leads. The results show that the wicking rate is highest when the cotton yarn is placed closer to either the cathode (*H* = 8 mm) or the anode (*H* = 4 mm). At 6 mm from the anode the wicking rate is lower. The conditions at *H* = 8 mm are favourable because the charged particle density increases towards the cathode, as found in [40], while for the region near the anode (*H* = 4 mm), the higher wicking rate can be

explained by the higher effective residence time of the yarn in the plasma due to an overlap of the different plasma columns (see front view of the discharge in Figure 4.3). In Figure 4.33, the position of the cotton yarn is changed in horizontal direction. At 1 mm downstream from the cathode, the plasma effect has a well defined maximum. The active species concentration is at a maximum here, due to the shape of the plasma profile which is influenced by the fast airflow (see side view of the discharge in Figure 4.3). For smaller values of *G*, the cotton yarn is not in the active, luminous region of the plasma. For higher values of *G*, the cotton yarn is in the afterglow of the plasma, where the density of active species gradually decreases in the downstream direction of the air flow.

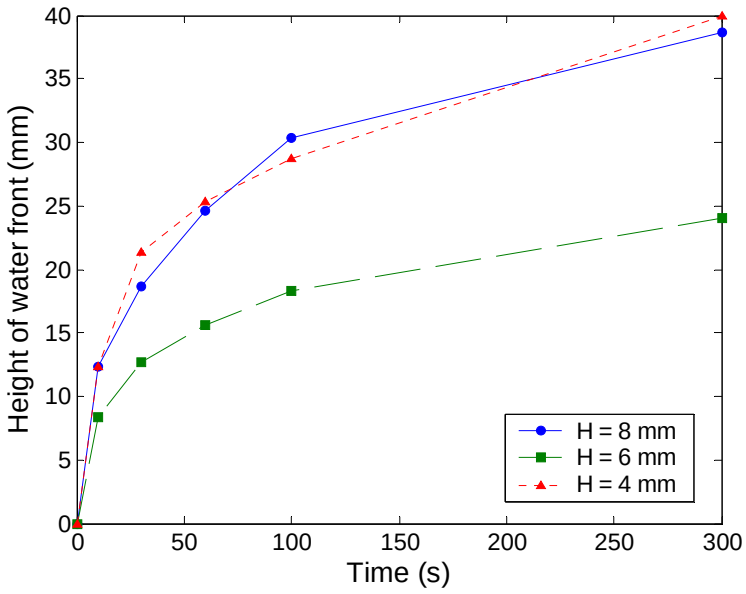

Figure 4.32 *Wicking rate for different vertical positions of the cotton yarn in the plasma region; H gives the height of the yarn relative to the anode (τ = 11 s, P = 209 W, G = 1 mm).*

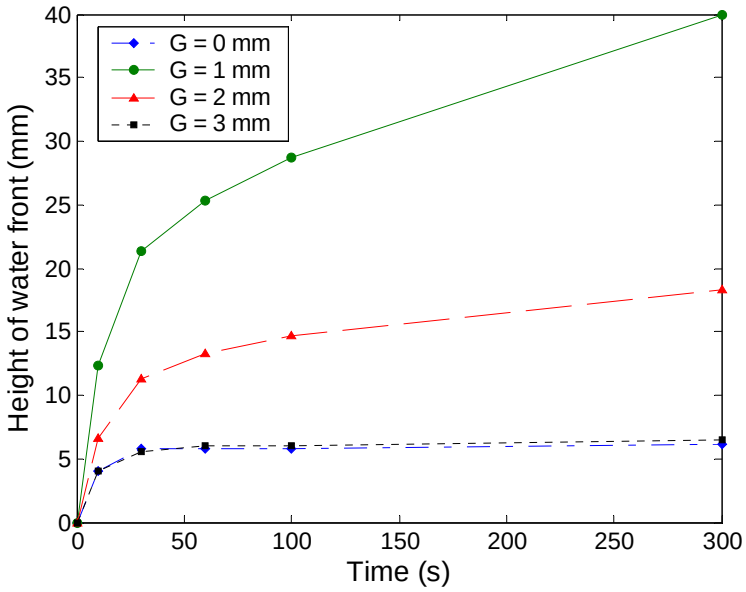

Figure 4.33 *Wicking rate for different horizontal positions of the cotton yarn in the plasma region; G gives the distance of the yarn relative to the cathode position in downstream direction (τ = 11 s, P = 209 W, H = 4 mm).*

4.4.5 STABILITY OF PLASMA EFFECT IN TIME

Figure 4.34 shows the stability in time of the wicking rate after plasma treatment. There seems to be a lowering in the wicking rate as a function of time after treatment. We can conclude that the plasma effect was not merely a physical etching of the waxy layer on the cotton fibres because the ageing effect indicates recovery of a structural modification of the surface. After 5 hours of ageing time, the wicking rate stabilizes at a value that is still considerably high.

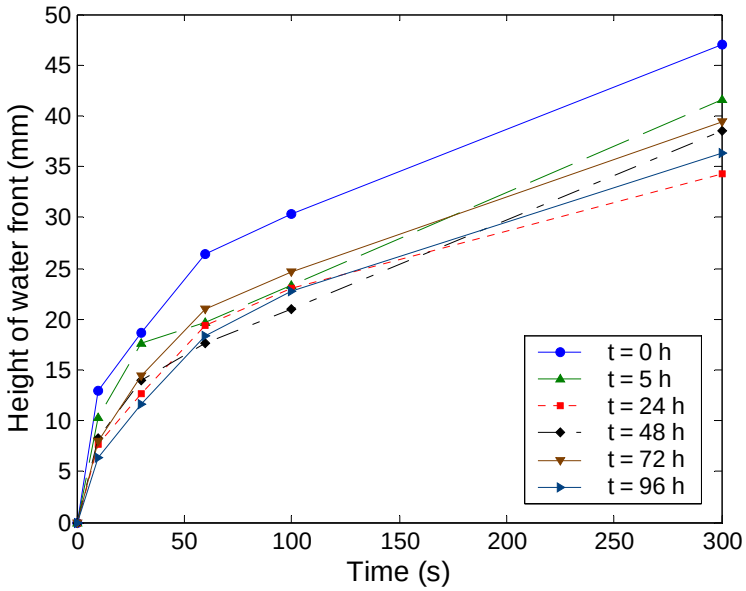

Figure 4.34 *Wicking rate at different ageing times t (τ = 17 s, P = 280 W, H = 4 mm, G = 1 mm).*

4.5 CONCLUSION

The DC glow discharge is evaluated to serve as source for a remote plasma treatment to improve surface characteristics. The results for PET-foil show that the contact angle decreases in the first second of treatment, while the value stabilizes at 33° for longer treatment times. The incorporation of oxygen containing functional groups, detected by means of XPS measurements, correlates well with this behaviour. Measurements on other materials show that plasma treatment in the remote setup can be used in various applications where improvement of hydrophilicity, adhesion or dyebility is desirable.

Measurements of the contact angle as a function of the position at the surface in the direction parallel to the pin alignment were performed to investigate the uniformity of the plasma effect. In spite of the intrinsic non-uniformity of the multi-pin discharge, the plasma effect appeared

to be homogeneous in the region of the surface that is directly exposed to the flowing afterglow. Intensive turbulence in the gas flow is responsible for an efficient mixing of the inhomogeneities in the density of the plasma-borne reactive species.

The intensive gas flow makes it possible for the active species to survive beyond the area directly exposed to the plasma. The extension of the treatment effect outside the directly treated zone is therefore strongly dependent on the local velocity of the gas flow. Enlarging the distance between the plasma zone and the sample decreases the treatment efficiency. Nevertheless, active species with sufficient modification ability seem to reach the surface at least up to 14 mm from the plasma.

It was observed that the contact angle increased again depending on the storage time after treatment due to a relaxation in the structure and orientation of plasma-created polar groups at the surface. However, after 50 hours of ageing the contact angle is still considerably lower than the value for an untreated surface and results in a wettability that is sufficient for many practical purposes.

To have an idea of the local influence of different parameters on the plasma effect, an active treatment in the DC glow discharge was carried out on cotton yarn. The results show that the wicking rate of the treated cotton yarn increases with the treatment time and the discharge power. The wicking rate tends to be higher when the yarn is positioned in the vicinity of the electrodes. The variation of the plasma effect in the direction of the airflow reflects the asymmetry in the plasma profile due to the fast gas flow. The plasma effect decreases during the first 5 hours after treatment, but this decrease levels off so that the remaining wicking rate is still remarkably higher than the wicking rate for an untreated yarn.

5 ATMOSPHERIC PULSED STREAMER DISCHARGE

5.1 INTRODUCTION

Although the remote treatment with the DC glow discharge can be sufficient for many applications, the activation of polymer films on industrial scale demands a very high roll speed and consequently shorter treatment times. In order to meet these requirements developments in the atmospheric linear plasma source should aim for higher treatment efficiency. The solution can be found in the streamer regime. The experimental setup for the remote DC glow discharge from the previous chapter is therefore redesigned to perform in a regime where the plasma consists of high density current filaments (streamers) that slide along the surface to be treated. The resulting intense contact between plasma streamers and surface ensures an in situ high concentration of active species and thus higher treatment efficiency [55]. The high repetition frequency of the streamers and the intensive turbulence in the gas flow promote uniform treatment of the surface, in spite of the intrinsic non-homogeneity of the streamer discharge.

5.2 EXPERIMENTAL SETUP

The discharge regime mainly depends on the current density and on the details of the electrode design. For the streamer regime, the discharge current is strongly non-steady and is transferred by many thin (about 100-300 µm in diameter) and bright current filaments (streamers), which are randomly distributed in space and time. The repetition frequency of the streamers and the current of a single streamer are determined by the values of the components in the

pulse-forming electrical circuit. In the experiments, these values are close to 10 kHz and 0.10 A respectively. The electrode design is also important to control the streamer regime. The positive electrode is a sharp needle, while the negative electrode is a metallic plate covered with a resistive coating. Figure 5.1 displays an electrode section that consists of 12 anode needles and 6 resistive cathode plates (1 plate for 2 needles). The distance between needle and plate is 4.5 mm. The plasma length of 1 section in the direction of the needles is 8 cm. Figure 5.2 shows the visual appearance of the streamers. The setup was built with 6 sections in parallel, corresponding to a total plasma length of 48 cm. In the results below only 1 section is connected.

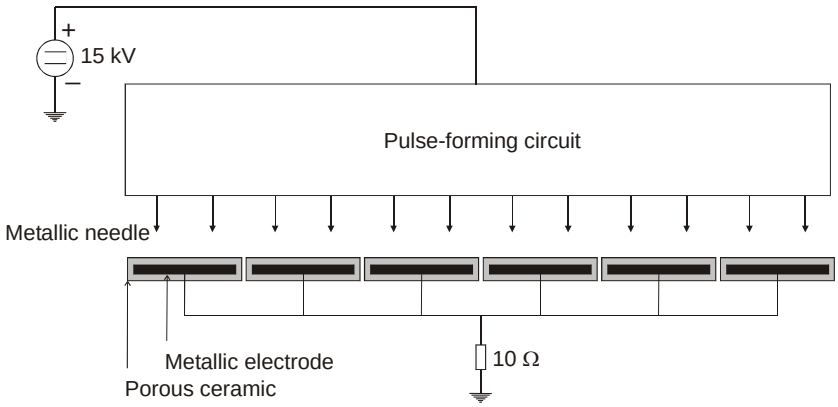

Figure 5.1 *Electrical scheme of the pulsed streamer discharge.*

Figure 5.2 *Photograph of the pulsed streamer discharge; the central needles are not connected.*

The streamers are blown out of the gap towards the sample and forced against the treated surface by the gas flow (with a gas velocity of 35 m s^{-1}). In this way, most of the active plasma species are generated immediately at the surface to be treated.

The value of the power density $\mathcal{P}$ in the body of a streamer is estimated to be in the range of 2000-4000 W cm^{-3}, i.e. much higher than in a diffusive glow discharge. However, the restriction of the streamer lifetime and of the current transferred by a single streamer, prevent local thermal damage of the treated surface.

The metallic needle has positive potential because streamers are formed more easily than in the case of a negative needle [42]. An anode needle has the additional advantage of a longer lifetime. High electric field strength and high current densities exist near the sharp electrode. In the case of a cathode needle the heavy positive ions are attracted to the needle and cause some sputtering of the electrode material, which is deposited on the ground electrode. In the case of an anode needle the positive ions are repelled and electrons are attracted. Since the electrons have only low mass, no sputtering of the needle electrode is observed.

5.3 SURFACE TREATMENT OF POLYPROPYLENE TAPE (PP-TAPE)

The laboratory setup is built for treatment of narrow polypropylene (PP) tapes (1.5 mm in width) with a view to introduce the plasma treatment in the production line of the tapes immediately after extrusion. PP-tapes are for example used in agro textiles where improvement of the hydrophilicity is desired to deal with the insufficient water transport of the PP material. The existing methods (sprays, finishes) are not permanent as the treated surface looses its hydrophilic property during the finishing processes or maintenance cycles that follow. The main focus of the plasma treatment is to

introduce hydrophilic properties with an improved permanency of the effect.

The PP-tape passes through the plasma zone in the direction perpendicular to the propagation of the streamers, i.e. from the right to the left in Figure 5.1 and 5.2. The resulting contact angles as a function of the treatment time are given in Figure 5.3. In this case the samples are not cyclically treated, so the treatment time is varied by changing the sample velocity. The value of the contact angle could be lowered by about 35° for velocities up to 45 m min^{-1}. A contact angle of 60° could be reached after 1.5 s of treatment (velocity = 3.5 m min^{-1}).

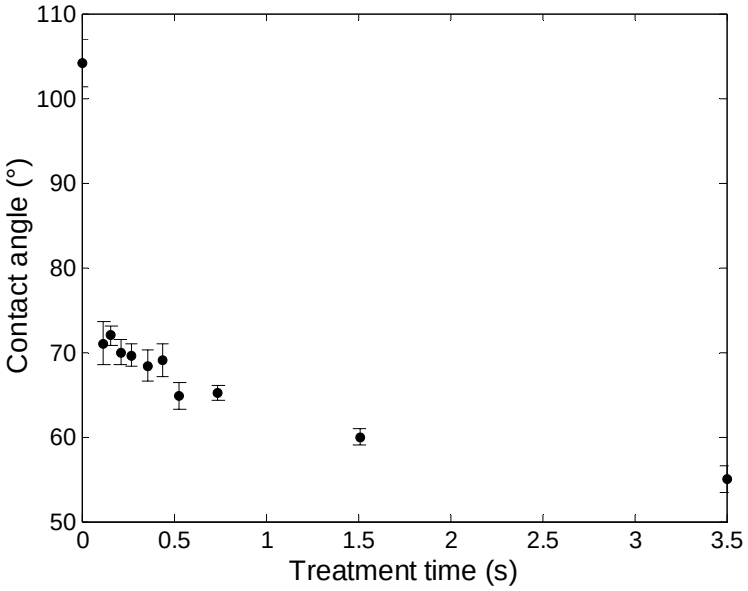

Figure 5.3 *Contact angle as a function of treatment time for small PP-tape in the pulsed streamer regime.*

Figure 5.4 shows the post-exposure change in the contact angle during 10 days after treatment. The contact angle increases only slightly as a function of the time after treatment. Even after 10 days,

the contact angle is only 3.5° higher compared to the value that was measured immediately after the plasma treatment.

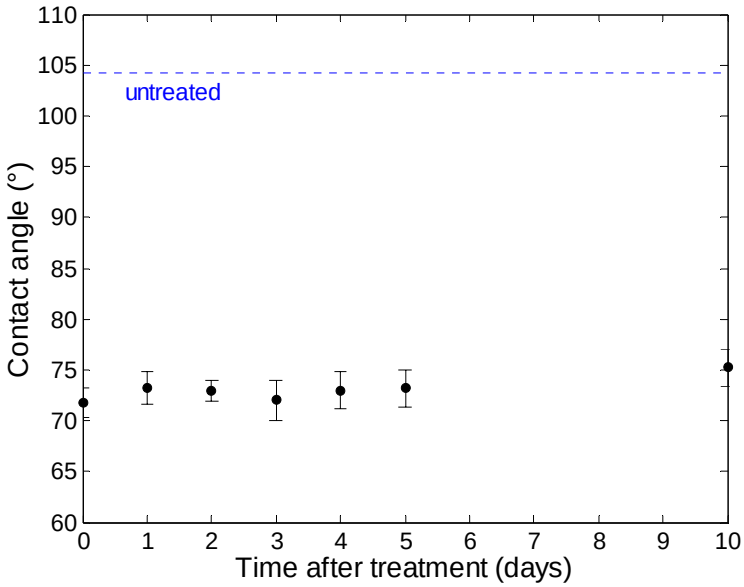

Figure 5.4 *Contact angle as a function of the time after treatment (ageing effect) for small PP-tape in the pulsed streamer regime (τ = 0.12 s).*

5.4 CONCLUSION

An experimental setup for remote treatment with a pulsed DC discharge in streamer regime was built to enhance the hydrophilicity of PP-tapes. With a roll velocity of 45 m min^{-1} and a plasma length of 8 cm an improvement of the contact angle from 105° to 70° was achieved. A plasma length with more electrode sections in parallel will enable treatment velocities in the range of the velocities in the extrusion line (100-300 m min^{-1}).

The results on the contact angle as a function of the time after treatment show a good permanency of the wettability. For a contact angle improvement of 33° only 3.5° are lost after 10 days. Due to this long-term permanency of the wettability improvement, the plasma treatment in streamer regime can be considered as a promising replacement of the existing methods.

6 GENERAL CONCLUSIONS

By means of a non-thermal atmospheric plasma, surface modification can be achieved without changing the bulk properties of the treated material. The motivation for using non-thermal plasma techniques in material processing lies mainly in the non-polluting dry method of treatment at low temperature. Working at atmospheric pressure offers additional advantages since the plasma treatment can be integrated in an existing production line. The already industrially wide-spread corona treaters lack in homogeneity and flexibility of sample dimension and geometry. The innovative remote plasma concepts investigated in this work, based on the DC glow discharge and the pulsed streamer discharge, avoid the difficulties encountered during the "classical" corona treatment and have the potential to reach higher linear process speed. Whether or not the technology can really penetrate into the industrial processing will depend on to which extent the plasma sources can combine efficiency, uniformity and permanency of the treatment with scalability up to relevant process velocities and dimensions.

Efficiency

In terms of efficiency, an active regime is preferred over a remote regime. In an active treatment, the sample is in direct contact with the plasma which means that the modifying species can react immediately with the surface. In remote treatment, where the plasma creation zone and the application zone are separated in space, the active species have to bridge the distance from plasma to surface. Although a fast gas flow is applied to accelerate the transport, the limited lifetime of the excited species causes their concentration to decrease outside the active plasma zone. Therefore, the electric power of the remote regime needs to be high enough to generate a sufficient concentration of active species. For the remote DC glow discharge a minimum energy dose of 58 J cm^{-2} is required to have a decrease in contact

angle of 40° on a PET-foil surface, while the dielectric barrier discharge (DBD) requires an energy dose of only 0.60 J cm^{-2} to reach the same decrease in contact angle.

In the streamer regime, the plasma streamers are guided closely along the treated surface by the gas flow so that the active plasma species are generated immediately at the surface. Local heating of the sample surface is restrained by the high repetition frequency of the streamers. The advantages of an active and a remote treatment are combined in this regime.

The results on the remote treatment with the atmospheric DC glow discharge have shown that the required energy dose depends on the material to be treated. Moreover, the desired treatment result – and consequently the energy dose – can vary depending on the considered application.

Uniformity

As the discharge in a DBD usually operates in a filamentary mode, the discharge consists of a large number of parallel current filaments between the electrodes. As the treated sample is directly exposed to these perpendicularly orientated filaments the DBD results in a non-uniform surface treatment. Consequently, there is also a risk of damaging the surface. For the remote DC glow discharge, contact angles on different positions on the treated PET-foil surface indicated a good homogeneity of the plasma effect. In spite of the intrinsic non-uniformity of the multi-pin discharge, the turbulence in the gas flow promotes a mixing of the inhomogeneities in the reactive species density before the surface is reached.

Permanency

It is observed that the improved wettability by a plasma treatment decays with time (ageing effect). The contact angle increases with the storage time after treatment due to a relaxation in the structure and

orientation of plasma-created polar groups at the surface. The rate of decay may also be affected by the temperature and humidity of the storage environment and by the tightness and handling of a roll of treated material.

Nevertheless, the surface does not return to the untreated state, but changes until a new equilibrium state is reached. Here, the contact angle value is still considerably lower than the value for an untreated surface and results in a wettability that is sufficient for many practical purposes. The preliminary results on PP-foil treated with the streamer discharge have shown an increase in contact angle of only 10 % after 10 days.

Scalability

The proposed setup for the remote treatment is based on a linear array of pin-to-plate glow discharges in ambient air. The plasma length can easily be scaled up to any roll width by putting more electrode elements in parallel. This flexibility in roll width, together with the wide variation in type and thickness of the treated material facilitates the implementation of the plasma treatment into the existing industrial production lines. Also on account of the low induced running costs (only electricity, no gas consumption), atmospheric plasma technology in air has the potential to be scaled up to industrially relevant dimensions and roll velocities.

This work represents the first step towards a feasibility study of the industrial implementation of the proposed atmospheric plasma techniques. The DC remote glow and the surface streamer discharge are interesting alternatives for the existing modification techniques of polymer and textile materials. Moreover, these innovative concepts also have the potential to be used for other types of application, as for example the deposition of thin functional coatings. The industrial integration and the expansion of the application field are therefore subjects of further research.

REFERENCES

[1] M.A. Lieberman, J.P. Booth, P. Chabert, J.M. Rax and M.M. Turner *Plasma Sources Sci. Technol.* **11** (2002) 283-293

[2] P. Chabert, J.L. Raimbault and J.M. Rax *Phys. Plasmas* **11** (2004) 1775-1785

[3] T. Uehara *Adhesion Promotion Techniques* ed. K.L. Mittal and A. Pizzi (New York, Dekker, 1999)

[4] E.M. Liston, L. Martinu and M.R. Wertheimer *J. Adhesion Sci. Technol.* **7** (1993) 1091-1127

[5] F. Massines and G. Gouda *J. Phys. D: Appl. Phys.* **31** (1998) 3411-3420

[6] A. Kruse, G. Kruger, A. Baalmann and O.D. Hennemann *J. Adhes. Sci. Technol.* **9** 12 (1995) 1611-1621

[7] Y.P. Raizer *Gas Discharge Physics* (Berlin, Springer-Verlag, 1991) chapter 1

[8] A. Grill *Cold Plasma in Materials Fabrication: from fundamentals to applications* (New York, IEEE Press, 1994)

[9] N. Inagaki *Plasma Surface Modification and Plasma Polymerization* (Lancaster, Technomic Publishing Company, 1996)

[10] A.A. Meyer-Plath, K. Schröder, B. Finke and A. Ohl *Vacuum* **71** (2003) 391-406

[11] C. Geβner, V. Bartels, T. Betker, U. Matucha, C. Penache and C.-P. Klages *Thin Solid Films* **459** (2004) 118-121

[12] J.R. Hollahan and A.T. Bell *Techniques and Applications of Plasma Chemistry* (New York, Wiley, 1987)

[13] B.N. Chapman *Glow Discharge Processes Sputtering and Plasma Etching* (New York, Wiley, 1980)

[14] J.R. Roth *Industrial Plasma Engineering, Volume 1: principles* (Bristol and Philadelphia, Institute of Physics Publishing, 1995)

[15] M.A. Lieberman and A.J. Lichtenberg *Principles of Plasma Discharges and Materials Processing* (New York, Wiley, 1994)

[16] B. Lamontagne, A.M. Wrobel, G. Jalbert and M.R. Wertheimer *J. Phys. D: Appl. Phys.* **20** (1987) 844-850

[17] D. Korzec, J. Rapp, D. Theirich and J. Engemann *J. Va. Sci. Technol. A* **12** (1994) 369-378

[18] H.J. Griesser *Vacuum* **39** (1989) 485-488

[19] J. Asmussen *J. Va. Sci. Technol. A* **7** (1989) 883-893

[20] A.P. Napartovich *Plasmas and Polymers* **6** 1-2 (2001) 1-14

[21] B. Eliasson and U. Kogelschatz *IEEE Trans. Plasma Sci.* **19** (1991) 309-323

[22] W. Siemens *Poggendorfs Ann. Phys. Chem.* **102** (1857) 66

[23] G. Borcia, C.A. Anderson and N.M.D. Brown *Plasma Sources Sci. Technol.* **12** (2003) 335-344

[24] U. Kogelschatz *Plasma Chem. Plasma Process.* **23** (2003) 1

[25] S. Meiners, J.G.H. Salge, E. Prinz and F. Förster *Surf. Coat. Technol.* **98** (1998) 1121-1127

[26] S. Kanazawa, M. Kogoma, T. Moriwaki and S. Okazaki *J. Phys. D: Appl. Phys.* **21** (1988) 838-840

[27] S. Okazaki, M. Kogoma, M. Uehara and Y. Kimura *J. Phys. D: Appl. Phys.* **26** (1993) 889-892

[28] F. Massines, A. Rabehi, P. Decomps, R.B. Gadri, P. Ségur and C. Mayoux *J. of Appl. Phys.* **83** 6 (1998) 2950-2957

[29] N. Gherardi, G. Gouda, E. Gat, A. Ricard and F. Massines *Plasma Sources Sci. Technol.* **9** (2000) 340-346

[30] V.I. Gibalov and G.J. Pietsch *J. Phys. D: Appl. Phys.* **33** (2000) 2618-2636

[31] M. Simor, J. Rahel, P. Vojtek and M. Cernak *Appl. Phys. Lett.* **81** 15 (2002) 2716-2718

[32] M. Simor, J. Rahel, M. Cernak, Y. Imahori, M. Stefecka and M. Kando *Surf. Coat. Technol.* **172** (2003) 1-6

[33] J. Rahel, M. Simor, M. Cernak, M. Stefecka, Y. Imahori, M. Kando *Surf. Coat. Technol.* **169** (2003) 604-608

[34] R.H. Stark and K.H. Schoenbach *J. Appl. Phys.* **85** 4 (1999) 2075-2080

[35] H. Sung-Spitzl. *Galvanotechnik* **90** (1999) 3426–3437

[36] S. Wu *Polymer Interface and Adhesion* (New York, Dekker, 1982)

[37] M. Zamfir, J. Verschuren and P. Kiekens *Int. Nonwovens Tech. Conf. 2002* (Atlanta GA, USA, 24-26 Sept. 2002)

[38] P.E.J. Flewitt and R.K. Wild *Physical Methods for Materials Characterisation* (Bristol and Philadelphia, Institute of Physics Publishing, 1994) chapter 5

[39] C.D. Wagner, W.M. Riggs, L.E. Davis, J.F. Moulder and G.E. Muilenberg *Handbook of X-ray Photoelectron Spectroscopy* (Minnesota, Perkin-Elmer Corporation, 1979)

[40] T. Callebaut, I. Kochetov, Yu. Akishev, A. Napartovich and C. Leys *Plasma Sources Sci. Technol.* **13** (2004) 245-250

[41] Z. Falkenstein and J.J. Coogan *J. Phys. D: Appl. Phys.* **30** (1997) 817-825

[42] Y.P. Raizer *Gas Discharge Physics* (Berlin, Springer-Verlag, 1991) chapter 12

[43] Yu. S. Akishev, O. Goossens, T. Callebaut, C. Leys, A. Napartovich and N. Trushkin *J. Phys. D: Appl. Phys.* **34** (2001) 2875-2882

[44] T.C. Manley *Trans. Electrochem. Soc.* **84** (1943) 83-96

[45] S. Okazaki, M. Kogoma, M. Uehara and Y. Kimura *J. Phys. D: Appl. Phys.* **26** (1993) 889-892

[46] J. Verschuren *The plasma treatment of textile products, taking into account their specific properties* (PhD thesis, Ghent University, 2004)

[47] Yu. S. Akishev, M. E. Grushin, A. P. Napartovich and N.I. Trushkin *Plasmas Polym.* **7** (2002) 261-289

[48] J.S. Townsend *Phil. Mag.* **28** (1914) 83

[49] A. Goldman, M. Goldman and J.E. Jones *Proc. 10th Int. Conf. on Gas Discharges and their Applications* (Swansea, UK, 1992) pp. 270-273

[50] G. Beamson and D. Briggs *High Resolution XPS of Organic Polymers, The Scienta ESCA300 Database* (New York, Wiley, 1992)

[51] Z. Fang, Y. Qiu and Y. Luo *J. Phys. D: Appl. Phys.* **36** (2003) 2980-2985

[52] S. Ishikawa, K. Yukimura, K. Matsunaga and T. Maruyama *Jpn. J. Appl. Phys.* **39** (2000) 5223-5228

[53] T. Wakida, K. Takeda, I Tanaka and T. Takagashi *Textile Res. J.* **59** (1989) 49-53

[54] R.M.A. Malek and I. Holme *Iran. Polym. J.* **12** 4 (2003) 271-280

[55] Yu. S. Akishev 2006 *European patent application* Appl. N° EPO5447062